Universitat Autònoma de Barcelona

Study and modelization of a neutrino-nucleus CCQE interaction model

Bruno Bourguille

UNIVERSITAT AUTONOMA DE BARCELONA

Study and modelization of a neutrino-nucleus CCQE interaction model

by

Bruno Bourguille

A thesis submitted for the
degree of Doctor of material science

Supervised by

Dr. Federico Sanchez Nieto (Supervisor)

Dr. Eva Pellicer Vila (Tutor)

in the

Institut de Fisica dAltes Energia

April 2020

UNIVERSITAT AUTONOMA DE BARCELONA

Abstract

Institut de Fisica dAltes Energia

Doctor of Particle Physics

by Bruno Bourguille

In the study of neutrinos oscillation, understanding neutrinos interaction with matter is an important subject to predict the expected number of events in the detector. At intermediate energies, between a few MeV and 10 GeV, neutrinos interact directly with the nucleons inside a nucleus. Among the different interaction processes, the charged (neutral) current quasi-elastic scattering is the main neutrino, or anti-neutrino, nucleus interaction around 1 GeV.

In oscillation experiments, Monte Carlo simulations are used to predict the expected number of events in function of the kinematics of the different interactions. By comparing the number of events in the near and the far detector with the oscillation model, it is possible to determine the oscillation parameter values.

In this thesis, we work with a charged current quasi-elastic scattering cross section calculation model. The same nucleus modelisation is used to calculate the 1p1h , one neutrino - one nucleon interaction, and the 2p2h, one neutrino - multiple nucleon interaction, cross section. We modified both of the calculation to extract the complete interaction kinematics of these interactions. With the kinematics plus cross section obtained, we build a Monte Carlo (MC) simulation.We then implement this MC simulation in a neutrino events generator, that simulate neutrino interaction inside a detector.

With this events generator, we work on a comparison between the improved model and the previous model used. Also we show some of the limitations of the new model.

UNIVERSITAT AUTONOMA DE BARCELONA

Resumen

Institut de Fisica dAltes Energia

Doctor of Particle Physics

para Bruno Bourguille

En el estudio de la oscilacin de neutrinos, comprender la interaccin de los neutrinos es importante para predecir el nmero esperado de eventos en el detector. A energas intermedias, entre pocos MeV y 10 GeV, los neutrinos interactan directamente con los nucleones dentro de un ncleo. Entre los diferentes procesos de interaccin, la dispersin cuasi-elstica de la corriente cargada (neutra) es la interaccin principal para los neutrinos, o antineutrinos, alrededor de 1 GeV.

En los experimentos de oscilacin, las simulaciones Monte Carlo se utilizan para predecir el nmero esperado de eventos en funcin de la cinemtica de las diferentes interacciones. Al comprar el nmero de eventos en el detector cercano y lejano con el modelo de oscilacin, es possible determinar los valores de lo parmetros de oscilacin.

En esta tesis, trabajamos con un modelo para calcular la seccin eficaz de las interacciones cuasi-elsticas de corriente cargada. El mismo modelo se usa para calcular la seccin eficaz utilizando interacciones de un neutrino con un nucleon, 1p1h, y las interacciones con ms de un nucleon, 2p2h. Ambos clculos son modificados para extraer la cinemtica completa de las interacciones. Con la cinemtica ms la seccin eficaz calculadas, construimos una simulacin Monte Carlo (MC). Posteriormente la simulacin es implementada en un programa para generar interacciones de neutrino, a fin de simular interacciones de neutrino en un detector.

Con el generador de eventos, trabajamos en comprar el nuevo y mejorado modelo con los anteriormente en uso. Finalmente las limitaciones del modelo son presentadas.

Acknowledgements

I would like to express my thanks to all the people that have helped me during this thesis. Particularly to my thesis advisor Federico Sanchez, he has been a great guide to me during this thesis.

I enjoyed my work with the T2K collaboration with many great physicists and great person in general. Particularly Dr Yoshinari Hayato and Luke Pickering from the NIWG group that helped in my work on the NEUT program.

I would like to thank the people from IFAE neutrinos group for providing me help when I needed it and a great working place, Dr. Thorsten Lux, Dr. Matteo Cavalli-Sforza and Dr. Alfonso Garcia.

Contents

Chapter 1

Motivation

The Standard Model of the particle physics is one of the most successful theories of physics. This theory describes the fundamental particles and their interactions. Neutrinos are fundamental particles that have shown a behavior beyond the prediction of the Standard Model. They can oscillate between their different flavors since their flavor Eigenstates, that are observable, are different from their mass Eigenstates. The knowledge of neutrino nucleus interaction is hence an important subject for the study of these oscillations.

In this thesis, we work with neutrinos of intermediate energies, between few MeV and 10 GeV. In this energy range, neutrinos interact directly with the nucleons inside the nucleus. The possible interactions include elastic scattering and the production of one or multiple pions inelastic scattering. The cross section of those interactions cannot be simulated by one single model. The direct interaction with nucleons means that the modelisation of the nucleus has an important effect on the cross section calculation. Since nucleus are complex multi-body object there are many different modelisations, thus leading to the development of different cross section calculation models. We will focus on one of the model for the fundamental interaction, the neutrino-nucleon scattering.

We have worked on the implementation of an interaction model in a neutrino nucleus interaction Monte Carlo simulation called NEUT. NEUT is the official neutrino nucleus event generator of the Tokai to Kamyokande (T2K) experiment. It is used to predict the number of events expected in the detector and their kinematics. We have used a more realistic model than the one already implemented in NEUT in respect of the prediction of the events kinematics. Once the implementation was done we had to verify this model using experimental data from three different experiments.

The thesis is organized in the following way. First, we will review neutrino physics history and their properties. In the following, we present the cross section calculation

model we are using. Then, we will talk about the modifications implemented to the cross section calculation model to extract a consistent kinematics and its implementation into the Monte Carlo simulation we are using in this thesis, NEUT. After that, we will shortly explain NEUT and how it works. In the last part, we will show the comparison between the model and experimental data. The last part contains comparison between the previous model used in NEUT and the one we implemented and some results showing the limits of these models.

Chapter 2

Neutrino Physics Review

2.1 Historical introduction

Neutrinos were first postulated in 1930 by W. Pauli. Until then it was assumed that matter consisted of positive protons and negative electrons. However this picture started to change with the apparent non-conservation of energy in the β decay. It was observed that electrons produced during this decay process were detected with a continuous kinetic energy spectrum and not a fixed one as it should have been in a 2 body decay [1]. Pauli wrote an open letter to the nuclear physicists, that was read during the Tbingen congress the 4 December 1930, with his postulate. In his letter Pauli proposed the name of "neutron" to this particle which he predicted to have a 1/2 spin and a mass close to the electron mass.

This particle also was considered to potentially explain another problem, the spin of the Nitrogen. It was observed to have an integer spin while a nucleus made of protons and electrons would have a half integer spin.

In 1932 a particle was discovered by J. Chadwick with a neutral charge and half integer spin but its mass was equivalent to the proton and it was named neutron [2]. This particle solved the problem of the spin of the Nitrogen with a nucleus being a bound state of neutrons and protons [3]. But it did not solve the issue of the beta decay spectrum as its heavy weight was incompatible with experimental observation. In the following 2 years, E. Fermi developed a theory for the beta decay with the emission of both an electron and a light neutral particle, which he called "neutrino" [4]. This beta decay model, although simplistic, was based on electromagnetic interaction, and was an important step toward a proper neutrino interaction model. The model predicted an interaction cross section of $\sigma < 10^{-44} cm^2$.

It took 20 years of experiments to have the first proof of the existence of neutrinos.

Reines and Cowan developed in 1956 [5] an experiment using 400 liters of a mixture of water and cadmium chloride to detect anti-neutrino created inside a nuclear reactor nearby. The anti-neutrino interacts with a target proton creating a neutron and a positron. The positron annihilates with an electron creating two simultaneous photons of 0.512 MeV and the neutron is captured by a cadmium nucleus emitting a photon a few microseconds later. The detection of those 3 signal proved the neutrino existence, although here anti-neutrino were detected. The averaged cross section was measured to be [6]

$$\sigma = (11 \pm 2.6)10^{-44} cm^2. \tag{2.1}$$

At the beginning of the 1950s, observations in the Kaon decays by Lee and Yang [7] lead to consider the possibility of parity violation in weak interactions. Parity conservation implies that any interaction and its mirrored one in space coordinate have the same probability and is invariant against the $\overrightarrow{X} \rightarrow -\overrightarrow{X}$ transformation. Until then, it was thought to apply to all interactions. To establish parity violation, one needs to find an observable quantity different for both process. This experiment was carried out by Wu et al [8], using polarized ^{60}Co β-decays. The experiment was based the detection of the electron emitted during polarized ^{60}Co decay, given by

$$^{60}Co \rightarrow ^{60} Ni^* + e^- + \overline{\nu}_e. \tag{2.2}$$

The polarization of the ^{60}Co was achieved with a magnetic field on very cold atoms, 0.01 K, and the mirror configuration is simply created by reversing the magnetic field. An scintillation detector, using an anthracene crystal, was fixed in one direction, detecting the electron produced during the β-decay, and a count of decays was made depending on the ^{60}Co polarization. If the parity was conserved, one would expect that this experiment and its mirror, where the magnetic field is reversed, would yield the same behavior with polarization. But the opposite behavior was observed, in one magnetic configuration electron detection was enhanced and in the other it was lowered. The results of the experiment showed that electrons are preferably emitted with the opposite spin direction to that of the mother nucleus. Hence the neutrino beta decays interaction violate the parity conservation.

This discovery changed the comprehension of weak interaction and lead to the development of the V-A theory. In 1958, R. Feynman and M. Gell-Mann, R. Marshak and G. Sudarshan, proposed a theory where all Fermions only interact through weak interaction with their left handed component, the V-A theory [9],[10]. According to this theory neutrinos were massless particles without flavor.

In parallel, the experimental particle physics was evolving rapidly. Muons were discovered in 1936 [11], as particle created by cosmic radiation, with properties similar to the

electron but heavier. Muons are fermions with a mass of 105.6 MeV that decay into one electron and two neutrinos. Pions were discovered in 1947 [12]. Pions are the lightest mesons, hadrons formed by two quarks, which can be charged or neutral (π^+, π^-, π^0). The main pions decays are

$$\pi^+ \rightarrow \nu + \mu^+ \tag{2.3}$$

$$\pi^- \rightarrow \overline{\nu} + \mu^- \tag{2.4}$$

$$\pi^0 \rightarrow 2\gamma \tag{2.5}$$

In 1959, Pontecorvo proposed the hypothesis that if the neutrino emitted in β-decay is the same as the one emitted by the pion decays [13] and the neutrinos are flavorless, the following reactions (2.6 and 2.7) should have the same rate.

$$\nu + n \rightarrow \mu^- + p \tag{2.6}$$

$$\nu + n \rightarrow e^- + p \tag{2.7}$$

To test this hypothesis, a quasi-pure ν beam, meaning without any other lepton than ν, was created using a high-energy (15 GeV) proton beam hitting a beryllium-target in Brookhaven by G.Danby et al [14]. The collisions created pions and kaons that, as we know today, decay into ν_μ and μ^+. A shield of iron was used to absorb hadrons and most of the muons. The neutrino beam was detected by spark chambers, with a small fraction of the ν that underwent the reaction 2.6. The resulting charged leptons, either muon or electron, in the spark chamber can be discriminated by their track characteristic: muons produce straight lines and electrons an electromagnetic shower. In the experiment 29 muon-like events were detected whereas only 6 electron-like events were observed, thus showing that muon neutrinos are not the same as electron neutrinos. This result established the concept of lepton flavor and the conservation of this flavor. In this concept, a neutrino of one flavor is created in coincidence with the lepton of the same flavor, so the ν_μ interacting with the neutron can only produce a muon and not an electron.

During the next decade, the theory of the Standard Model was developed by Glashow [15], Weinberg [16] and Salam [17]. The Standard Model predicted the existence of 3 gauge bosons for the electroweak interaction, W^+,W^- and Z^0. They were discovered in 1983 at CERN by the two experiments UA1 and UA2 [18],[19]. We will explain in chapter 3 the neutrino weak interaction model with W^+ and W^- propagator.

2.2 Neutrinos and the Standard Model

The Standard Model (SM) is the theory that combines electromagnetic, weak and strong interactions. The SM is based on a gauge theory with a group formed by a direct product of three groups SU(3)⊗SU(2)⊗U(1), with SU(3) the color for the quantum chromodynamics(QCD or strong interaction), and SU(2)⊗U(1) the electroweak group, also called quantum flavor dynamics. The electroweak theory predicted the existence of the charged current bosons $W^{\pm}$, the massless gamma boson and the neutral current and its boson Z^0. The $W^{\pm}$ is responsible of the β decay and the other interactions described above. In 1973, the weak neutral current interaction was detected in a bubble chamber experiment, Gargamelle at CERN [20]. The different interactions have been studied in several experiment allowing the determination of various free parameters in the theory with high precision: the Fermi Constant G_F and the Weinberg angle Θ_W [21].
In the Standard Model theory all particles are massless in order to have gauge invariance, and the concept of spontaneous symmetry breaking is added to provide mass [22]. This is the "so-called" Higgs mechanism. This process gives mass to the bosons, whose masses are related to G_F, Θ_W and the gauge coupling constant of the electroweak group. The quarks and leptons also gain mass through this mechanism. But this mechanism cannot predict the absolute mass values of the particles.
In the SM, as a result of the parity violation, ν are predicted to only exist as chiral[1] left-handed particle (right-handed for $\overline{\nu}$). The right-handed ν, if it exists, does not interact through weak interaction and is called "sterile". Right-handed νs have not been found yet. Thus, under the hypothesis that there is no "sterile" neutrino, neutrinos are massless through the use of the Higgs mechanism as it requires both chirality to provide mass to a particle through the Dirac equation with ψ the neutrino 4-component wavefunction:

$$L = \overline{\psi}\big(i\gamma_\mu \frac{d}{dx_\mu} - m_D\big)\psi. \tag{2.8}$$

The Dirac mass term is $L_m = \overline{\psi} m_D \psi$. The wavefunction can be written as a sum of the left and right handed component $\psi = \psi_L + \psi_R$. Then, the Dirac mass term, using the fact that $\overline{\psi_L}\psi_L = 0$, is rewritten as

$$L_m = m_D(\overline{\psi_L}\psi_R + \overline{\psi_R}\psi_L). \tag{2.9}$$

Therefore in the hypothesis that there is no right-handed neutrino their mass term is not possible.
A summary of the particles is given table 2.1.

[1] chirality: fundamental property of of particle referring to the behavior of this particle's quantum mechanical wave function when rotated

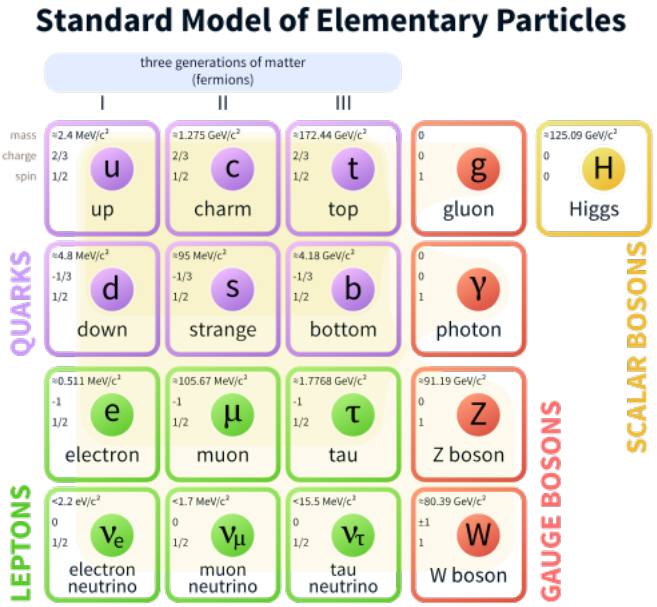

FIGURE 2.1: Elementary particle of the standard model (Image from Wikipedia)

2.3 Neutrino oscillation

The Homestack experiment observed in 1970 a large deficit of neutrinos coming from the sun compared to the expected flux [23]. This observation confirmed a theory proposed by Pontecorvo [24] in 1968 and Maki, Nakagawa and Sakata [25] in 1962, in which the neutrino could oscillate between the different flavors. This oscillation mechanism requires the neutrino to have a mass, with the flavor Eigenstates $|\nu_\alpha>$ not identical with the mass Eigenstates $|\nu_i>$. Each flavor Eigenstate can be written as a linear combination of the mass Eigenstates through a unitary matrix U:

$$|\nu_\alpha> = \sum_i U_{\alpha i}|\nu_i> \qquad |\nu_i> = \sum_\alpha U^\dagger_{i\alpha}|\nu_\alpha> \qquad = \sum_\alpha U^*_{\alpha i}|\nu_\alpha> \tag{2.10}$$

with [2]

$$U^\dagger U = 1 \qquad \sum_i U_{\alpha i}U^*_{\beta i} = \delta_{\alpha\beta} \qquad \sum_\alpha U_{\alpha i}U^*_{\alpha j} = \delta_{ij} \tag{2.11}$$

$|\nu_\alpha>$ are neutrinos flavor Eigenstates of the Hamiltonian H_f at a time t and $|\nu_i>$ are mass Eigenstates with an energy E_i and a momentum $\overrightarrow{p}$. With the Schroedinger equation, a neutrino of mass state i propagating freely in a vacuum can be written as a plane wave solution

$$|\nu_i(t)> = e^{-iH_f t}|\nu_i(0)> . \tag{2.12}$$

[2] $U^\dagger is the transpose conjugate matrix and U^* is the conjugate matrix$

Whereas $|\nu_i(t) >$ are the mass Eigenstate with a energy E_i and momentum $\overrightarrow{p}$ of the Hamiltonian H which is diagonal in the vacuum. Then $H|\nu_i(t) >= E_i|\nu_i >= \sqrt{m_i^2 + |\overrightarrow{p}|^2}|\nu_i >$. Since neutrinos are assumed to fulfil $m_i << p$, the energy can be approximated by $E_i \approx |\overrightarrow{p}| + m_i^2/(2|\overrightarrow{p}|)$.

Combining the previous equations, the flavor neutrino at a time t is a coherent superposition of mass neutrino states of energy E_i:

$$|\nu_\alpha(t) >= \sum_i U_{\alpha i} e^{-iE_i t} |\nu_i > . \tag{2.13}$$

Using the previous relation and the hypothesis that neutrinos are relativistic particles (assuming $E \approx |\overrightarrow{p}|$), one can derive the probability for a neutrino of flavor α to change to a β flavor after traveling a time t:

$$\begin{aligned} P(\alpha \to \beta) &= | < \nu_\beta(0)|\nu_\alpha(t) > |^2 \\ &= \delta_{\alpha\beta} - 4 \sum_{i>j=1}^{3} Re(U_{\alpha i} U^*_{\beta i} U^*_{\alpha j} U_{\beta j}) sin^2\Big(\frac{\Delta m^2_{ij} L}{4E}\Big) \\ &+ 4 \sum_{i>j=1}^{3} Im(U_{\alpha i} U^*_{\beta i} U^*_{\alpha j} U_{\beta j}) sin\Big(\frac{\Delta m^2_{ij} L}{4E}\Big) cos\Big(\frac{\Delta m^2_{ij} L}{4E}\Big) \end{aligned} \tag{2.14}$$

with Δm_{ij} the difference of masses between two mass Eigenstates and $L = ct$ the distance between source and detector. In the 3 flavors scenario, the mixing matrix is called the Pontecorvo, Maki, Nakagawa and Sakata matrix (U_{PMNS}) that can be parametrized with 3 angles (θ_{13},θ_{23},θ_{12}) and one phase δ:

$$U_{PMNS} = \begin{pmatrix} 1 & 0 & 0 \\ 0 & c_{23} & s_{23} \\ 0 & -s_{23} & c_{23} \end{pmatrix} \begin{pmatrix} c_{13} & 0 & s_{13}e^{-i\delta} \\ 0 & 1 & 0 \\ -s_{13}e^{-i\delta} & 0 & c_{13} \end{pmatrix} \begin{pmatrix} c_{12} & s_{12} & 0 \\ -s_{12} & c_{12} & 0 \\ 0 & 0 & 1 \end{pmatrix} \tag{2.15}$$

In these matrices, s_{ab} is the contraction for $\sin(\theta_{ab})$ and c_{ab} is the contraction of $\cos(\theta_{ab})$ with $ab = 13, 23, 12$.

In this parametrisation for the PMNS matrix, the first matrix is referred to Atmosphere sector (23), the second matrix is referred to Accelerator sector (13) and the third is referred to Solar sector (12). Their name corresponds to the neutrino source used to study the dominant mixing angles. This choice of parametrisation has been done due to the different value of the 3 angles and is independent of the difference of square masses. The flavor oscillation properties can be parametrized with 3 masses, 3 angles and one complex phases. The complex phase is linked to the CP symmetry in the lepton sector and if it is non-zero, the particle-antiparticle symmetry is broken. The neutrino mass

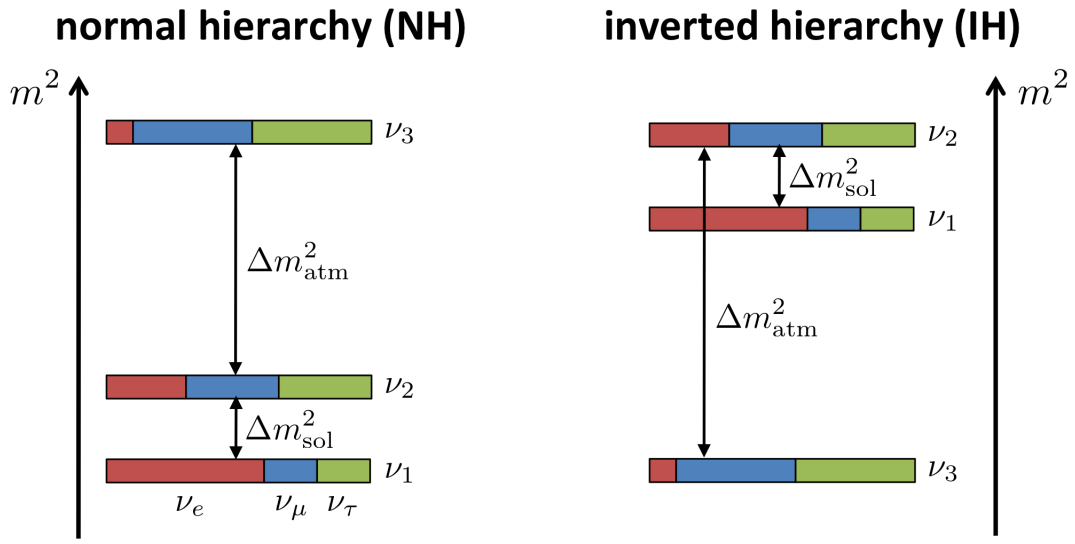

FIGURE 2.2: representation of two possible mass hierarchy. color indicate the flavor composition of each state .

term is not directly used in oscillation, only the difference in squared mass Δm^2_{ij} as seen in equation 2.14, around a few $10^{-3}eV^2$ for the atmospheric sector and a few $10^{-5}eV^2$ for the solar sector [26]. This is because the oscillation is an interference process occurring due to the different velocity of the neutrinos. The main convention is to use $\Delta m^2_{21} = m^2_2 - m^2_1$ also written as Δ_{sol} and $\Delta m^2_{32} = m^2_3 - \frac{m^2_1+m^2_2}{2}$ also written as Δ_{atm}. In this convention $\Delta m^2_{21} > 0$, but either $\Delta m^2_{32} > 0$ and it is called normal hierarchy, NH, or $\Delta m^2_{32} < 0$ and it is called inverted hierarchy, IH, this is shown figure 2.2.

2.4 Source and detection

As stated before, neutrinos used for oscillation searches can be produced by several sources. The most important ones are:

- nuclear power plants,
- the sun,
- the atmosphere,
- accelerators.

2.4.1 Nuclear power plants

Nuclear power plants are the strongest terrestrial source of anti-neutrinos. The fission of ^{235}U,^{238}U,^{239}Pu and ^{241}Pu atoms produce unstable neutron-rich atoms that will go through β decay to stabilize. There is two different β decay processes possible inside a nucleus, the β^- decay where a neutron decay to a proton, an electron and an anti-neutrino and the β^+ decay where a proton decay to a neutron, a positron and a neutrino. As inside a power plant neutron-rich atoms are produced, most of the decay happening in the power plant are β^- decay. So, per fission reactions an average of 6 anti-neutrinos are produced. The anti-neutrino flux density for a solid angle in a power plants is computed the following way:

$$\Phi_\nu = 1.5 * 10^{12} \frac{P/MW}{L^2/m^2} cm^{-2} s^{-1} \tag{2.16}$$

where P is the thermal power (in MW) of the reactor and L (in m) is the distance from the reactor core. This is a low nuclear energy process, with $\overline{\nu}_e$ or ν_e produced and neither $\overline{\nu}_\mu$ (ν_μ) nor $\overline{\nu}_\tau$ (ν_τ)as in the β-decay only an electron or a positron is emitted. The conservation of the Lepton number induces therefore the production of an electron anti-neutrino. The anti-neutrinos produced have an energy spectrum peaked at 2-3 MeV and extended up to 8 MeV.
As such the detection reaction used is mostly the inverse β-decay:

$$\overline{\nu}_e + p \rightarrow e^+ + n \tag{2.17}$$

that has an energy threshold of 1.806 MeV for hydrogen atoms and a cross section of $\sigma = 9.23 * 10^{-42} \left(\frac{E_\nu}{10MeV}\right)^2 cm^2$ [27]. The energy threshold changes depending on the bounding of the proton inside the nucleus. The strength of the bounding in a nucleus is linked to the number of neutrons and protons inside it. This is the method that was used by Reines and Cowan to detect the first neutrino [6].

2.4.2 the Sun

The sun (and every star) creates its energy via nuclear fusion and is one of the most interesting sources of neutrinos. First, it is a pure source of ν_e resulting from fusion chains. Second, it was a deficit in the predicted number of solar neutrinos that lead to the first indications of neutrino flavor oscillations. This deficit was first seen by the Homestake experiment [28] and it was confirmed by subsequent experiment such as Kamioka Observatory and Sudbury Neutrino Observatory. Third, study of solar neutrinos is nearly the only way to have a direct probe in the solar interior.

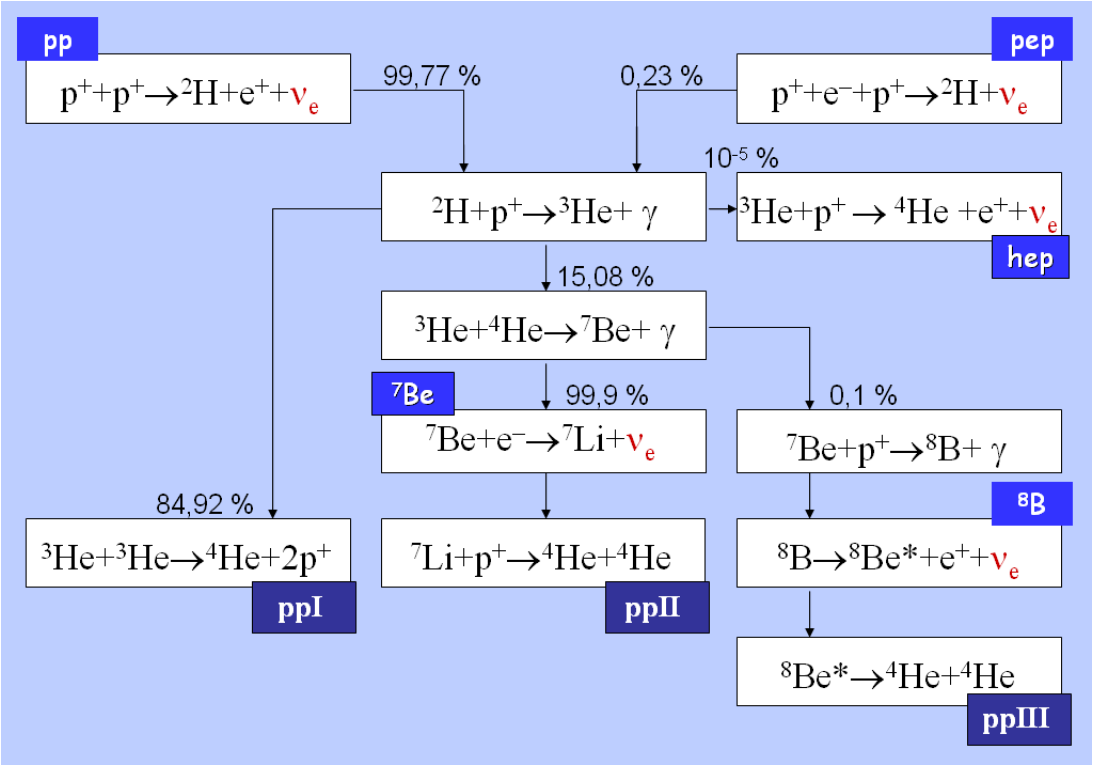

FIGURE 2.3: pp cycle in the sun. It produce 98.4% of the solar energy. (Image from Wikipedia)

The dominant hydrogen thermonuclear fusion in the sun is the following interaction

$$4p \rightarrow {}^4He + 2e^+ + 2\nu_e \tag{2.18}$$

Each of these ^{4}He fusion produces an energy of $Q = 2m_e + 4m_p - m_{He} = 26.73MeV$, then with the Luminosity of the sun $L_{sun} = 3.8x10^{26}W$ [29] it is possible to estimate the flux of neutrinos at the Earth:

$$\Phi_\nu = 2\frac{L_{sun}}{Q}\frac{1}{4\pi R^2} \approx 6.3x10^{10}cm^{-2}s^{-1} \tag{2.19}$$

with R the mean distance Sun to Earth. The details of the neutrino flux are more complex, there are two different processes, the *pp* cycle [30] and the CNO cycle [31]. In the Sun, the *pp* cycle is the main cycle and accounts for almost all energy production. It is shown figure 2.3. In the *pp* cycle neutrinos are produced in different reactions, so they have different energy. The primary *pp* fusion has two different reactions but one proceeds with 99.77% as the *pp* reaction, the other one being the pep reaction.

$$p + p \rightarrow {}^2H + e^- + \nu_e \qquad pp \tag{2.20}$$

$$p + e^- + p \rightarrow {}^2H + \nu_e \qquad pep \tag{2.21}$$

Neutrinos produced in *pp* reaction have a continuous energy spectrum with energies going up to 0.42 MeV whereas neutrinos from the *pep* reaction have a fixed energy at 1.44 MeV. In the later stage of the cycle, other neutrinos can be produced with a lower probability than in the *pp* cycle going from the *pp* process to the *ppI* process such as the *hep* process with a continuous energy spectrum up to 18.77 MeV.

$$^3He + p \rightarrow {}^4He + e^+ + \nu_e \qquad hep \tag{2.22}$$

$$^7Be + e^- \rightarrow {}^7Li + \nu_e \qquad {}^7Be \tag{2.23}$$

$$^8B \rightarrow {}^8Be^* + e^+ + \nu_e \qquad {}^8B \tag{2.24}$$

The ^7Be reaction produces neutrinos at a fixed energy. In this case with two possible energies, either 0.862 MeV or 0.384 MeV and the last reaction creating neutrinos in the *pp* cycle is the ^8B process with a continuous energy spectrum up to 15 MeV. Therefore solar neutrinos are emitted as electron neutrinos with an energy spectrum from sub-MeV to nearly 20 MeV.

Detection of solar neutrinos is done through two types of methods: radiochemical and real-time experiments. The principle for a radiochemical experiments is the generic reaction

$$^A_N Z + \nu_e \rightarrow {}^A_{N-1}(Z+1)^* + e^- \tag{2.25}$$

where the daughter nucleus is unstable and the decays has a half-life long enough to allow for isotope extraction and detection. The production rate of the daughter nucleus is written as

$$R = N \int \Phi(E_\nu)\sigma(E_\nu)dE_\nu \tag{2.26}$$

with Φ the solar neutrino flux, N the number of target atoms and σ the cross section for the reaction of equation 2.25. Given an incident neutrino flux around $10^{10} cm^{-2} s^{-1}$ and a cross section expected around $10^{-45} cm^2$, about 10^{30} target atoms are required to produce one event per day. This kind of experiment has a low threshold but carries no information on the time of the event, direction and energy of the incident neutrino. Indeed one can only count the average number of unstable daughter nuclei over a certain period of time. An example of such detector is the Homestake experiment [32] using Chlorine neutrino capture changing to Argon with a threshold of 0.8 MeV.

The principle of real-time experiments is to detect the electron scattered by an neutrino-electron interaction. There two method are used, the first consists of detecting the Cerenkov light [33] emitted by the electron going faster than the light-speed in the medium, usually water. The second is to detect the energy deposited by the lepton in the detector medium, for example liquid scintillator or liquid Argon, using a Time Projection Chamber. The advantage of the method is that the neutrino direction can be retrieved as the electron direction is correlated to the direction of the incoming neutrino.

The problem with this method comes with the energy threshold of this interaction that is about 5 MeV, meaning that only neutrino emitted by the ^8B and hep reactions can be detected so only a very small fraction of all solar neutrinos. An example of this kind of detector is the Sudbury Neutrino Observatory [34].

2.4.3 The atmosphere

Atmospheric natives neutrinos have been used to study oscillations via the large range of the ratio L/E, between 1 and 10^5 km GeV^{-1}. They are produced from the decay of secondary particles produced in the interaction of primary cosmics rays with the atmosphere. The primary cosmic rays consist to nearly 98% of hadrons and 2% of electrons whose energy can reach from a few GeV to hundreds of TeV. The hadronic showers produced contains mesons, mostly pions which decay via:

$$\pi^+ \rightarrow \mu^+ + \nu_\mu \qquad \mu^+ \rightarrow e^+ + \nu_e + \overline{\nu}_\mu \tag{2.27}$$

$$\pi^- \rightarrow \mu^- + \overline{\nu}_\mu \qquad \mu^- \rightarrow e^- + \overline{\nu}_e + \nu_\mu \tag{2.28}$$

For higher energy showers, it is possible to have Kaon production, leading to the production of more neutrinos through the following decays:

$$K^\pm \rightarrow \mu^\pm + \nu_\mu(\overline{\nu}_\mu) \tag{2.29}$$

$$K_L \rightarrow \pi^\pm + e^\pm + \nu_e(\overline{\nu}_e) \tag{2.30}$$

Atmospheric neutrinos are produced in the atmosphere, hence they can have a path-length to the ground anywhere between a few km to 10000 km if they cross the earth. Due to the primary particle broad energy spectra, neutrinos can have a wide range of energy from hundreds of MeV to a few TeV. The cosmic ray flux uncertainties, the neutrino production cross section and the atmosphere model make it very difficult to calculate the absolute neutrino flux [35],[36],[37] . The predictions on the flux have disagreements on the level of 20 % to 30 % in the spectra and overall normalization. Those study still reached a consensus that the ratio of fluxes:

$$R = \frac{\nu_e + \overline{\nu}_e}{\nu_\mu + \overline{\nu}_\mu} \tag{2.31}$$

can be predicted with a 5% accuracy due to some uncertainties cancelling out. Atmospheric neutrinos have enough energy to interact directly with nucleons inside nucleus (see next chapters for interaction details) and detection is done through the lepton resulting from those interactions.

2.4.4 The accelerator

Neutrinos produced using an accelerator are used to study oscillation as one can choose the distance between production and detector and have a neutrino energy flux well defined so it is possible to target specific regions of L/E for the study. Since the first neutrino beam of the Brookhaven experiment, the neutrino beam production principle has not changed significantly. A high energy proton beam is collided with a fixed target, resulting in a high yield of secondary mesons, mostly pions and kaons.on the other side of the collision, optical devices called horns are installed. The horns are pulsed with high currents synchronously with the accelerator pulse, forming a magnetic azimuted field concentric around the beam axis. The magnetic field focuses particles with the appropriate charge towards the beam axis and deviate the others reducing wrong-sign backgrounds. The secondaries decay following the reactions 2.27,2.28,2.29 with a branching ratio of 100% for pions and 63% for kaons. This ensures a nearly pure ν_μ beam (or $\overline{\nu}_\mu$ beam if the opposite signed charged mesons are focused). With a length L_D for the tunnel, only a portion of the meson decays. The probability of decay P is given as

$$P = 1 - exp(-L_D/L_0) \tag{2.32}$$

with L_0 the mean decay length for a meson M of 4-vector $(E_M, \overrightarrow{p_M})$ and mean life τ_M under the relativistic assumption

$$L_0 = \beta\gamma\tau_M = \frac{p_M}{m_M}\tau_M \tag{2.33}$$

So the decay length depends on the meson momentum via

$$L_0(\pi) = 55.9m \times p_\pi/GeV \tag{2.34}$$

$$L_0(K) = 7.51m \times p_K/GeV \tag{2.35}$$

This probability multiplied by the decay branching ratios gives the number of neutrinos as a functions of its energy. The neutrino flux and energy distribution can be chosen not only with the initial particle momentum but also with the decay tunnel length. At the end of the decay tunnel, there is a large muon shield, to absorb the remaining mesons by nuclear reactions and stop the muons by ionization and radiation losses. This way, one limits the beam contamination due to electron neutrinos from muon decays as shown in the second equation of line 2.27. Contamination of the muon neutrino beam by electron neutrinos also came from others decays like the K_{e3^-} decay

$$K^\pm \to \pi^0 + e^\pm + \nu_e(\overline{\nu_e}) \tag{2.36}$$

with a branching ratio of 4.8%. The last source of contamination are the decays from mesons produced in the absorber. The neutrino spectrum is then determined from the kinematics of the two body decays mesons. In the laboratory frame Energy (E_ν) and angle ($\cos\theta_\nu$) are related to the same quantities in the rest frame (marked with a *) by

$$E_\nu = \gamma E^*_\nu(1 + \beta\cos\theta^*_\nu) \qquad \cos\theta_\nu = \frac{\cos\theta^*_\nu + \beta}{1 + \beta\cos\theta^*_\nu} \tag{2.37}$$

$$\beta = \frac{p_M}{E_M} \qquad \gamma = \frac{E_M}{m_M} \qquad E^*_\nu = \frac{m_N^2 - m_\mu^2}{2m_N} \tag{2.38}$$

So in the laboratory frame we have neutrino energy dependent on the angle with

$$E_\nu(\theta) = \frac{m_N^2 - m_\mu^2}{2(E_M - p_M\cos\theta_\nu)} \tag{2.39}$$

In conclusion the (anti)neutrino flux depend first the beam meson composition after the proton target collision, second the horn charge selection, third the decay length. In addition, one can choose to install the detector either in the neutrino beam direction, "on-axis", to maximize neutrino energy and width, or with an angle respect to the neutrino beam direction, "off-axis", to have the flux peak at lower energy. In the "off-axis" configuration, there is less events than with the "on-axis" but there will be less background interactions.

2.4.5 detection in accelerator and atmospheric neutrino experiments

Detection of accelerator and atmospheric neutrinos is done through neutrino-nucleon scattering, and the different detectors for this need to fulfill many requirements

- identification of a charged lepton to distinguish CC and NC events,
- measurement of energy and scattering angle of the charged lepton to determine the kinematic variable of the events,
- measurement of the hadronic energy to reconstruct the neutrino energy,
- identification of the secondary hadron and his momentum to investigate the final final state,
- detection of short living particles, the potential secondary mesons for example,
- use of different target materials.

It is challenging to fulfill all the requirements, and the actual design of the detector depend on the physics question under study.

2.4.6 Oscillation Study

The study of neutrinos oscillations can be done in two different ways, the appearance and the disappearance modes. In the first case, you are searching for a new neutrino flavor which do not exist in the original beam. In the second case, one searches whether less neutrinos than expected, of one produced flavor, are detected after traveling a certain distance. The identification of the neutrino flavor is made through the detection of the corresponding charged lepton produced in the charged current interaction:

$$\nu_l + N \rightarrow l^- + X \tag{2.40}$$

with $l^{\pm}$ being one of the three leptonic flavor. and N and X the hadron initial and final state. Among the source of neutrinos, accelerators permit to chose the distance L between source and detector, an large neutrino energy spectrum and also have a good event rate.
With equation 2.14, there is threes case to be considered with respect to a possible observation of oscillations:

- $L/E \ll \frac{4}{\Delta m^2}$. In this case, the experiment will not see any oscillation as it is too close to the source.It is in this position that near-detector are installed.In an oscillation experiment a near detector is used to measure the neutrino flux and reduce uncertainties.
- $L/E\frac{\Delta m^2}{4} \approx 1$. This is a necessary condition to observe oscillations, also it is the most sensitive region.
- $L/E \gg \frac{4}{\Delta m^2}$. This is the regime of decoherence, the three neutrino masses do not interfere anymore so there is no oscillation anymore.

The parameters space explored depends on the ratio L/E, with the most sensitive range of an experiment at

$$\Delta m^2 \approx E/L. \tag{2.41}$$

Concerning near detector, They are also used to study neutrino cross section.

2.5 Three accelerator-based Experiments

This work is related to the interactions of ν on nucleus for $E_\nu > 100MeV$. This is an energy regime for atmospheric and accelerator experiments. We will focus on presenting the three accelerator-based experiments whose data will be compared to in this thesis: T2K, MiniBooNE and MINERvA.

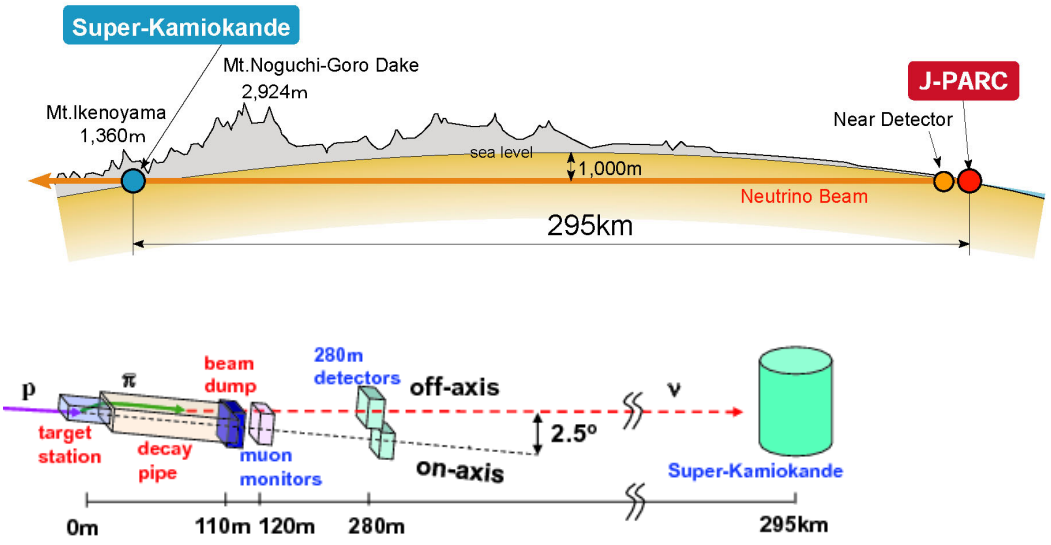

FIGURE 2.4: schematic view of T2K experiment configuration

2.5.1 T2K

The T2K (Tokai to Kamiokanda) experiment is a long baseline neutrino oscillation experiment. It was designed to probe disappearance of the muon neutrino and appearance of the electron neutrino in a nearly pure muon neutrino beam. Another aim was to study neutrino oscillation parameters with high precision and it was the first experiment to detect ν_e appearance [38].
The T2K configuration is shown in figure 2.4. An accelerator is used to produce neutrinos that are detected in a far detector, Super-Kamionkande (SK) , 295 km away from the target. A detailed description of SK can be found in [39]. To control the flux, there is a near detector facility 280 m away from the tunnel with 2 near detectors, INGRID [40] and ND280. One of the particularities of T2K experiment is the neutrino beam is not directed toward the far detector but with an angle of 2.5°. This allows the neutrino beam to be peaked around 0.6 GeV, which maximize the oscillation effect at 295 km and minimize the electron neutrino contamination for the electron neutrino appearance study. The flux prediction of ν is based on the data from the NA61/SHINE experiment from CERN, a complete description about the T2K flux is available in [41].

Another particularity is the fact that near detector and far detector does not use the same detector technology, SK is a water Cherenkov detector whereas Ingrid is composed of an array of iron and scintillator sandwiches and ND280 is composed of a 2 Fine Grained Detectors (FGD)[42] using water and scintillator as target, 3 Time Projection Chambers (TPC)[43] in a metal basket box surrounded by Electromagnetic Calorimeters (ECal)[44] enveloped in a magnet. Inserted in the magnet yokes is placed a Side Muon Range Detector (SMRD)[45] to trigger or veto on interaction outside the basket such as

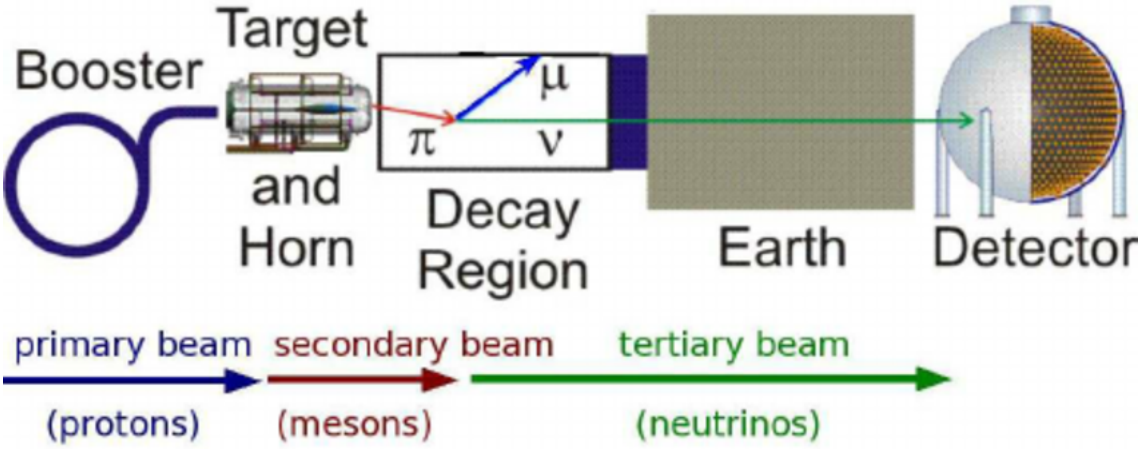

FIGURE 2.5: schematic view of MiniBooNE experiment

cosmic rays. Before the TPC and FGD there is a Pi-Zero Detector (POD) [46] composed of 26 scintillator modules interleaved with water layers and brass sheets. The aim of the POD detector is to observe neutral current interactions, in which a π^0 is emitted. Construction of the experiment began in 2004 and the experiment began to take data in 2010. As of today, it is still taking data and an upgrade of the near detector (ND280 upgrade) and the building of a new far detector (Hyper Kamiokande) have started.

2.5.2 MiniBooNE

The MiniBooNE (Mini Booster Neutrino Experiment) experiment was a short baseline neutrino oscillation experiment. This experiment is the first stage of the BooNE experiment, The primary aim was to verify the result from the LSND experiment, which observed a $\nu_\mu \rightarrow \nu_e$ oscillation for $\Delta m^2 = 1\ eV^2$ implying physics beyond the classical neutrino oscillation scheme. MiniBooNE looked for the possibility of sterile neutrinos influencing neutrino oscillation. This experiment has been build at Fermilab to look for $\nu_\mu \rightarrow \nu_e$ oscillation and it also is made to search for anti-neutrino mode, $\overline{\nu}_\mu \rightarrow \overline{\nu}_e$. MiniBooNE schematic configuration is shown figure 2.5, the muon neutrino beam is created by decay of pions produced by collision of the Fermilab Boosters proton beam and a Be target. Neutrinos are detected 500 meters away from the end of the decay tunnel by a mineral oil Cherenkov and scintillation detector.

The MiniBooNE experiment started taking data in 2002. The data obtained with the neutrino muonic beam showed some evidence for oscillations but not where they were expected creating a new controversy. Indeed, the results excludes the oscillation for anti-neutrinos at $\Delta m^2 = 1eV^2$ proposed by the LSND experiment [47]. An excess of electron neutrino events was detected at lower energies and is still unexplained. This anomaly leads to the creation of a new dedicated experiment called microBooNE [48].

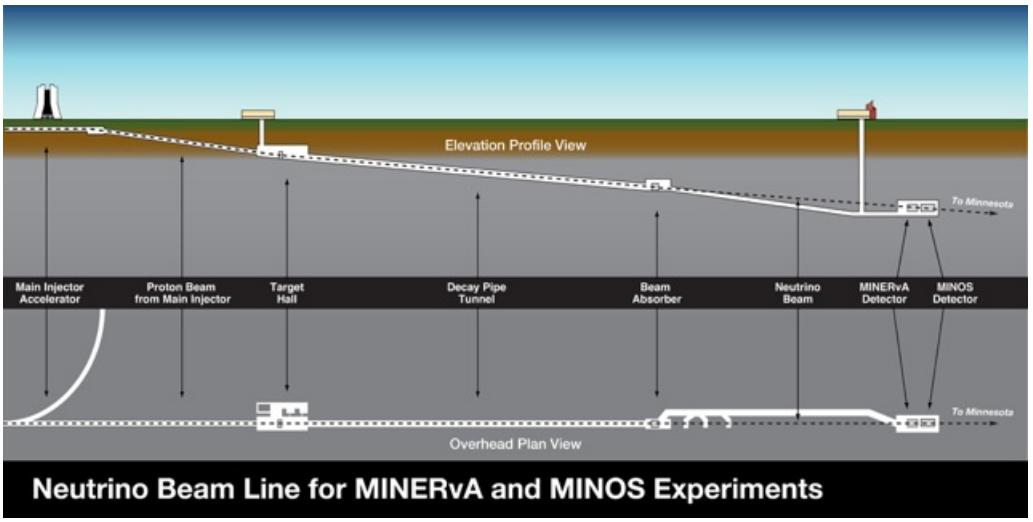

FIGURE 2.6: schematic view of MINERvA experiment

2.5.3 MINERvA

The MINERvA (Main INjector ExpeRiment $\nu - A$) experiment is a short baseline neutrino cross-section calculation experiment. The goal is to perform a precision study of cross sections relevant to oscillation studies, aiming to have a solid comprehension of neutrino-nucleus interactions.

MINERvA uses a compact design shown in figure 2.6, with the far detector only 1000 m away from the proton target usig the same beam as MiniBooNE. The neutrino beam is produced at FermiLab by a collision between a proton beam and a proton target then after focusing with magnets the resulting pion and letting them decays in a 675 m decays volume we have a neutrino beam. This neutrino energy is spread between a few hundred MeV to 15 GeV. The neutrino are then detected by the MINERvA detector approximately 250 m away from the end of the decay volume, putting the detector 1000 m away from the target. The MINERvA detector is composed of a nuclear target, made of either C, Fe, Pb, LHe or water, a Solid Scintillator tracker surrounded by Electromagnetic Calorimeter and Hadron Calorimeter. A particularity of this design is that the Minos near detector is situated 20 m behind the Minerva detector. The Minos near detector is a tracking calorimeter composed of iron and plastic scintillator in a magnet, used for muon spectrometry.

MINERvA detector started taking data in 2010 and is still running.

Chapter 3

Cross Section theory and modelisation of CCQE interactions

Neutrinos interact through weak interaction, with a cross sections of about $10^{-38}/E_\nu$ (cm^2/GeV), with E_ν being the neutrino energy in GeV. As such, there are different interaction physics processes involved as function of the energy. In this thesis, I study neutrinos of energies between few hundreds of MeV and a few GeV. Figure 3.1 shows the total cross section of neutrinos in this range and also introduces the different interaction processes contributions and their neutrino energy ranges. The different interaction mechanism at this energy range are called Quasi-Elastic Scattering (QE), Resonant Production (RES) and Deep Inelastic Scattering (DIS).

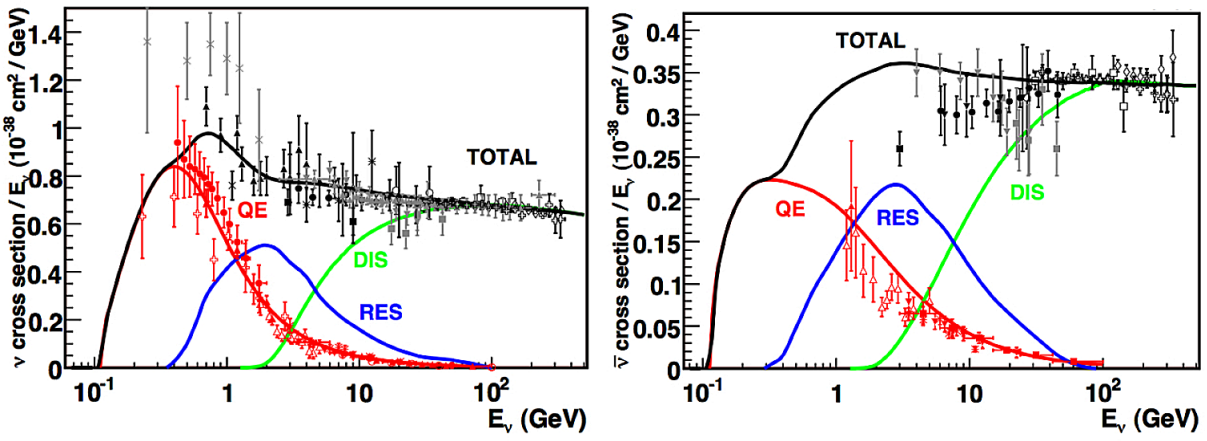

FIGURE 3.1: Cross section versus neutrino Energy for an energy range between 100 MeV and 20 GeV.left is for neutrino and right for anti-neutrino. Plot from [49]

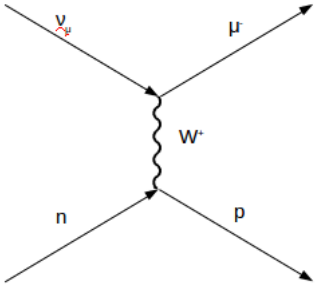

FIGURE 3.2: a) Feynman diagram for a CCQE interaction with a muon neutrino

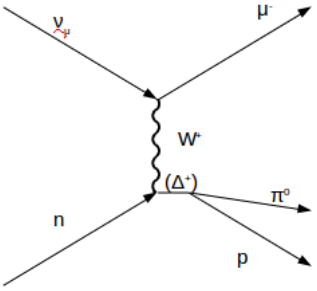

FIGURE 3.3: b) Feynman diagram for a neutrino resonant pion production with a Δ

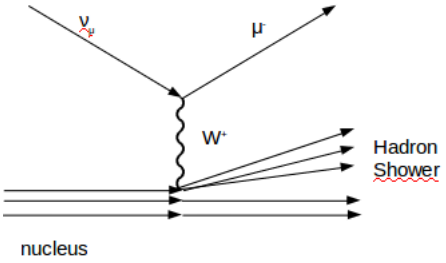

FIGURE 3.4: c) Feynman diagram for a neutrino DIS interaction

The scattering interaction mechanism extracts one or more nucleons from the nucleus. In the case of a Charged Current $W^{\pm}$ exchange, this interaction is called Quasi-Elastic (CCQE). The process (equation 3.1) Feynman diagram is show in figure 3.2. The Neutral Current with Z^0 exchange is shown by equation 3.2 and is called Elastic (NCE).

$$\nu_l + n \rightarrow l^- + p \tag{3.1}$$

$$\nu_l + n \rightarrow \nu_l + n \tag{3.2}$$

Resonant production interaction (RES) corresponds to an excitation of the nucleon by the neutrino to a baryon resonance state. This results in the production of a baryon afterwards decaying with the emission of a meson:

$$\nu_l + p \rightarrow l^- + \Delta^{++} \rightarrow l^- + \pi^+ + p. \tag{3.3}$$

This interaction has many channels that leads to the production of a different meson: Δ^{++}, Δ^{+}, Δ^{0}, Δ^{-}, K^{+}, K^{0}, K^{-}.The Feynman diagram of one of the several channel of resonant interaction is shown in figure 3.3. There also exist case where the meson is directly produced during the interaction without excitation of, it is called the non-resonant production.

DIS is an interaction that appears only if the neutrino has enough energy to resolve the quark constituents of the nucleon.

$$\nu_l + N \rightarrow l^- + X \tag{3.4}$$

with N the target nucleus and X the final nucleus, a hadron shower is also emitted during this interaction. The quark scattered by the neutrino will create an hadron shower by hadronization as shown in figure 3.4.
This thesis is centered around CCQE interactions. I will now describe the process to calculate CCQE cross sections. In CCQE interactions there exist two different processes 1p1h and 2p2h. 1p1h refers to interaction with only one nucleon whereas 2p2h is when 2 nucleons interact coherently with the scatered neutrino.
Cross sections are computed using the impulse approximation [50], in which the neutrino interacts with free nucleons in a nuclear potential. More importantly, this approximation state that the target nucleon is considered as a quasi-free particle during the interaction. The resulting cross section is then corrected for nuclear effects for initial and the final states.

3.1 Cross Section of Neutrino-Nucleus Scattering

3.1.1 Definition and formulae

The interaction integrated cross section is defined as the number of interactions during a period of time "t" for a target divided by the flux, the number of incident particles per time unit. Using the Fermi Golden rule, the cross section can be expressed with a transition matrix M_{fi}, which describes the evolution from initial state i to final state f. For a scattering, with at least four particles, two initial particles i_1 and i_2, and at least 2 final particles f_α:

$$\sigma = \frac{1}{4E_{x_1}E_{x_2}(v_{x_1}+v_{x_2})} \int \prod_{f_\alpha} \frac{d^3p_{f_\alpha}}{(2\pi)^3 2E_{f_\alpha}} (2\pi)^2 \delta^4(\sum_{f_\alpha} p_{f_i} - p_{x_1} - p_{x_2}) |M_{fi}|^2 \tag{3.5}$$

with E_a, v_a and p_a the energy, velocity and momentum of particle a ($a = i_1, i_2, f_\alpha$).
Electroweak charged current interactions are written as follow:

$$\begin{aligned} \nu_l + A_i &\rightarrow l^- + A_f \\ \overline{\nu}_l + A_i &\rightarrow l^+ + A_f \end{aligned} \tag{3.6}$$

with A_i the initial nucleus and A_f the final nucleus and the ejected hadrons. The double differential cross section can be written by using equation 3.5, with the assumption of

being in the center of mass frame:

$$\frac{d^2\sigma_{\nu l}}{d\Omega(k')dE'_l} = \frac{|\overrightarrow{k'}|}{|\overrightarrow{k}|}\frac{G_F^2}{4\pi^2}L_{\mu\tau}W^{\mu\tau} \tag{3.7}$$

with $\overrightarrow{k}$ and $\overrightarrow{k'}$ neutrino and lepton momentum respectively[1], $E'_l = (\overrightarrow{k'}^2 + m_l^2)^{1/2}$ the energy of the outgoing lepton, $\Omega(k')$ the solid angle of the outgoing lepton, $G_F = 1,1664.10^{-11} MeV^{-2}$ the Fermi constant and L and W the Leptonic and Hadronic tensor respectively. We take μ and $\tau = 0,1,2,3$ the indices for the tensor and vector. By convention the metric is written as $g^{\mu\tau} = (+,-,-,-)$ and $\epsilon_{\mu\tau\alpha\beta}$ is the Levi-Civita tensor.

The leptonic tensor represents the leptonic part of the interaction and is given by equation 3.8

$$L_{\mu\tau} = k'_\mu k_\tau + k'_\tau k_\mu - g_{\mu\tau}k.k' + i\epsilon_{\mu\tau\alpha\beta}k'^\alpha k^\beta \tag{3.8}$$

The hadronic tensor containts all information about the electroweak interaction inside the nucleus, from initial state, $|i>$, to all possible final states, $|f>$.

$$W^{\mu\tau} = \frac{1}{2M_i}\sum_f (2\pi)^3\delta^4(P'_f - P_i - q) < f|j^\mu_{cc}(0)|i >< f|j^\tau_{cc}(0)|i > \tag{3.9}$$

with P_i the four-momentum of the initial nucleus and M_i its mass, P'_f the four-momentum of the final hadronic state f, q is the transferred four-momentum. The current, J^μ_{cc}, is written using the quark fields Ψ_u,Ψ_d,Ψ_s and the Cabibbo angle ($cos(\Theta_C = 0.974)$ as in the equation 3.10.

$$j^\mu_{cc}(0) = \overline{\Psi_u}\gamma^\mu(1-\gamma_5)(\cos(\Theta_C)\Psi_d + \sin(\Theta_C)\Psi_s) \tag{3.10}$$

The hadronic tensor $W^{\mu\tau}$ can be described by 6 structure functions $W_i(q^2)$.

$$\begin{aligned} W^{\mu\tau} = &-g^{\mu\tau}W_1 + \frac{P^\mu P^\tau}{M_i^2}W_2 + i\frac{\epsilon^{\mu\tau\gamma\delta}P_\gamma q_\delta}{2M_i^2}W_3 + \frac{q^\mu q^\tau}{M_i^2}W_4 + \\ &+ \frac{P^\mu q^\tau + q^\mu P^\tau}{2M_i^2}W_5 + i\frac{P^\mu q^\tau + q^\mu P^\tau}{2M_i^2}W_6 \end{aligned} \tag{3.11}$$

The structure functions are probability density function describing the spatial distributions of charge and current inside the nucleon, they are among the most basic observables of the nucleon. The understanding of these structure functions is one of the most important challenges for nuclear physics.

We choose the reference system such that the transferred momentum $\overrightarrow{q}$ is alone the z

[1] their value is calculated in the laboratory frame

direction and the initial nucleus is at rest, $P = (M_i, \overrightarrow{0})$, and after multiplying with the leptonic tensor we can write the double differential cross section as:

$$\frac{d^2\sigma_{\nu l}}{d\Omega(k')dE'_l} = \frac{|\overrightarrow{k'}|E'_l M_i G_F^2}{\pi^2}\Bigg\{2W_1\sin^2(\frac{\theta'}{2}) + W_2\cos^2(\frac{\theta'}{2}) - W_3\frac{E_\nu + E'_l}{M_i}sin^2(\frac{\theta'}{2}) + \\ + \frac{m_l^2}{E'_l(E'_l + |k'|)}\Bigg[W_1\cos(\theta') - \frac{W_2}{2}cos(\theta') + \frac{W_3}{2}\left(\frac{E'_l + |k'}{M_i} - \frac{E_\nu + E'_l}{M_i}\cos(\theta')\right) + \\ + \frac{W_4}{2}\left(\frac{m_l^2}{M_i^2}\cos(\theta') + \frac{2E'_l(E'_l + |k'|)}{M_i^2}\sin^2(\theta')\right) - W_5\frac{E'_l + |k'|}{2M_i}\Bigg]\Bigg\} \tag{3.12}$$

with E_ν the incoming neutrino energy and θ' the outgoing lepton scattering angle with respect to the neutrino. Equation 3.12 is a general formula that could be applied to any neutrino-nucleon scattering as no assumption is made on the final hadronic state.

3.1.2 Nucleus, hadronic tensor and boson self-energy in a medium

The interactions happen inside the nucleus, thus the hadronic tensor has to take into account different effects due to the nuclear media. There are different ways to describe the nucleus, the most simple one is the Relativistic Fermi Gas (RFG), where the density is the same in the whole nucleus and the nucleon momentum is fixed to the Fermi momentum. Another model is called the Spectral Function (SF), here the nucleus is described as a sum of particle and hole spectral functions. The model used to describe the nucleus in this thesis is the Local Fermi Gas (LFG) approximation. It assumes a density dependent on the radial position in the nucleus. This model is a reasonable description between the RFG and the SF that provide accurate predictions for electron scattering cross section.
For the RFG and LFG model, the Fermi momentum p_F can be written as:

$$p_F(r) = (3\pi^2\rho_t)^{\frac{1}{3}} \tag{3.13}$$

with ρ_t the density of the target nucleon in the media, whether it is a neutron or a proton depending on neutrinos or anti-neutrinos interaction. The total density is defined as $\rho_t = \rho_n + \rho_p$, so that one can take into account the case of nuclei non isoscalar. The density does not depend on the radial position in the nucleus for the RFG model but it does for the LFG model.
The hadronic tensor is determined by calculating the self-energy of the neutrino in the medium, which depends on the self-energy[2] of the W-boson $\Pi_W^{\eta\rho}(q)$. The concept of neutrino self-energy is described in figure 3.5. In this figure, the neutrino has a 4-vector $k = (k^0, \overrightarrow{k})$ and an helicity r, the position inside the nucleus has a density ρ. The self

[2]energy that a particle has as a result of interacting with itself in its environment

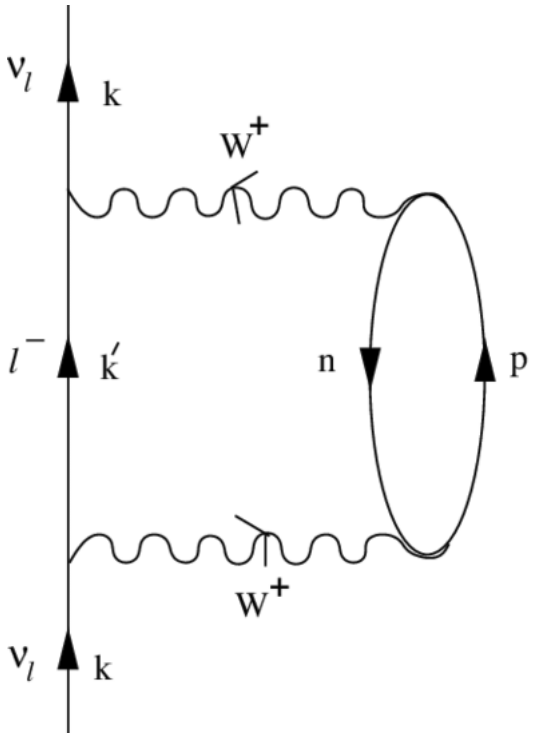

FIGURE 3.5: Diagram representing the neutrino self-energy in the nuclear matter.

energy of this neutrino, written $\Sigma^r_\nu(k,\rho)$, is the interaction through a W-boson exchange with itself. For the notation, the virtual lepton is written with a 4-vector k' and the boson with a 4-vector $q = k - k'$. Using the formalism developed in reference [51], the neutrino self energy can be expressed in the following way

$$-i\Sigma^r_\nu(k,\rho) = \int \frac{d^4q}{(2\pi)^4}\overline{u}_r(k)\Big[-i\frac{g}{2\sqrt{2}}\gamma^u_L iD_{\eta\alpha}(q)(-i)\Pi^{\alpha\beta}_W(q;\rho) \\ iD_{\beta\rho}(q)i\frac{\not{k}' + m_l}{k'^2 - m_l^2 + i\epsilon}(-i\frac{g}{2\sqrt{2}})\gamma^\rho_L\Big]u_r(k) \quad (3.14)$$

With $D_{\eta\alpha}(q)$ the virtual boson W^+ propagator and $\Pi^{\alpha\beta}_W(q;\rho)$ its self-energy, $u_r(k)$ the Dirac spinors. The Dirac spinors are normalized to $u\overline{u} = 2m$, and are projected only to left handed neutrinos by the equation term $\gamma^\mu_L = \gamma^\mu(1-\gamma_5)$. The boson propagator is written $D_{\eta\alpha}(q) = (-g_{\eta\alpha} + q_\eta q_\alpha/M^2_W)/(q^2 - M^2_W + i\epsilon)$.
Neutrinos only interact with matter if they are left-handed, so only the left handed self-energy is non-zero. Then the sum over helicities, $\Sigma_\nu(k,\rho) = \sum_r \Sigma^r_\nu(k,\rho)$, results in the computation of a trace in the Dirac space. After this sum we have:

$$\Sigma_\nu(k,\rho) = \frac{8iG}{\sqrt{2}M^2_W}\int \frac{d^4q}{(2\pi)^4}\frac{L_{\eta\rho}\Pi^{\eta\rho}_W(q;\rho)}{k'^2 - m_l^2 + i\epsilon} \quad (3.15)$$

with $L_{\eta\rho}$ the virtual lepton tensor.
Using the optical theorem, the self energy of the neutrino is related to the decay width

of the particle through the imaginary part of the self-energy [52]

$$\Gamma(k;\rho) = -\frac{1}{k^0} Im\Sigma_\nu(k,\rho) \tag{3.16}$$

The Cutkoskys rules [53] are used to calculate the discontinuity across a cut arising from from a physical-region singularity. By using those rules, it is then possible to calculate the imaginary part of Σ_ν. These rules are applied in figure 3.5, cutting a vertical line between the intermediate lepton state and the virtual interaction of the W-boson. Those states are placed "on shell" by taking the imaginary part of the propagator, allowing to integrate over the energy assuming $k^0 > 0$

$$Im\Sigma_\nu(k,\rho) = \frac{8iG}{\sqrt{2}M_W^2} \int \frac{d^3k}{(2\pi)^3} \frac{\Theta(q^0)}{2E_l'} Im L_{\eta\rho} \Pi_W^{\eta\rho}(q;\rho) \tag{3.17}$$

with $\Theta(q^0)$ being the Heaviside function.
The probability of decay per unit area is given by $\Gamma dt dS$. Using relation 3.16 and the relation between an integration over time and over space, we can write

$$d\sigma = \Gamma dt dS = -\frac{1}{q^0} Im\Sigma_\nu(k,\rho) dt dS = -\frac{1}{|\overrightarrow{k}|} Im\Sigma_\nu(k,\rho) d^3r \tag{3.18}$$

Thus, the nuclear cross section can be written as

$$\sigma = -\frac{1}{|\overrightarrow{k}|} \int Im\Sigma_\nu(k,\rho) d^3r \tag{3.19}$$

The LFG assumption, as shown in [54], is an excellent approximation for volume processes like the one studied here. Using equations 3.17 and 3.19 one can write

$$\sigma = -\frac{1}{|\overrightarrow{k}|} \frac{8G}{\sqrt{2}M_W^2} \int d^3r \int \frac{d^3q}{(2\pi)^3} \frac{\Theta(q^0)}{2E_l'} Im L_{\eta\rho} \Pi_W^{\eta\rho}(q;\rho) \tag{3.20}$$

By construction the lepton and the hadron tensor can be decomposed between a symmetric and an anti-symmetric part, written as $L_{\eta\rho} = L^s_{\eta\rho} + iL^a_{\eta\rho}$ and $W^{\eta\rho} = W_s^{\eta\rho} + iW_a^{\eta\rho}$. The comparison between equations 3.7 and 3.20 allows relating the hadron tensor to the gauge boson self-energy. It is then possible to decompose the contraction $L_{\mu\tau}W^{\mu\tau}$

$$\frac{d^2\sigma_{\nu l}}{d\Omega(k')dE_l'} = \frac{|\overrightarrow{k'}|}{|\overrightarrow{k}|} \frac{G_F^2}{4\pi^2} (\frac{2\sqrt{2}}{g})^2 \int \frac{d^3r}{2\pi} [L^s_{\eta\rho} Im(\Pi_W^{\eta\rho} + \Pi_W^{\rho\eta}) - L^a_{\eta\rho} Re(\Pi_W^{\eta\rho} - \Pi_W^{\rho\eta})] \Theta(q^0) \tag{3.21}$$

Finally the hadronic tensor reads

$$W_s^{\rho\eta} = -\Theta(q^0)(\frac{2\sqrt{2}}{g})^2 \int \frac{d^3r}{2\pi} Im[\Pi_W^{\eta\rho} + \Pi_W^{\rho\eta}](q;\rho(r)) \tag{3.22}$$

$$W_a^{\rho\eta} = -\Theta(q^0)(\frac{2\sqrt{2}}{g})^2 \int \frac{d^3r}{2\pi} Re[\Pi_W^{\eta\rho} - \Pi_W^{\rho\eta}](q;\rho(r)) \tag{3.23}$$

This self energy should be calculed taking into account the relevant absorption modes, some of them are shown in figure 3.6, such as absorption by one or more nucleons (π, ρ,..), production of a real or virtual mesons or excitation of a resonant degree of freedom (Δ,..). In addition nuclear effects have to be taken into account, such as random phase approximation (RPA), short range correlation or Final State Interaction (FSI). Those effects correspond to either the nuclei as a whole or the other nucleons affecting the interaction. This leads to corrections to the cross section. Until now the formalism has not been restricted to the quasi-elastic region, so it can be applied to any interaction.

3.2 Quasi-elastic cross section (1p1h)

The "so-called" 1 particle - 1 hole (1p1h) is the CCQE interaction in which the neutrino interacts with only one nucleon which then try to escape from the nucleus.

3.2.1 Hadron tensor calculation

For 1p1h interactions, equation 3.6 take the form:

$$\nu_l + n \to l^- + p \tag{3.24}$$

In the previous section, the cross section was computed in function of the self energy of the gauge boson. Therefore to have the cross section for the 1p1h interaction, we have to calculate the contribution of the one nucleon $W^+(W^-)$ absorption to the self-energy. This corresponds to the first diagram of figure 3.6. Applying the Cutkoskys rules give the self energy diagram to be calculated. This self-energy diagram shows an interaction vertex between a boson W^+ and two nucleons propagator in the nuclear medium. This propagator in a medium is written as

$$G(p,\rho) = \frac{1}{p^2 - M^2 + i\epsilon} + \frac{2\pi i}{2E(\overrightarrow{p})}\delta(p^0 - E(\overrightarrow{p}))\Theta(k_F - |\overrightarrow{p}|) \tag{3.25}$$

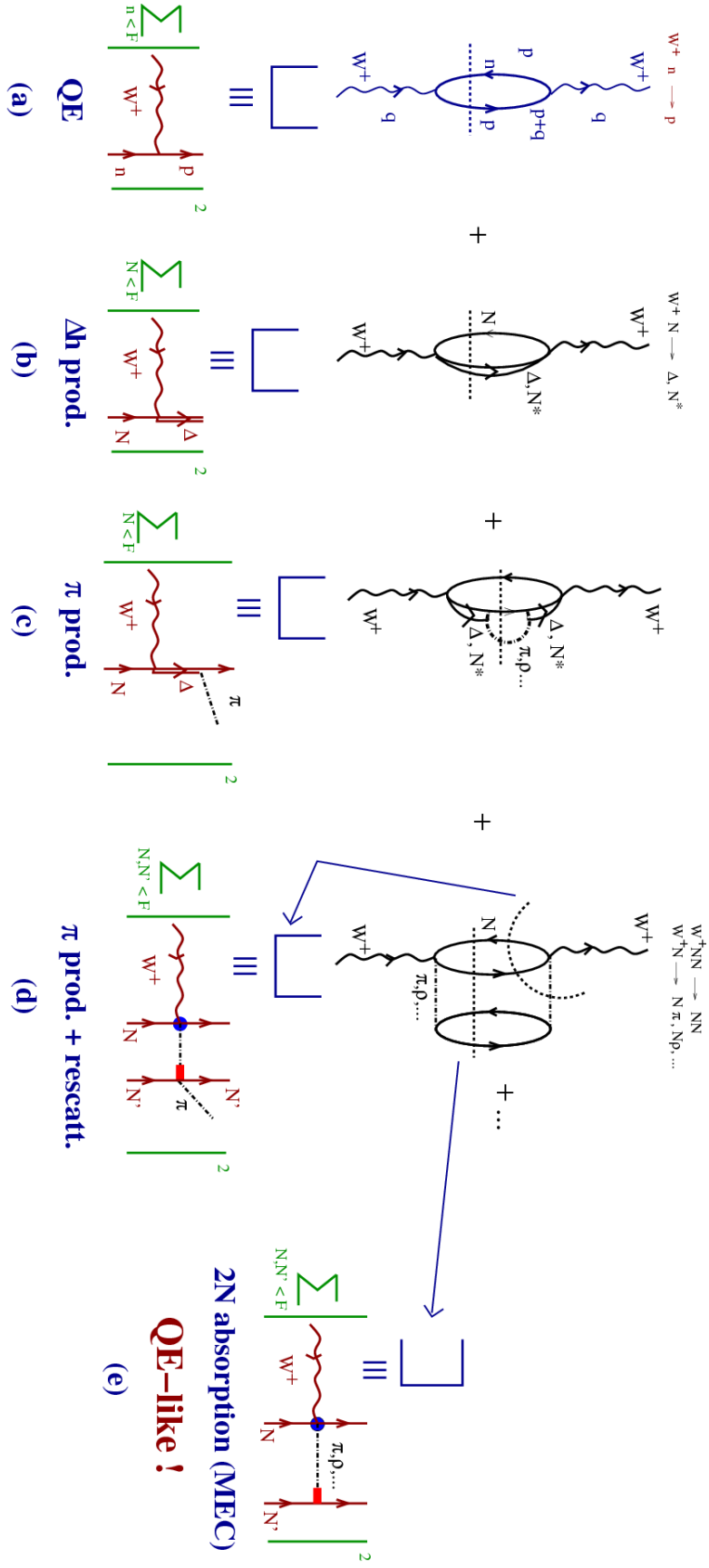

FIGURE 3.6: Representation of some of the contribution to the boson W^+ self-energy

being M the target nucleon mass, $\overrightarrow{p}$ the target nucleon momentum and $E(p)$ its energy. For the W^+pn vertex we separate into axial and vector nucleon currents

$$V^\alpha = 2cos(\theta_C)\big(F_1^V(q^2)\gamma^\alpha + i\mu_V \frac{F_2^V(q^2)}{2M}\sigma^{\alpha\nu}q_\nu\big) \tag{3.26}$$

$$A^\alpha = cos(\theta_C)G_A(q^2)\big(\gamma^\alpha\gamma_5 + \frac{2M}{m_\pi^2 - q^2}q^\alpha\gamma_5\big) \tag{3.27}$$

with $m_\pi = 139.57MeV$. The vectorial form factor, $F1$ and $F2$, and the axial one, G_A, are used to describe the internal structure of the nucleon. The vector form factors can be related to the form factor from the electron scattering (using isospin symmetry), it is the so called Conserved Vector Current (CVC) approximation, and they can be expressed using the Sachs form factors of the nucleon [55]

$$F_1^V(q^2) = \frac{1}{2}[\frac{G_E^p + \tau G_M^p}{1+\tau} - \frac{G_E^n + \tau G_M^n}{1+\tau}] \tag{3.28}$$

$$\mu_V F_2^V(q^2) = \frac{1}{2}[\frac{G_M^p - G_E^p}{1+\tau} - \frac{G_M^n - G_E^n}{1+\tau}] \tag{3.29}$$

This is using the Galster et al parametrization [56],

$$G_E^p = \frac{G_M^p}{\mu_p} = \frac{G_M^n}{\mu_n} = -(1+\lambda_n\tau)\frac{G_E^n}{\mu_n\tau} = (\frac{1}{1 - q^2/M_D^2})^2 \tag{3.30}$$

with $\tau = -q^2/(4M^2)$, $M_D = 0.846GeV$, $\mu_p = 2.792847$, $\mu_n = -1.913$ and $\lambda_n = 5.6$.

The axial form factor is only accessible through weak interaction and here we use the simplest way to define it, a dipole form factor

$$G_A(q^2) = \frac{g_A}{(1 - q^2/M_A^2)^2} \tag{3.31}$$

with $g_A = 1.257$ and $M_A = 1.05GeV$. Those values are obtained through the study of the charged (neutral) current (quasi-)elastic (anti)neutrino scattering off protons, deuterons and other nuclei.

With the propagator and the vertex, the W^+ self energy for the 1p1h interaction becomes

$$-i\Pi_W^{\eta\rho}(q;\rho) = -cos^2(\theta_C)(\frac{q}{2\sqrt{2}})^2 \int \frac{d^4p}{(2\pi)^4} A^{\eta\rho}(p,q)G(p;\rho_n)G(p+q;\rho_p) \tag{3.32}$$

$A^{\eta\rho}(p,q)$ is the nucleon tensor described by the following expression

$$\begin{aligned} A^{\eta\rho}(p,q) = Tr\Big\{ & \big[2F_1^V(q^2)\gamma^\eta - 2i\frac{\mu_V F_2^V(q^2)}{2M}\sigma^{\eta\alpha}q_\alpha - G_A(q^2)(\gamma^\eta\gamma_5 - \frac{2M}{m_\pi^2 - q^2}q^\eta\gamma_5)\big] \\ & (\not{p} + \not{q} + M)\big[2F_1^V(q^2)\gamma^\rho + 2i\frac{\mu_V F_2^V(q^2)}{2M}\sigma^{\rho\alpha}q_\alpha - G_A(\gamma^\rho\gamma_5 + \frac{2M}{m_\pi^2 - q^2}q^\rho\gamma_5)\big] \\ & (\not{p} + M)\Big\} \end{aligned} \tag{3.33}$$

After the traces computation,

$$\begin{aligned} A^{\eta\rho}(p,q) = & 16(F_1^V(q^2))^2\big\{(p+q)^\eta p^\rho + (p+q)^\rho p^\eta + \frac{q^2}{2}g^{\eta\rho}\big\} + \\ & + 2q^2(\mu_V F_2^V(q^2))^2\big\{4g^{\eta\rho} - 4\frac{p^\eta p^\rho}{M^2} - 2\frac{p^\eta q^\rho + q^\eta p^\rho}{M^2} - q^\eta q^\rho(\frac{4}{q^2} + \frac{1}{M^2})\big\} - \\ & - 16F_1^V(q^2)\mu_V F_2^V(q^2)(q^\eta q^\rho - q^2 g^{\eta\rho}) + \\ & + 4(G_A(q^2))^2\big\{2p^\eta p^\rho + q^\eta p^\rho + p^\eta q^\rho + g^{\eta\rho}(\frac{q^2}{2} - 2M^2) - \frac{2M^2(2m_\pi^2 - q^2)}{(m_\pi^2 - q^2)^2}q^\eta q^\rho\big\} - \\ & - 16iG_A(q^2)(F_1^V(q^2) + \mu_V F_2^V(q^2))\epsilon^{\eta\rho\alpha\beta}q_\alpha p_\beta \end{aligned} \tag{3.34}$$

As it is an hadron tensor, it can be decomposed in the same tensor as the one of 3.11:

$$A^{\eta\rho}(p,q) = a_1 g^{\eta\rho} + a_2(p^\eta p^\rho + \frac{p^\eta q^\rho + p^\rho q^\eta}{2}) + ia_3\epsilon^{\eta\rho\alpha\beta}p_\alpha q_\beta + a_4 q^\eta q^\rho \tag{3.35}$$

with

$$\begin{aligned} a_1(q^2) &= 8q^2\big\{(F_1^V(q^2) + \mu_V F_2^V(q^2))^2 + (G_A(q^2))^2(\frac{1}{4} - \frac{M^2}{q^2})\big\} \\ a_2(q^2) &= 32(F_1^V(q^2))^2 - 8(\mu_V F_2^V(q^2))^2\frac{q^2}{M^2} + 8(G_A(q^2))^2 \\ a_3(q^2) &= 16G_A(q^2)(F_1^V(q^2) + \mu_V F_2^V(q^2)) \\ a_4(q^2) &= -\frac{8q^2}{M^2}(\mu_V F_2^V(q^2))^2(\frac{M^2}{q^2} + \frac{1}{4}) - \frac{8M^2(G_A(q^2))^2}{m_\pi^2 - q^2}(\frac{q^2}{(m_\pi^2 - q^2)} + 2) \end{aligned} \tag{3.36}$$

with $a_5(q^2)$ the same as $a_2(q^2)$ and $a_6(q^2) = 0$ to complete the decomposition in the same structure function as 3.11.

Finally, we can compute the hadron tensor for 1p1h interactions:

$$W^{\rho\eta}(q^0, \overrightarrow{q}) = -\frac{cos^2(\theta_C)}{2M^2}\int_0^\infty dr r^2\big\{2\Theta(q^0)\int\frac{d^3p}{(2\pi)^3}\frac{M}{E(\overrightarrow{p})}\frac{M}{E(\overrightarrow{p}+\overrightarrow{q})}\Theta(k_F^n(r)-|\overrightarrow{p}|)$$
$$\Theta(|\overrightarrow{p}+\overrightarrow{q}|-k_F^p(r))(-\pi)\delta(q^0+E(\overrightarrow{p})-E(\overrightarrow{p}+\overrightarrow{q}))A^{\eta\rho}(p,q)\big\} \quad (3.37)$$

If the form factors are known, this hadron tensor can be analytically calculated, leading to the cross section for 1p1h interaction in a nucleus. We still have to take into account the different nuclear corrections to be applied to this tensor such as Pauli Blocking, RPA correction at low and intermediates transfer energy, Coulomb field distortion and FSI effects.

3.2.2 Nuclear corrections

The Pauli Exclusion Principle in quantum mechanics states that two or more identical fermions cannot have the same quantum state, and in the nucleus this is represented by the Pauli Blocking that forbids nucleons to have the same final state, including the momentum. In this model, the Pauli Blocking effect is modelized in the hadron tensor by

$$\int_0^\infty dr\, r^2\Theta(k_F^n(r)-|\overrightarrow{p}|)\Theta(|\overrightarrow{p}+\overrightarrow{q}|-k_F^p(r)). \quad (3.38)$$

Random Phase Approximation (RPA) [57] response is used to modelize the medium polarization effects in the 1p1h cross section. Medium polarization means that the nucleons in the medium can affect the electroweak couplings due to a strong interaction between the target nucleon and the surrounding nucleons. RPA response is described diagrammatically in figure 3.7 with the interaction modelized using effective particle hole interactions of the Landau-Midgal type [58]

$$V = c_0 f_0(\rho) + f_0'(\rho)\overrightarrow{\tau_1}\overrightarrow{\tau_2} + g_0(\rho)\overrightarrow{\sigma_1}\overrightarrow{\sigma_2} + g_0'(\rho)\overrightarrow{\sigma_1}\overrightarrow{\sigma_2}\overrightarrow{\tau_1}\overrightarrow{\tau_2} \quad (3.39)$$

where $\overrightarrow{\sigma}$ and $\overrightarrow{\tau}$ are Pauli matrices acting on the nucleon spin and isospin spaces respectively. The different coefficients, c_0, f_0, f_0', g_0, g_0', were determined in [59] from calculations of electric and magnetic moments of nuclei, transition probabilities and electric and magnetic multipole resonances. Those interaction include virtual pion creation such as π, ρ, Δ[3]. The nucleon tensor $A^{\eta\rho}$ is then modified by the sum of the RPA

[3] the loop in figure 3.7

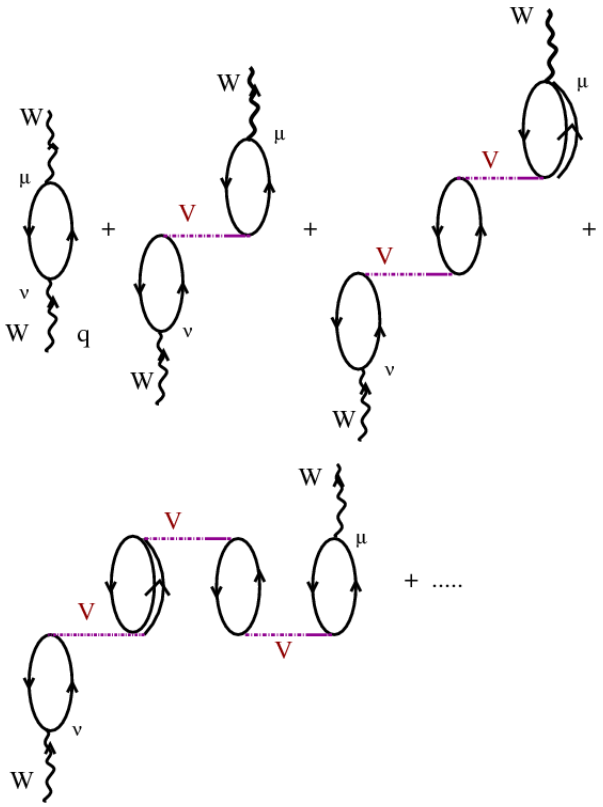

FIGURE 3.7: Set of diagrams describing the RPA effects in the 1p1h cross section

series representing those medium polarization effect.

Medium polarization is not the only nuclear effect that has to be taken into account. It is also necessary to correct the energy balance in the reaction. In the LFG model creating a particle hole excitation requires to excite the initial state nuclei to the final state nuclei. So the nuclei needs a minimum excitation energy in order to transit from the initial to the final state, both being supposed to be a the Fermi level. This minimum energy is equal to the difference of mass between the initial and final state of the hadron part of the interaction. Then the minimum energy, q_{val}, depends on the nucleus, defined by A nucleons and Z protons, and if the interaction was with a neutrino or an anti-neutrino and we can write:

$$q_{val}(\nu) = M(A - 1_Z) - M(A_Z) + m_p \tag{3.40}$$

$$q_{val}(\overline{\nu}) = M(A - 1_{Z-1}) - M(A_Z) + m_n + m_e \tag{3.41}$$

Those energy corrections are taken into account by removing them from the transfer energy:

$$q'^0 = q^0 - q_{val} \tag{3.42}$$

Since the charged lepton produced in the 1p1h interaction is moving inside the nucleus, it is affected by the Coulomb field of the nucleus described by a charge distribution, $\rho_{ch}(r)$. The approach was developed in reference [60], with the inclusion of a self-energy in the intermediate lepton propagator as shown in figure 3.5. This self-energy in LFG is approximated by

$$\Sigma_C = 2k'^0 V_C(r) \tag{3.43}$$

$$V_C(r) = -4\pi\alpha(\frac{1}{r}\int_0^r dr' r'^2 \rho_{ch}(r') + \int_r^\infty dr' r' \rho_{ch}(r')) \tag{3.44}$$

with $\alpha = 1/137.036$ the fine-structure constant and k' is the energy momentum four-vector of the intermediate lepton. Due to the Coulomb potential, the momentum conservation of the outgoing lepton is broken and one defines via energy conservation $\hat{E}'_l(r)$ the momentum of the outgoing lepton as:

$$\hat{E}'_l(r) = E'_l - V_C(r) = \sqrt{m_l^2 + |\overrightarrow{\kappa}(r)|^2} \tag{3.45}$$

This lepton momentum $\overrightarrow{\kappa}$ depends of the radial position of the interaction in the nucleus and will serve to calculate a local transfer momentum $\overrightarrow{q}' = \overrightarrow{k} - \overrightarrow{\kappa}(r)$ between the neutrino and the outgoing lepton. Also a correction due to the Coulomb potential is applied to the d^3k' integration in equation 3.17:

$$|\overrightarrow{\kappa}(r)|\hat{E}'_l(r)/|\overrightarrow{k'}|E'_l. \tag{3.46}$$

With these corrections, the hadronic tensor takes finally the form:

$$\begin{aligned} W^{\rho\eta}(q^0, \overrightarrow{q}) = -\frac{cos^2(\theta_C)}{2M^2}\int_0^\infty dr r^2 \frac{|\overrightarrow{\kappa}(r)|\hat{E}'_l(r)}{|\overrightarrow{k'}|E'_l}\Theta(\hat{E}'_l(r) - m) \\ \{2\Theta(q'^0)\int \frac{d^3p}{(2\pi)^3}\frac{M}{E(\overrightarrow{p})}\frac{M}{E(\overrightarrow{p}+\overrightarrow{q}')}\Theta(k_F^n(r) - |\overrightarrow{p}|) \\ \Theta(|\overrightarrow{p}+\overrightarrow{q}'| - k_F^p(r))(-\pi)\delta(q^0 + E(\overrightarrow{p}) - E(\overrightarrow{p}+\overrightarrow{q}'))A^{\eta\rho}_{RPA}(p,q')\} \end{aligned} \tag{3.47}$$

with $q'^0 = q^0 - qval$, $\overrightarrow{q}' = \overrightarrow{k} - \overrightarrow{\kappa}(r)$ and $A^{\eta\rho}_{RPA}(p,q')$ being the nucleon tensor modified by RPA correction.

3.3 2p2h

The "so-called" 2 particles - 2 holes (2p2h) interactions are interactions where the transferred energy has enough energy to extract 2 nucleons from the nucleus during the primary interaction. This interaction has an important contribution to the total cross section in the "dip region" corresponding to excitation energies lying between the quasielastic and pion resonant production peak. One of the diagram of the 2p2h self-energy is shown in figure 3.6 with the contribution (e). It has to be noted that this diagram participates to 2p2h self-energy when the cut is made horizontal. The other contributions that can be obtained, like (d) with a vertical cut, is part of the pion production self-energy. Also one can see that the processes contributing to 2p2h exchange a pion. This interaction is described with the pion propagator D_π and the pion form factor $F_\pi^2(k_\pi)$. The hadronic tensor that is calculated using the Cutkosky rule for those $W^+N \to N'\pi^\lambda$ processes is the following [61]:

$$W_{2p2h}^{\mu\tau} = \Theta(q^0)\frac{1}{M^2}\int\frac{d^3r}{2\pi}\sum_{N,N',\lambda}\int\frac{d^4k_\pi}{(2\pi)^4}\Theta(q^0-k_\pi^0)F_\pi^2(k_\pi)Im\overline{U}_R(q-k_\pi,k_F^N,k_F^{N'})A^{\mu\tau}$$
$$D_\pi^2(k_\pi)F_\pi^2(k_\pi)\frac{f_{\pi NN}^2}{m_\pi^2}\overrightarrow{k}_\pi^2\Theta(k_\pi^0)ImU_\lambda(k_\pi) \tag{3.48}$$

with U_λ is the Lindhard function for a particle-hole excitation by an object of charge λ. This function needs to take into account the correction from the interaction with other nucleons in the nucleus.
First, the self-energy of the pion of charge λ is defined as:

$$\Pi(k_\pi) = F_\pi^2(k_\pi)\frac{f_{\pi NN}^2}{m_\pi^2}\frac{U(k_\pi)}{1-\frac{f_{\pi NN}^2}{m_\pi^2}g'U(k_\pi)} \tag{3.49}$$

where $U(k_\pi) = U_N(k_\pi) + U_\Delta(k_\pi)$ is the Lindhard function for the particle-hole and Δ-hole excitations. To compute this self-energy, the particle-hole excitation have been replaced by a series of RPA interactions.
It is also necessary to remove from the W-self energy the contribution that can be obtained from the quasi-elastic 1p1h interaction and have already been taken into account in the RPA nuclear correction. So it is necessary to subtract this contribution from equation 3.48.
In the interaction it is possible that a pion is emitted from the first particle-hole excitation and couples to the second excitation. This is modelized through an effective longitudinal interaction V_l

$$V_l(k) = \frac{f_{\pi NN}^2}{m_\pi^2}(F_\pi^2(k)\frac{k^2}{k^2-m_\pi^2} + (g_l')^2) \tag{3.50}$$

which beside the pion exchange term include a short range interaction term(SRC) driven by a Landau-Midgal parameters g_l'. Another interaction channel that has to be considered is the ρ meson exchange, leading to a transverse contribution for W-self energy.

3.4 Pion resonant production

For energies above 0.2 GeV, the production of a π during a neutrino-nucleus interaction becomes feasible by means of the weak excitation of the $\Delta(1232)$ resonance and it subsequent decays into a nucleon and a π. Those processes are called single pion resonant production (RES). A Feynman diagram of such interaction is shown in figure 3.3 and some of the contributions to the self-energy are shown in diagrams b, c and d of figure 3.6. For a W^+ boson exchange, there are 3 different channels:

$$\begin{aligned} \nu_l + p &\to l^- + p + \pi^+ \\ \nu_l + n &\to l^- + p + \pi^0 \\ \nu_l + n &\to l^- + n + \pi^+ \end{aligned} \tag{3.51}$$

with l being one of the lepton flavors.The calculation of all contributions to the RES hadron tensor is based on effective calculation of the Lagrangian. It is parametrized by a vector and an axial form factor. These can be extracted using data from μ and ν scattering [62]. It is worth mentions that the experimental data still have large uncertainties and even contradictory results for some channels.
At higher energies, there are other inelastic resonant processes that have to be considered, such as multi-pion, photon or kaon production. The prediction of these processes have not been extensively tested due to lack of experimental data. Moreover, around 1 GeV they are expected to be negligible.

3.5 DIS

At higher energy, neutrinos can interact directly with the quarks forming the nucleon. In this interaction the scattered quark produces an hadronic jet. The Feynman diagram associated to this interaction is sketched figure 3.4.
As the actual target of the neutrino has changed the double differential cross section is rewritten using another formalism in which:

$$\frac{d\sigma}{dxdy} = \frac{G_F^2 m_t}{\pi} E_\nu \big(xy^2 \frac{m_t}{q^0} W_1(q^0, q^2) + (1 - y - \frac{m_t xy}{2E_\nu}) W_2(q^0, q^2) \pm xy(1 - \frac{y}{2}) W_3(q^0, q^2) \big) \tag{3.52}$$

with x the Bjorken scaling variable and y the relative energy transfer (also called the Bjorken y), they are defined as :

$$x = \frac{-q^2}{2q.p_n} \tag{3.53}$$

$$y = \frac{q.p_n}{p_\nu.p_n} \tag{3.54}$$

with $q = (q^0, \overrightarrow{q})$ the tranferred 4-momentum, p_n the target 4-momentum and p_ν the neutrino 4-momentum. For inelastic systems the mass of the final state hadron is higher than the mass of the inital state. In this case, the Bjorken variables are lower than 1 (x=1 means an elastic scattering). For high values of transfer momentum and energy, the structure functions do not depend on the two variables independently but only on the dimensionless Bjorken scaling variable [63]. This is called the scaling invariance, leading to the following replacement:

$$m_t W_1(q^0, q^2) = F_1(x) \tag{3.55}$$

$$q^0 W_2(q^0, q^2) = F_2(x) \tag{3.56}$$

$$q^0 W_3(q^0, q^2) = F_3(x). \tag{3.57}$$

The parton model provides a physical interpretation to this scaling [64]. DIS can be seen as a superposition of elastic neutrino-parton scattering. Here, the parton is a point-like structure with a fraction x of the momentum and energy of the nucleon. In this model structure functions F_i are linked to distributions of partons:

$$F_1(x) = \sum q_i(x) + \sum \overline{q}_i(x) \tag{3.58}$$

$$F_2(x) = 2x \sum q_i(x) + 2x \sum \overline{q}_i(x) \tag{3.59}$$

$$F_3(x) = 2 \sum q_i(x) - 2 \sum \overline{q}_i(x) \tag{3.60}$$

The $q_i(x)$ are defined as the parton distribution functions (PDF) within the nucleon. They are the probability of finding a Dirac parton of type i with a momentum fraction x. The summation runs over all quark components that can be scattered inside the nucleon. Currently PDFs have been studied using QCD-based models [65].

3.6 SUperScaling Approach (SUSA model)

In the thesis, we have have studied the possibility to use the scaling properties described by this method to the comparison between data sets and our MC.
The scaling concept has been developed for lepton-nucleus interactions first by G. B.

West [66]. The ansatz is that the quasi elastic electron-nucleus scattering process inclusive cross section can be approximated by a single nucleon cross section times a specific function depending on transfer momentum and energy. In this case, the lepton interacts with a nucleus as if the transfer energy q^0 and the transfer momentum $\overrightarrow{q}$ are given to individual constituents of the complex system. The scaling occurs at some specific kinematics, where the specific function scales. This means that this function becomes directly dependent only on one single quantity, the scaling variable Ψ. The scaling has different concepts:

- Scaling of the zeroth kind. This concept is used when the longitudinal and transverse part of the cross section have the same scaling function.
- Scaling of the first kind. This concept is satisfied when the scaling function only depends explicitly on the scaling variable (the scaling variable is still dependent of the transfer energy and momentum).
- Scaling of the second kind. This is observed when the scaling function does not depend on the nuclear species.
- Superscaling. It is used when both scaling, the first and second kind, occur at the same time.

The scaling concept has been modified to be used for neutrino scattering interaction. This was done in the SUSA model [67], using a Relativistic Fermi Gas model (RFG). The SUSA model is then based on the hypothesis that the neutrino scattering cross section scale as does the electron scattering. This hypothesis is observed in the model based on impulse approximation, for example in [68].
The Superscaling Approach is based on a function extracted from QE electron scattering data. The superscaling function $f(\Psi')$ is defined as the ratio between the experimental cross section and the appropriate single nucleon one [69]

$$f(\Psi') = k_f \frac{\left(\frac{d^2\sigma}{d\Omega_e dq^0}\right)_{exp}}{\sigma_{Mott}(\nu_L G_L^{ee'} + \nu_T G_T^{ee'})} \tag{3.61}$$

where σ_{Mott} is the Mott cross section, the ν_L and ν_T terms are the leptonic factors associated to electromagnetic interactions and $G_L^{ee'}$ and $G_T^{ee'}$ are transverse and longitudinal form factors of the electron scattering. The scaling variable is defined in the following way

$$\Psi' = \frac{1}{\sqrt{\epsilon_F}} \frac{\lambda' - \tau'}{\sqrt{(1+\lambda')\tau' + \kappa\sqrt{\tau'(\tau'+1)}}} \tag{3.62}$$

Nucleus	k_F(MeV/c)	E_{shift}(MeV)
Helium	165	15
Carbon	228	20
Aluminium	236	18
Calcium	241	28
Iron	241	23
Tin	245	28
Lead	248	31

TABLE 3.1: Estimation of the k_F and E_{shift} parameters for different nuclear species with the RFG model

Introducing the dimensionless variables as

$$\epsilon_F = \sqrt{1+\eta_F^2} - 1 \tag{3.63}$$

$$\eta_F = \frac{k_F}{M_N} << 1 \tag{3.64}$$

$$\kappa = q/(2M_N) \tag{3.65}$$

$$\lambda' = q^{0\prime}/(2M_N) \tag{3.66}$$

$$\tau' = \kappa^2 - \lambda'^2 \tag{3.67}$$

with k_F the Fermi momentum in the RFG, $q^{0\prime} = q^0 - E_{shift}$, E_{shift} being the used to account for a phenomenological shift of the quasi-elastic peak. Those two parameters depend on the nuclear species considered during interaction as shown in the table 3.1. A comparison of the experimental SUSA model to a phenomenological parametrization of electron scattering is shown figure 3.8 and complete explanation on this model can be found in [70].

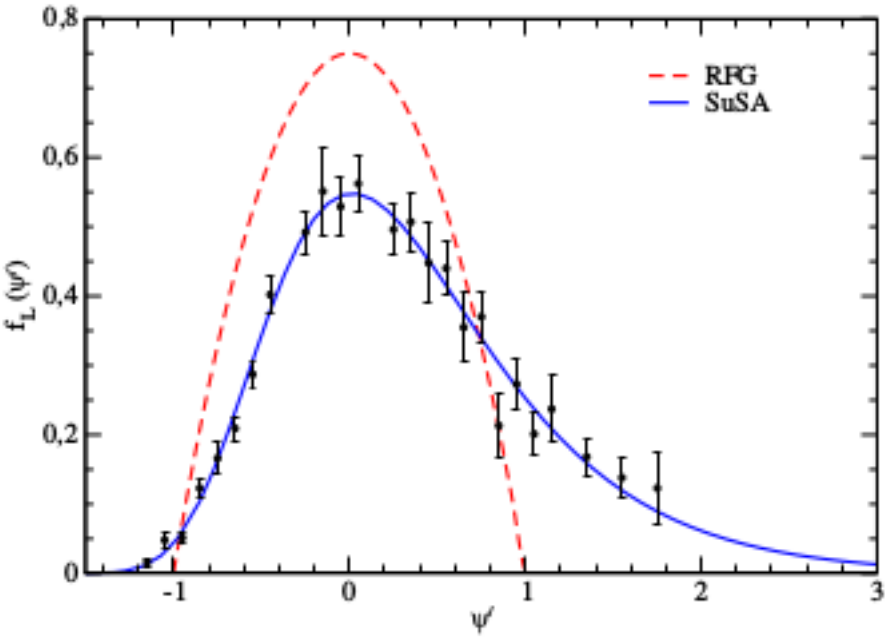

FIGURE 3.8: Average experimental $f_{SuSA}(\Psi')$ versus Ψ' in the quasi-elastic region together with a phenomenological paramterization of the selected (e,e') longitudinal scaling data ($f^{e,e'}_{L,exp}$) obtained from the R_L data on [71]. The integral curve has been normalize to unity. The RFG scaling function is shown as reference. The figure is from [70]

Chapter 4

Full kinematics event generation

In this section, we will discuss the details of the Monte Carlo (MC) generator developed during the thesis. We take the model of cross section calculations for 1p1h developed by Nieves et al. [72] and presented in the previous chapter. From this model, we want to extract the kinematics of each event to build a MC simulation with the complete kinematic information of the interaction. This MC has then been implemented in the main MC generator for T2K, NEUT [73]. If the form factors are known, this hadron tensor can be analytically calculated, leading to the cross section for 1p1h interaction in a nucleus.

4.1 Cross section calculation and interaction kinematic

The 1p1h interaction is a a four body interaction with two particles in the initial state, the neutrino and the target nucleon, and two particles in the final state, the lepton and the product nucleon. For the reaction we define neutrino propagation along the z-axis.In principle we have 10 degrees of freedom, the momentum of the neutrino and the momenta and both angles of the 3 other particles. However, they are related to 3 equations, the energy-momentum conservation rules, leaving us with 7 degrees of freedom. In our work the neutrino momentum is chosen during the input so it is not a degree of freedom. In the reaction the lepton is invariant with respect to the ϕ angle. Also we assume that the ϕ angle is also invariant for the proton, so there is no component transverse to the reaction plane. This reduce the degree of freedom of the interaction to 4.
The initial program was written as a double differential cross section calculation $\frac{d^2\sigma(E_\nu)}{dt_l d\cos(\theta_{\nu l})}$, with t_l being the kinetic energy of the lepton, l, and $\theta_{\nu l}$ the angle between the neutrino and the lepton. This way, the cross section is calculated for the complete lepton kinematics of the interaction. Thus, we need to obtain the hadron part of the kinematics,

as it is integrated in the hadron tensor part of the cross section computation.
The first step is to describe the nucleon initial state. The initial state information is defined by two parameters, the radial position of interaction, R, and the Fermi momentum, p_F, of the interacting nuclei.
In the hadron tensor, the radial position of interaction is integrated over the nucleus radius, determining a position of interaction for each event means undoing the integration. In the code integration over the radial position of interaction is a numerical approximation. To obtain the radial position, for each event we eliminate the integral and select, with a uniform distribution, a randomly chosen radius between $R_{min} = 0$ and R_{max}, corresponding to the edge of the nucleus according to the selected nuclear density model.
The integration over the target momentum is done through an analytical method, using the imaginary part of the relativistic isospin asymetric Lindhard function. Consequently, in the code, the target momentum is not directly computed as the integration of the target nucleon is replaced by an analytical function that does not need that. The first modification to be done was to recover the integral expression before the use of the Lindhard function. Then, the selection for the target momentum is done randomly with a uniform distribution between $p_F^{min} = 0$ and $p_F^{max} = (3\pi^2\rho_t)^{\frac{1}{3}}.p_F^{max}$ is the Fermi momentum for the LFG so by definition it has to depend on the radial position of interaction. It is done using the target nucleon density, ρ_t, that is defined either using a modified harmonic oscillator density or a two parameters Fermi distribution depending on the target nucleus. The parameters of few relevant nuclei are shown in table 4.1. In both cases, the density depends on the radial position inside the nucleus with, for Carbon and Oxygen, a modified harmonic oscillator density with $\rho(r) = \rho_0(1 + a(r/R)^2)\exp(-(r/R)^2)$ (a is dimensionless for this density form), while for the rest of the nuclei a two parameters Fermi distribution is used with $\rho(r) = \rho_0/(1 + \exp((r - R)/a))$. In those formula r the radial position inside the nucleus and R either R_p or R_n depending whether we want neutron of proton density.
With these two modifications, the code is now providing a four differential cross section for a neutrino energy depending on the lepton kinetic energy, neutrino lepton angle, radial position of interaction in the nucleus and target nucleon momentum.With this we can have access to the cross section versus radial position and Fermi momentum (figure 4.1 and 4.2).
To simplify the discussion we will be referring to the interaction of a 1 GeV muon neutrino on a carbon target. We will discuss the implementation of the neutrino flux, the use of other nuclei and the anti-neutrinos in the next chapters.

Figure 4.1 shows that neutrinos interact inside the carbon nucleus mostly between 1 and 3.6 fm with a peak around 2.1 fm away from the center and nearly no interaction happens

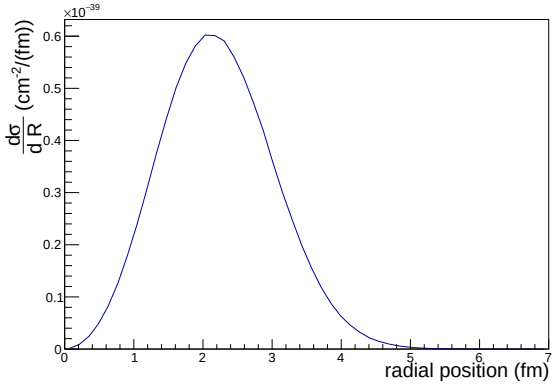

FIGURE 4.1: Cross section vs Radial position of interaction for a 1 GeV neutrino on a carbon atom

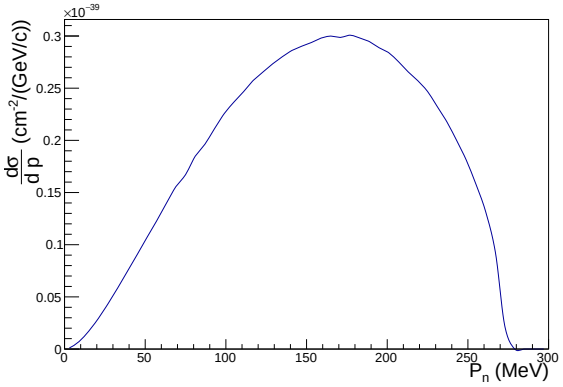

FIGURE 4.2: Cross section vs Fermi momentum for a 1 GeV neutrino on a carbon atom

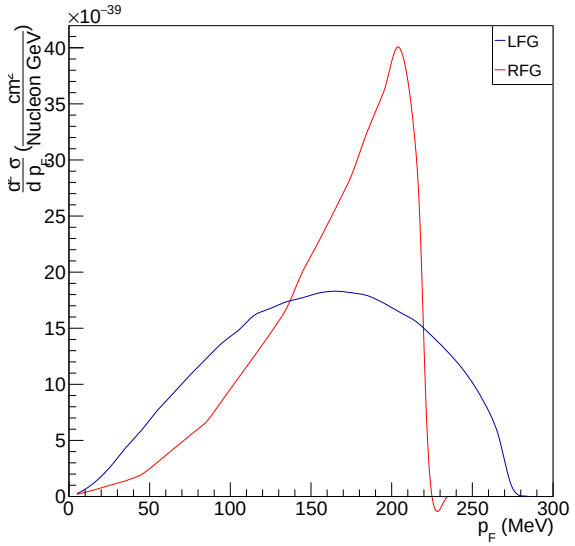

FIGURE 4.3: Comparison between Fermi momentum for LFG and RFG

in the center due to the phase space effect. As shown in figure 4.2, the target nucleon has a momentum between a few MeV and 270 MeV, and the highest probability of interaction happens for momenta between 120 to 250 MeV. The neutron momentum distribution (figure 4.2) is characteristic for the LFG model with most of the interactions happening at lower energy than the maximal Fermi momentum of the RFG, $p_F(RFG) = 225$ MeV. But there exists the possibility to have momentum higher than this value. The difference between LFG model and RFG model for the target momentum is shown figure 4.3.

The LFG modelization of an atom is based on the dependency between the radial position in the nucleus and the density of nucleon in the nucleus. Hence the relation between the maximum Fermi momentum and the radius is shown in figure 4.4. The maximum

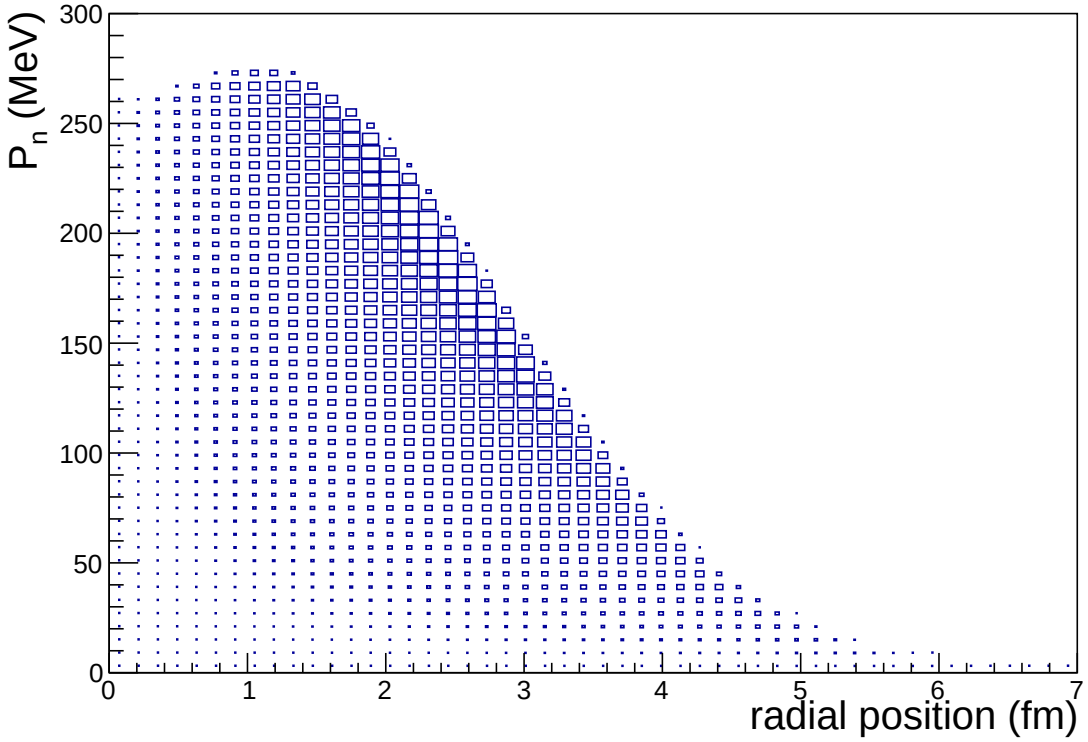

FIGURE 4.4: Cross section dependency between the initial state nucleon (in this case a neutron) momentum and interaction position for a 1 GeV neutrino on a carbon atom

Fermi momentum can be calculated through the formula:

$$p_F^{max}(R) = (3\pi^2\rho(R))^{\frac{1}{3}} \tag{4.1}$$

The dependency $p_F^{max}(R)$ is not linear and the maximum value is not at the center of the nucleus but at a radius around 1 fm for Carbon. Figure 4.4 shows that the cross section is higher when closer to the maximum target momentum at a given radius ($p_F^{max}(R)$). With the following information extracted from each event, E_ν, t_l, $\theta_{\nu l}$, R, p_F , we can reconstruct the complete kinematics of a four-body interaction using the following equations:

$$P_\nu - P_l = P_q \tag{4.2}$$

$$P_t + P_q = P_f \tag{4.3}$$

With $P_\nu = (E_\nu, \overrightarrow{p_\nu})$, $P_l = (E_l, \overrightarrow{p_l})$, $P_q = (q0, \overrightarrow{q})$, $P_t = (E_t, \overrightarrow{p_F})$, $P_f = (E_f, \overrightarrow{p_f})$ the

four-vectors of neutrino, lepton, virtual W boson, target nucleon and final nucleon respectively. We calculate the first equation that corresponds to the lepton current:

$$q^0 = E_\nu - E_l \tag{4.4}$$

$$\begin{aligned} |\overrightarrow{q}| &= |\overrightarrow{p_\nu} - \overrightarrow{p_l}| \\ &= \sqrt{E_\nu^2 + p_l^2 - 2E_\nu\, p_l\, cos(\theta_{\nu l})} \end{aligned} \tag{4.5}$$

with the known parameters, $E_l = m_l + t_l$ and $p_l = \sqrt{E_l^2 - m_l^2}$. The binding energy and Coulomb potential effect on the kinematics are taken into account by modifying the transfer momentum four-vector accordingly. We name this local transfer momentum $q^{loc} = (q^{loc^0}, \overrightarrow{q^{loc}})$

$$q^{loc^0} = q^0 - E_{bind} \tag{4.6}$$

$$\begin{aligned} |\overrightarrow{q^{loc}}| &= |\overrightarrow{p_\nu} - \overrightarrow{p_l^{loc}}| \\ &= \sqrt{E_\nu^2 + (p_l^{loc})^2 - 2E_\nu p_l^{loc} cos(\theta_{\nu l})} \end{aligned} \tag{4.7}$$

where $p_l^{loc} = \sqrt{(E_l - E_{bind} - V_c(R))^2 - m_l^2}$ with E_{bind} being the binding energy of the nucleus and $V_c(R)$ the Coulomb potential at the interaction point computed with the definition from the previous chapter. It is important to note that those corrections imply that the overall energy-momentum is no longer conserved as the calculation of the kinematics of the hadron part is rewritten as

$$P_t + P_q^{loc} = P_f \tag{4.8}$$

From this equation and the known parameters we can calculate the final state particle kinematics:

$$E_f = E_t + q^{0loc} \tag{4.9}$$

$$\begin{aligned} |\overrightarrow{p_f}| &= |\overrightarrow{p_F} + \overrightarrow{q}^l oc| \\ &= \sqrt{p_F^2 + (q^{loc})^2 + 2p_F q^{loc} cos(\theta_{tw})} \end{aligned} \tag{4.10}$$

We just have to solve the system of equations created by the energy-momentum conservation rules to be able to resolve all kinematic information for the hadron part:

$$\begin{aligned} (P_t + P_q^{loc})^2 &= (P_f)^2 \\ m_f^2 &= m_t^2 + (q^{0loc})^2 + 2(E_t q^{0loc} - 2p_t q^{loc} cos(\theta_{tw})) \\ cos(\theta_{tw}) &= \frac{1}{2} \frac{(E_t + q^{0loc})^2 - (m_f^2 + p_t^2 + (q^{loc})^2)}{p_t q^{loc}} \end{aligned} \tag{4.11}$$

The resulting final state of the hadron will be indirectly affected by the position of interaction (shown in figure 4.5). This figure shows the interaction cross section for proton momentum versus radial position of interaction, with protons having momenta mainly between 300 MeV and 1.2 GeV. The resulting nucleon momentum, in this case the proton momentum, show a very slight dependency to the radial position of interaction. This was expected as no radial dependence in our model affects the kinematics for more than a few MeV, be it the binding energy or the coulomb potential or even the Fermi momentum. For protons with momenta lower than approximately 400 MeV, we can see a shift of the maximal radial position of interaction from the 2 fm position toward the edge of the nucleus. The protons with the lowest momenta are concentrated at the edge of the nucleus. These low momentum protons, below 200 MeV, do not exist in the RFG model due to Pauli Blocking, but the Fermi momentum depends on the radial position inside the nucleus. The Fermi level is almost vanishing at the surface of the nucleus allowing for very low energy protons peripheral interactions. This is a prediction exclusive to the LFG model and the Spectral Function approaches. The confirmation of this point in an experiment would be complicated as those protons have very low momentum and therefore cannot pass the threshold of detection for the current experiment, such as the ND280 near detector of T2K. They may not even leave the nucleus in some cases. One possible method developed by the experiments is to look at the energy deposited near the vertex as the so-called "available energy" measurement carried out by MINERvA [74].

Figures 4.6 and 4.7 show the effect of the RPA on the kinematics of the interaction. RPA correction lowers the cross section and creates also a shift in momentum direction of the proton and muon, with more energetic and more forward going protons and muons [1]. This is explained by the fact that RPA effects could account for a low $Q^2 = -q^2 = -\left((q^0)^2 - \overrightarrow{q}^2\right)^2$ deficit of CCQE events observed by several experiments. Higher energetic protons, receiving higher transferred energy, are nearly not affected by RPA corrections.

4.2 Monte Carlo implementation

The Monte Carlo (MC) simulation is used to model the probability of an interaction for a chosen kinematics. The first step in the MC is to select the nucleus and the neutrino type. This selection fixes many parameters of the interaction such as the radial size of the nucleus, the binding energy, the type and the mass of the outgoing lepton and the final hadron.

[1] i.e. high transferred momentum

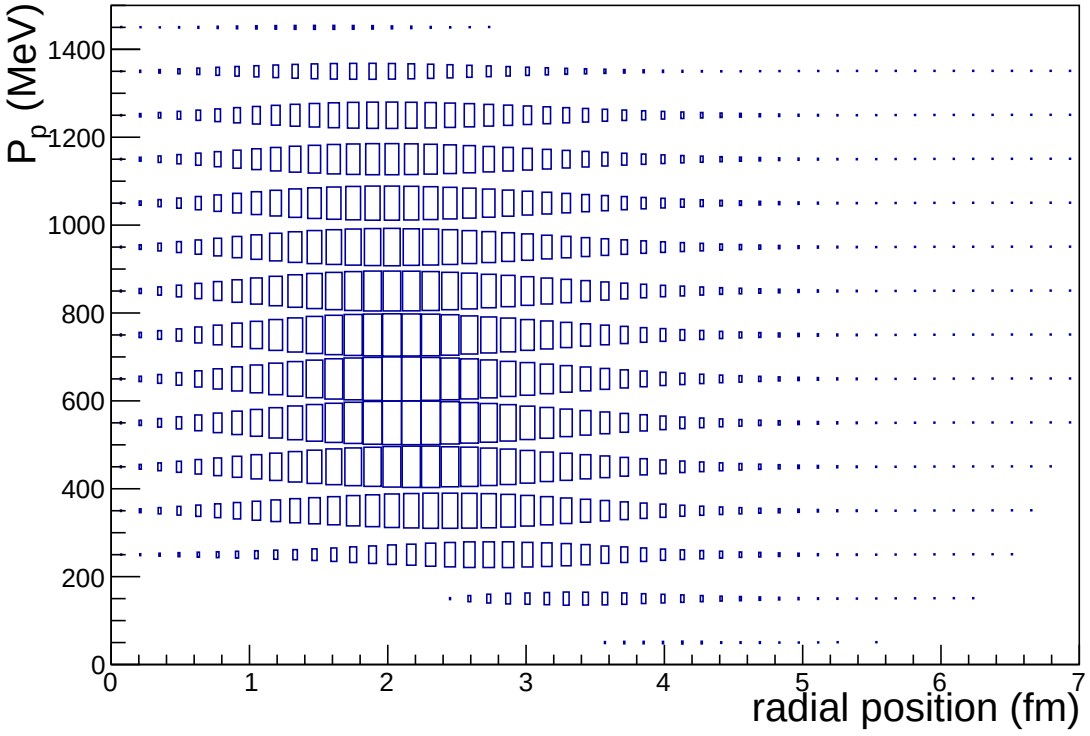

FIGURE 4.5: Final state nucleon (here a proton) momentum versus radial position of interaction

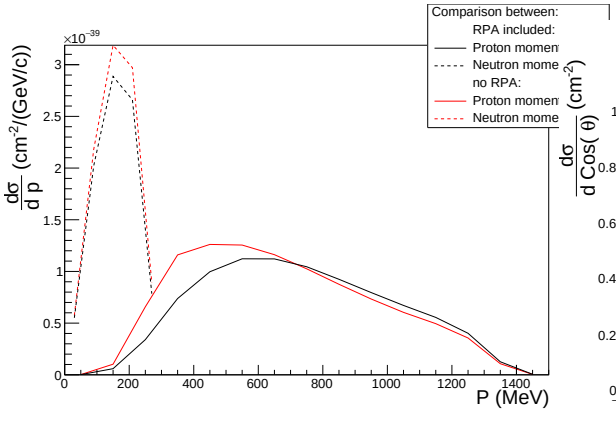

FIGURE 4.6: Comparison between nucleon momentum for a 1 GeV neutrino on carbon using RPA and not using RPA, where neutron is the initial state nucleon and proton is the final state nucleon

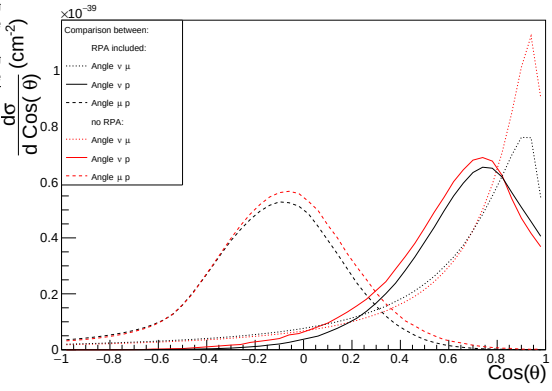

FIGURE 4.7: Comparison for angle between different particles of the interaction for a 1 GeV neutrino on carbon using RPA (blue line) and not using RPA (red line)

Nucleus	R_p (MeV)	R_n (MeV)	a_p (fm)	a_n (fm)	Q (MeV)	$\overline{Q}$ (MeV)
^{6}C	1.692	1.692	1.082	1.082	17.428	17.250
^{8}O	1.833	1.833	1.544	1.544	14.371	13.421
^{13}Al	3.05	3.05	0.535	0.535	11.767	9.568
^{14}Si	2.93	2.93	0.569	0.569	15.890	12.878
^{18}Ar	3.47	3.64	0.569	0.569	8.576	13.82
^{26}Fe	3.971	4.05	0.5935	0.5935	9.935	11.478
^{82}Pb	6.624	6.89	0.54	0.54	6.075	9.296

TABLE 4.1: Charge (R_p,a_p), neutron matter(R_n,a_n) density parameters, Q,$\overline{Q}$ binding energies for different nuclei for neutrino and anti-neutrino respectively.

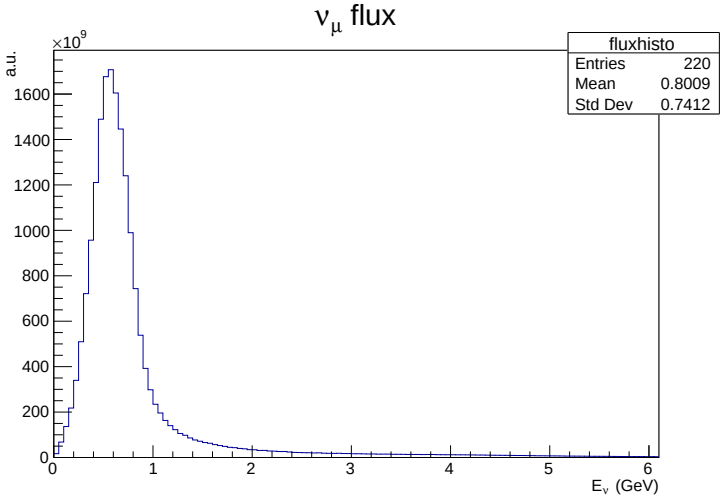

FIGURE 4.8: Neutrino flux at nd280

For each event we apply the following kinematic selection: the neutrino energy is chosen either by selecting one particular energy or using a random value weighted by an experimental neutrino flux, for example the one from T2K shown in figure 4.8, weighted by the the interaction cross section.

We improved the MC efficiency, before obtaining kinematics for every events, by first calculating the cross section in function of the energy, $\sigma(E)$, and save it in a look-up table. These table are computed automatically by the MC code if they are not available and store them in file. The cross section is computed for all three lepton flavors, including neutrinos and anti-neutrinos and for all available nuclei. The look up table is smoothen by a simple interpolation function to evaluate the cross section at each energy. Thus, when we want to select the neutrino energy according to an experiment flux and interaction cross section, we only have to multiply the flux by the pre-computed cross section to have the weight of each energy value.

For the lepton kinematic parameters, the angle $\theta_{\nu l}$ is chosen between 0 and π and the kinetic energy between 0 and $E_\nu - m_l - q_{val}$ with m_l being the lepton mass and q_{val} being the binding energy of the nucleus. The radial position or interaction R is selected

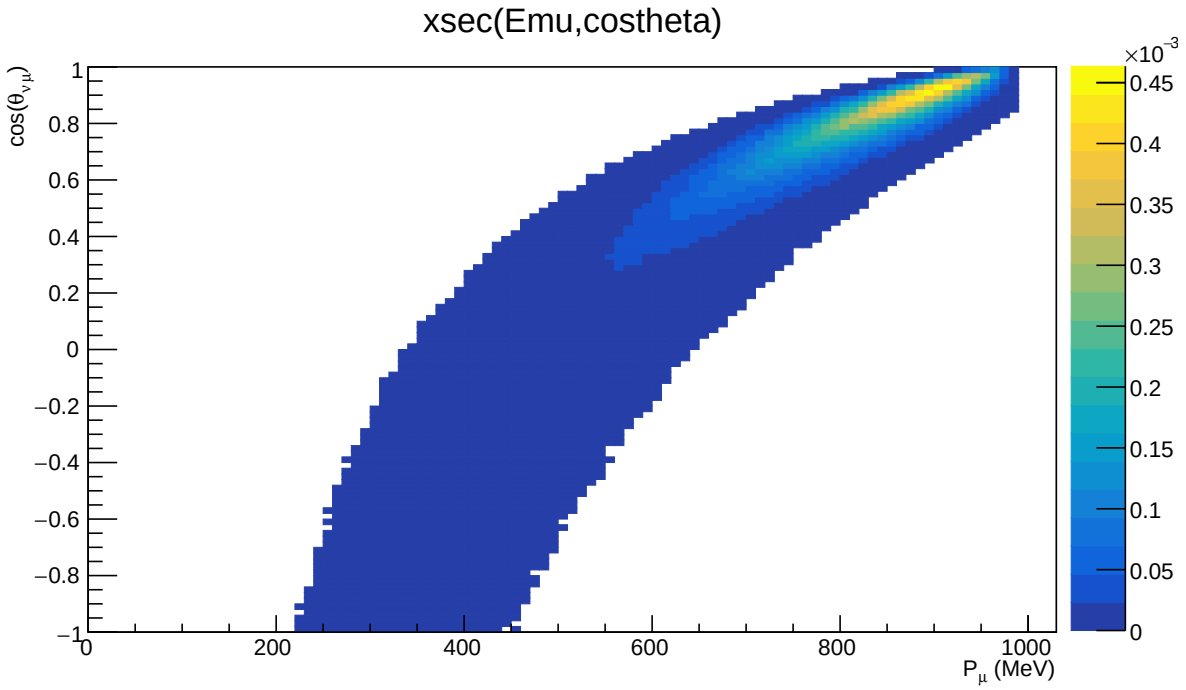

FIGURE 4.9: Neutrino-muon angle versus muon momentum distribution for a 1 GeV muon neutrino

between 0 and the maximum size of the nucleus, and then the Fermi momentum is also selected randomly between 0 and the maximum Fermi momentum at a given R value. Figure 4.9 shows the relation between the lepton momentum and the neutrino-lepton angle. One can see that there is a limitation on the possible values of $\theta_{\nu\mu}$ given a value of p_μ. To speed up the generation, we select event between θ_{min} and θ_{max} and correct for the phase space. Thus we use the following replacing our previous event generation. First, the angle $\theta_{\nu l}$ is selected between 0 and π the same way as before. Second, we chose the radial position of interaction still using the previous selection method. Then, assuming the maximum Fermi momentum[2], and either the angle between target and product nucleon to be 0, for maximum, or π, for minimum, it is possible to extract the extreme values from the system of equations 4.12. The numerical Newton method is used to find the solution of the system of equations:

$$\begin{aligned} \overrightarrow{p_\nu} + \overrightarrow{p_F} &= \overrightarrow{p_l} + \overrightarrow{p_f} \\ \overrightarrow{p_\nu} - \overrightarrow{p_l} &= \overrightarrow{p_f} - \overrightarrow{p_F} \\ E_\nu^2 + p_l^2 - 2E_\nu p_l \cos(\theta_{\nu l}) &= (p_f \pm p_F)^2 \end{aligned} \tag{4.12}$$

Beginning the convergence of the method with $p_l^{min} = 0$ and $p_l^{max} = ((E_\nu - q_{val} + E_t^F - E_f^F)^2 - m_l^2)^{\frac{1}{2}}$,with E_t^F and E_f^F the energy of the target and the product nucleon at Fermi momentum. Once the new lepton momentum maximum and minimum have been

[2]still dependent of the radial position of interaction

computed, the lepton momentum is chosen randomly between them.
In order to further improve the performance it is then possible to calculate a minimum momentum of the target by solving the following quadratic equation to obtain the following equation:

$$(q0^2-q^2)p_F^2+q(q0^2-q^2+\Delta_M)p_F+(q0^2-q^2+\Delta_M).(q0^2-q^2+\Delta_M)-4.m_t^2.q0^2=0 \quad (4.13)$$

with $\Delta_M = m_t^2 - m_f^2$. So the selection of the target momentum is between this lower value of this equation and the maximum Fermi momentum.
Those two improvements of the selection ensure a valid kinematics and to have the correct cross section value, while ensuring a faster MC simulation.

As stated earlier, before calculating cross sections and kinematics for all events, we have to initialize the program. To be able to work with other nuclei efficiently, we decided to store each nucleus information necessary for the LFG computation in memory during initialization. Those information are retrieved when we need any nucleus specific. The memory contains information about the nucleus, the number of protons and neutrons, the binding energy q_{val} for neutrino and anti-neutrino interactions, the RPA parameters and the maximum radius of the nucleus. The memory contains the method to calculate the density and the maximum Fermi momentum at R. Most importantly, we pre-compute the radial distribution of the interaction and the corresponding Coulomb potential $V_c(R)$. We do not need to calculate it again only to interpolate numerically. This is done to speed up the generation since we only initialize once, but we need to use the information over a vast number of events. In our program, we have stored data for Carbon, Oxygen, Aluminium, Silicon, Argon, Iron and Lead. The information stored are shown in table 4.1. It is to be noted that Hydrogen is computed using a free nucleon cross section process. Therefore we calculate it separately. This way of treating the nuclei information allows us to be able to add others in the future, if necessary.

Chapter 5

NEUT

NEUT, together with GENIE, is one the neutrino Monte Carlo event generators used by SK and T2K to simulate neutrino interactions inside the different detectors [73]. It was originally developed in order to study the atmospheric neutrinos that are the background of the nucleon decay in the Kamiokande detector. It was then extended and used in other experiments such as SK, K2K, SciBooNE and T2K.
NEUT produces a list of neutrino interactions and their product particles according to a neutrino flux and energy spectrum. Each interaction NEUT generates is composed of a primary neutrino-nucleon interaction. The particles produced in the interaction undergo a number of secondary interactions as they propagate out of the nucleus. For the primary interactions all possible interactions in the energy range between 100 MeV and 1 TeV are considered.This means the main interaction models considered are :

- charged and neutral current (quasi-)elastic scattering (1p1h)
- charged and neutral current 2 particles - 2 holes interaction (2p2h)
- charged and neutral current single π, K and η resonance production
- charged and neutral current deep inelastic scattering.
- charged and neutral current coherent pion production.

The secondary interactions are modelized using a particle cascade routine.
For each neutrino event simulated, the neutrino event generator NEUT does the following procedure: It fixes the neutrino energy and then the primary interaction is determined depending on each interaction cross section. Afterwards simulates the corresponding interaction and applies the secondary interaction. This implies to know the cross section of each channel. The output is composed of the full kinematics of the ingoing and

outgoing leptons, nucleons and hadrons implicated in the interaction. Each of the events are weighted by the cross section convoluted by the flux in order to be used directly in detector simulation.

5.1 Neutrino-Nucleus interaction models

Since the beginning of NEUT, models used for the interactions have changed with the theory improvement and experimental results. Thus new interaction models have been implemented in the event generator without losing the possibility to use the previous model. In this section, we shortly present the different models implemented in NEUT.

5.1.1 (Quasi-)Elastic scattering

The 1p1h scattering is the dominant interaction channel around 1 GeV and is the main interaction at T2K. This interaction channel is also useful since knowing the lepton kinematics allows the reconstruction of the incident neutrino energy. We implemented the 1p1h Local Fermi Gas (LFG) model of Nieves et al [72] presented in chapter 3 in the newest NEUT version (v5.4.0). For this interaction, including the model we implemented, there are 3 different models available in the current NEUT version: the Smith-Moniz Relativistic Fermi Gas (RFG) model [75], the spectral function model by Benhar et al [76] and the LFG model by Nieves et al [72]. The first 1p1h has been used from the beginning, whereas the spectral function model is available since version 5.3.2 and as stated we have now implemented the Nieves model. As mentioned in the chapter 3, section 1.2, the main difference between the models is the modelization of the nucleus.

5.1.2 2 particles - 2 holes scattering

The 2p2h interaction, with an important contribution between the 1p1h and the resonance region, is implemented in NEUT using the model proposed by Nieves et al [61]. Others models exist but only this one is implemented in NEUT. The 2p2h model use a LFG approach for the nucleus modelization. This interaction can sometimes be misidentified as a 1p1h interaction.

5.1.3 Resonance production

For the pion resonance production, two models have been implemented: the Rein and Sehgals model [77] and the Graczyk and Sobczyks model [78]. The Graczyk and Sobczyks

model is an improved version of the Rein and Seghal model which correct for the zero mass lepton assumption used. The Rein and Sehgals model was implemented since the first version, whereas the Graczyk and Sobcyks one has been implemented for the version 5.3.2 of NEUT. To obtain the cross section for each meson production channel, the amplitude of the excitation of a baryon resonance is multiplied by the decay probability of the excited baryon into a meson and a baryon.

5.1.4 Deep inelastic scattering

In the NEUT event generator, for the DIS interaction, the parton distribution function necessary to calculate the cross section, as presented chapter 3, section 5, are taken from [79]. Furthermore corrections proposed by Bodek and Yang [80] are applied for the low q^2 disagreement with the experiment. The cross section is further tuned with experimental results from [81].

5.1.5 Coherent pion production

The coherent pion production interaction is an interaction that is known to exist at high energy, above several GeV and modeled by Rein and Seghal [82]. At lower energies, this channel was predicted as a continuity of the interaction model but it was only first detected in 2016 in the T2K near detector ([83]). In NEUT, in addition to the Rein and Seghal model [84], the Berger and Seghal model [85] have been implemented.

5.2 NEUT input card

NEUT input consists of a card containing information about the incoming particle, the target and the interactions which should be considered. The card is a text file that will be read by NEUT to initialize a run of events.
For the incoming particle, one needs to select whether it is a neutrino or an anti-neutrino and its flavor. It is also possible to define their directions and their energies. The direction is either fixed or randomized. The neutrino energy can be fixed, flatly randomized or selected using an external flux file.
The target information that are contained in the card are the type of nuclei or atoms used and how the interaction vertex should be determined. The target nucleus type is defined with the numbers of protons, neutrons and free protons, for example the H2O is defined as 8 protons, 8 neutrons and 2 free protons. The interaction vertex of each is chosen between a fixed position or at a random position alongside a distance defined

between 0, the center of a nucleus, and a chosen maximum, taken as the limit of the nucleus.
One can select whether one want to have all neutrino mode of interactions possible or only a few to a minimum of 1. Then it is possible to choose which of the interaction model one want to use as all model that have been previously implemented in NEUT are not removed with new model addition. In addition some of the parameters of each model can be selected in the card, such as axial mass value, particle mean free path or even the form factor parametrization. These options have been added to follow the theory development and to be able to tune model with experimental results.

5.3 NEUT output, flux and cross section

The NEUT output is a root file containing the kinematics of each event. This section presents how we retrieve the double differential cross section for one root file created with a neutrino flux Φ. By using the cross section definition given in the previous chapter,

$$\sigma = \frac{N_{int}}{\Phi N_t} \tag{5.1}$$

with N_{int} the number of interaction and N_t the target density.
We want to have MC results reflecting the dependency on muon momentum and angle between neutrino and muon for a given neutrino energy. The NEUT output provides the neutrino flux depending on the neutrino energy and the event rates as function of energy. The double differential cross section is computed the following way:

$$\frac{d^2\sigma}{dp_l dcos(\theta_{\nu l})} = \frac{N}{\Phi_{int} \cdot N_{ev}/Evrate_{int} \cdot \Delta_{p_l} \cdot \Delta_{cos(\theta_{\nu l})}} \tag{5.2}$$

with $\Phi_{int} = \int \Phi(E)dE$ and $Evrate_{int} = \int Evrate(E)dE$ the integral over the neutrino energy of the flux and the events rate. N_{ev} is the total number of events simulated during the run. Δ_{p_l} and $\Delta_{cos(\theta_{\nu l})}$ are the bin width chosen for the histogram.

Chapter 6

Comparison of the model to experimental data

In this chapter, We will compare the model implemented in NEUT to experimental results from T2K, MiniBooNE and MINERvA. After discussing the fluxes of the various experiments and the different data sets used during the thesis, we will show the comparison between the LFG model and the different data sets. Moreover, we will show a comparison between the previous NEUT 1p1h model, the RFG model, and the one we implemented, the LFG model. Also we will show the study we performed with the SUSA model and how it points toward the model limits.

6.1 Experimental Neutrino Fluxes

In this section, we present the different experiment fluxes. Those fluxes are shown as they are when used as input for NEUT.

6.1.1 T2K

For the study using T2K data, we use the predicted neutrino flux at the near detector ND280. This flux is shown in figure 6.1, with a peak energy around 750 MeV and an average energy around 800 MeV. A detailed description of the T2K neutrino flux modelling can be found in [86]. Most of the neutrinos have energies between a few MeV and 1.2 GeV with a peaked distribution. The narrow peak in the distribution is due to the fact that the ND280 near detector and the SK far detector are off-axis in respect to the beam direction. Around this energy, neutrinos interacts primarly through the 1p1h

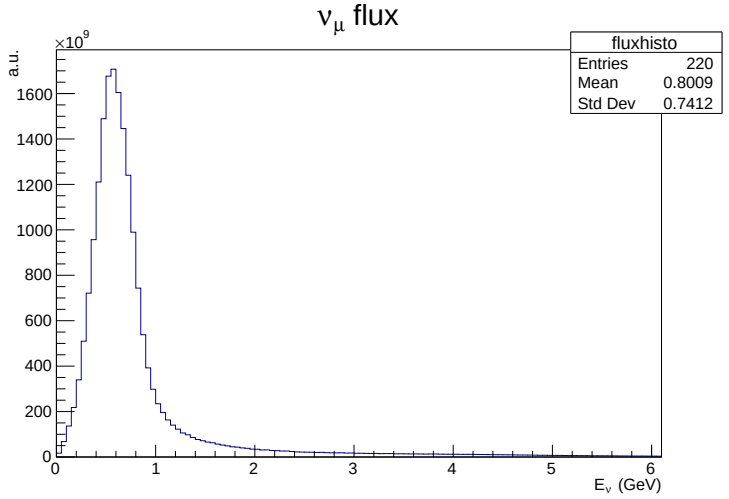

FIGURE 6.1: Neutrino flux at ND280

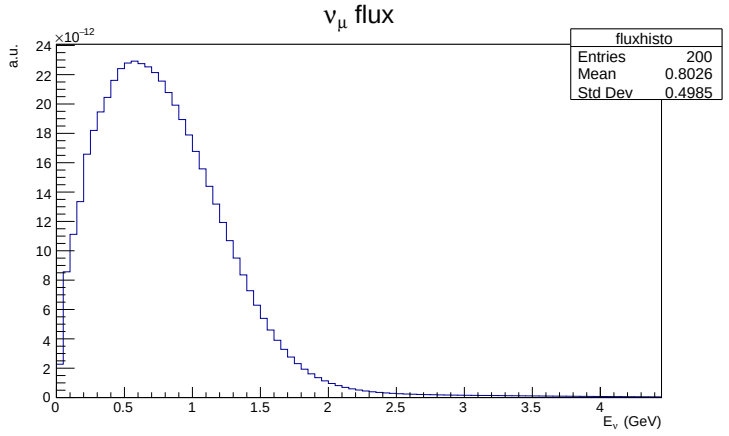

FIGURE 6.2: Neutrino flux at MiniBooNE

channel. While the other important interaction channels are the 2p2h and the RES channels.

6.1.2 MiniBooNE

For the study with MiniBooNE data, the flux used is shown in figure 6.2. More details on the MiniBooNE neutrino flux can be found in [87] The ν_μ flux has a peak energy of around 550 MeV and an average energy (over $0 < E_\nu < 3GeV$) around 800 MeV. Compared to the T2K flux, this one shows a widespread distribution of neutrino energies between a few MeV to 2.5 GeV as the detector is on-axis. In this energy range, interactions happening in the detector will be mostly 1p1h, 2p2h and RES, with a smaller contribution from DIS.

6.1.3 MINERvA

The flux of the MINERvA experiment is shown in figures 6.3 for neutrinos and in 6.4 for anti-neutrinos. A more detailed explanation on the MINERvA flux can be found in [88]. The purpose of the MINERvA experiment is to study the background relevant to oscillation studies. The neutrino flux has been chosen to be of higher energy than the usual oscillation experiment due to two factors , one the already existing beam of Minos with a longer baseline and energy, second the first idea of the MINERvA experiment was to study DIS. With the peak energy of the flux around 3.5 GeV and an average energy around 3.3 GeV for the neutrinos flux and 3.1 GeV for the anti-neutrinos flux the interactions happening in the detector are primarly resonant production, while 1p1h, 2p2h and DIS are secondary interaction around this energy.

6.2 Data sets used

In this section, we present the studies from which we obtain the data and their selection method.

6.2.1 T2K CCinclusive

This study compares data from Ref [89]. The selection only requires a muon in the final state to accept the event. What is new with this study is the inclusion of events with high angle and also backward with a new timing-based method. Accordingly for the NEUT data only the existence of a muon is requested. So we apply to the events of the NEUT output file the following condition: "has a muon alive". This means we only have to have a muon outside of the nucleus, effectively removing every neutral current events. We then identify the event interaction for the MC between the different models 1p1h, 2p2h, RES, DIS, coherent scattering and diffraction to see the contribution of each interaction.

6.2.2 T2K CC0pion

This study is using data from Ref [90]. In this study, the CC0pion events correspond to events where a muon and no pions are detected in ND280. This means that the selections we apply to the NEUT file resulting from the MC simulation are:

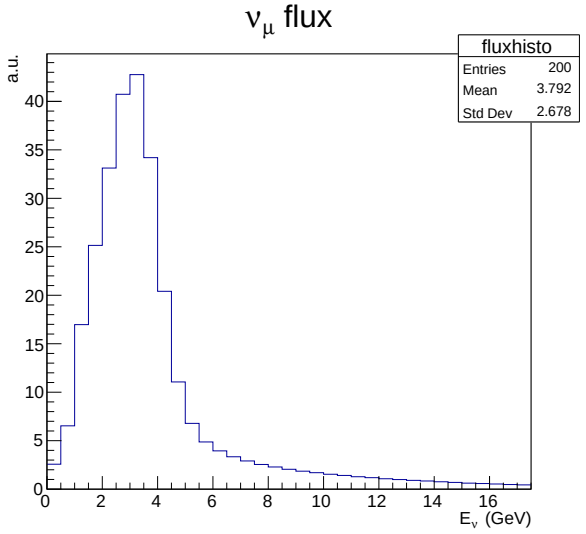

FIGURE 6.3: Neutrino flux at Minerva

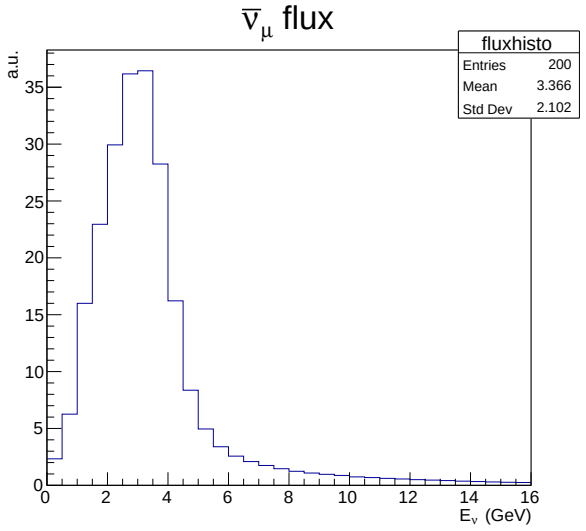

FIGURE 6.4: Anti-neutrino flux at Minerva

- we have a muon "alive", meaning that a muon is escaping from the nucleus after the interaction. This ensure that the interaction in the nucleus was a charged current interaction and not a neutral current one.

- no pion "alive", meaning that no pion, charged or neutral, are escaping from the nucleus.

In these conditions, the important part is that the selection is done outside the nucleus without considering what happens inside. By doing so we reproduce the experimental conditions and create the expected background. In terms of events selected in the simulation, we will have three different interaction cases:

- 1p1h events, signal and majority of the selected events.
- 2p2h events, cannot be distinguished from 1p1h events using π information.
- Other interactions with a pion produced during the interaction but this pion is absorbed inside the nucleus and thus does not leave it so it is the main background source.

Since we are using MC data we can tag those events with their "true" interaction and separate them.

6.2.3 MiniBooNE

This study uses data published by the MiniBooNE collaboration in the following article [91]. It measures the CCQE neutrino interactions on carbon, with the main background being resonant production events with an intranuclear absorption. Thus, to reproduce this CCQE-like study, we use the following selection for the MC:

- the event has a muon "alive", so it can be detected outside the nucleus.
- the final state must not contain a charged pion, cutting resonant interactions except for the predicted background.
- in the MiniBooNE experiment, another source of background is the non detection of the π^0 produced during the resonant production process $\nu_\mu + n \rightarrow \mu^- + \pi^0 + p$. So we have to consider the events with a π^0 in the final state as a background, adding those events to the selected one.

6.2.4 MINERvA

6.2.4.1 Anti-neutrino data

This study uses data published by the MINERvA collaboration in Ref [92]. This article studies the muon anti-neutrino charged current quasi elastic interaction on hydrocarbon, meaning that in my simulation we have to select anti-neutrinos but also that the target is not a carbon, C, but a hydrocarbon, CH. We will have two different CCQE interactions, anti-neutrinos on C and anti-neutrinos on a free nucleon, the H. The selection of events in the study is based on the requirement to have a CCQE-like final state with an angle of less than 20 degrees along the beam direction. This acceptance angle is used to match the region where both MINERvA and MINOS can reconstruct the momentum with good accuracy. So the conditions applied to each event are

- to have a μ^+ exiting the nucleus.
- to not have any meson outside of the nucleus.
- the angle of the μ^+ with respect to the beam direction must be lower than 20 degrees.

With the condition given by the angle of the μ^+ and the neutrino energy flux, the MINERvA analysis imposes also the following limits of $1.5\ GeV < p_L < 15\ GeV$ and $p_T < 1.5\ GeV$ for the μ^+ longitudinal (p_L) and transverse (p_T) momentum respectively.

6.2.4.2 Neutrino data

This study uses data from the article [93] published by the MINERvA collaboration. In this article, the process studied is QE-like, with a muon and a proton in the final state. Following the signal definition used in the study, the simulated events are selected with the following conditions:

- a muon exiting the nucleus with a kinematic properties of $1.5\ GeV/c < p_\mu < 10\ GeV/c$, $\theta_\mu < 20°$,
- no meson outside the nucleus,
- a proton exiting the nucleus with a kinematic properties of $0.45\ GeV/c < p_p < 1.2\ GeV/c$, $\theta_p < 70°$,

where p_μ and θ_μ (p_p and θ_p) are the muon (proton) momentum and polar angle angle with respect to the neutrino beam direction, respectively, when exiting the nucleus.

6.3 Data and MC prediction

We show in this section the different study realized with the MC output and the different data sets.

6.3.1 T2K CCinclusive

The results are presented using a double differential cross section with respect to muon momentum and neutrino muon angle. The angular binning is finner than in the other data sets as one of the principal aim of this study was to have a better accuracy for high

	selected						not selected
interaction	1p1h	2p2h	RES	DIS	coherent	diffraction	neutral current
events (%)	34.6	5.9	27.8	5.3	0.3	0.001	26.1

TABLE 6.1: Composition of the different interactions for a NEUT file output using the T2K flux and the CC inclusive selection method

angle and backward angle muons, corresponding to $cos(\theta_{\nu\mu}) < 0.6$. The distribution of interaction, according to our selection method, in our sample is shown in table 6.1. We can see that the main interaction is, as expected, 1p1h (34.6%) with an important contribution from RES interaction (27.8%). In addition there are less relevant contributions from both 2p2h and DIS interactions.

The comparison between data and model is shown figure 6.5. NEUT predictions reproduce properly the data except for a few differences. For a few angle, for $cos(\theta)$ between 0.25 and 0.8, we can see that the NEUT prediction seems to be slightly shifted compared to the data, particularly for the $0.25 < cos(\theta) < 0.45$ and $0.6 < cos(\theta) < 0.71$ bin angle. We also see that the peak differential cross section predicted by NEUT is a bit too low compared to the actual peak differential cross section. The last small difference is for forward angle, $cos(\theta) > 0.92$, around 1500-2000 MeV of muon momentum the predicted cross section is lower than the cross section. The first two differences are in the region where the 1p1h interaction is the main interaction contributing to cross section but not the last one. So, potentially, improving the 1p1h model could improve the cross section prediction. But other interaction models should also be improved as they are likely to be involved in the differences.

We will now present the difference between the previous 1p1h model implemented in NEUT and the one we have implemented. Effectively it is a comparison between the classic Smith-Moniz RFG model and the Nieves LFG model. As stated in the previous chapters 3 and 5, the main difference between those models is the nuclear tensor treatment. Others than the model themself, there is a difference in the initialization phase of NEUT, the axial mass value determination. For the RFG model, the axial mass used is 1.21 GeV as default value whereas, for the LFG model, the default value used is 1.05 GeV. The difference in axial mass between models is a well-known problem, with the axial mass for free nucleon being 1.014 ± 0.014 GeV. This axial mass was calculed using scattering data from electrons and neutrinos on hydrogen and deuterium. The disagreement between low energy ν_μ cross section predictions and data has lead to a change in the axial form factor due to additional nuclear effects. Thus the difference between the axial mass value can be explained by the choice of this value to absorb

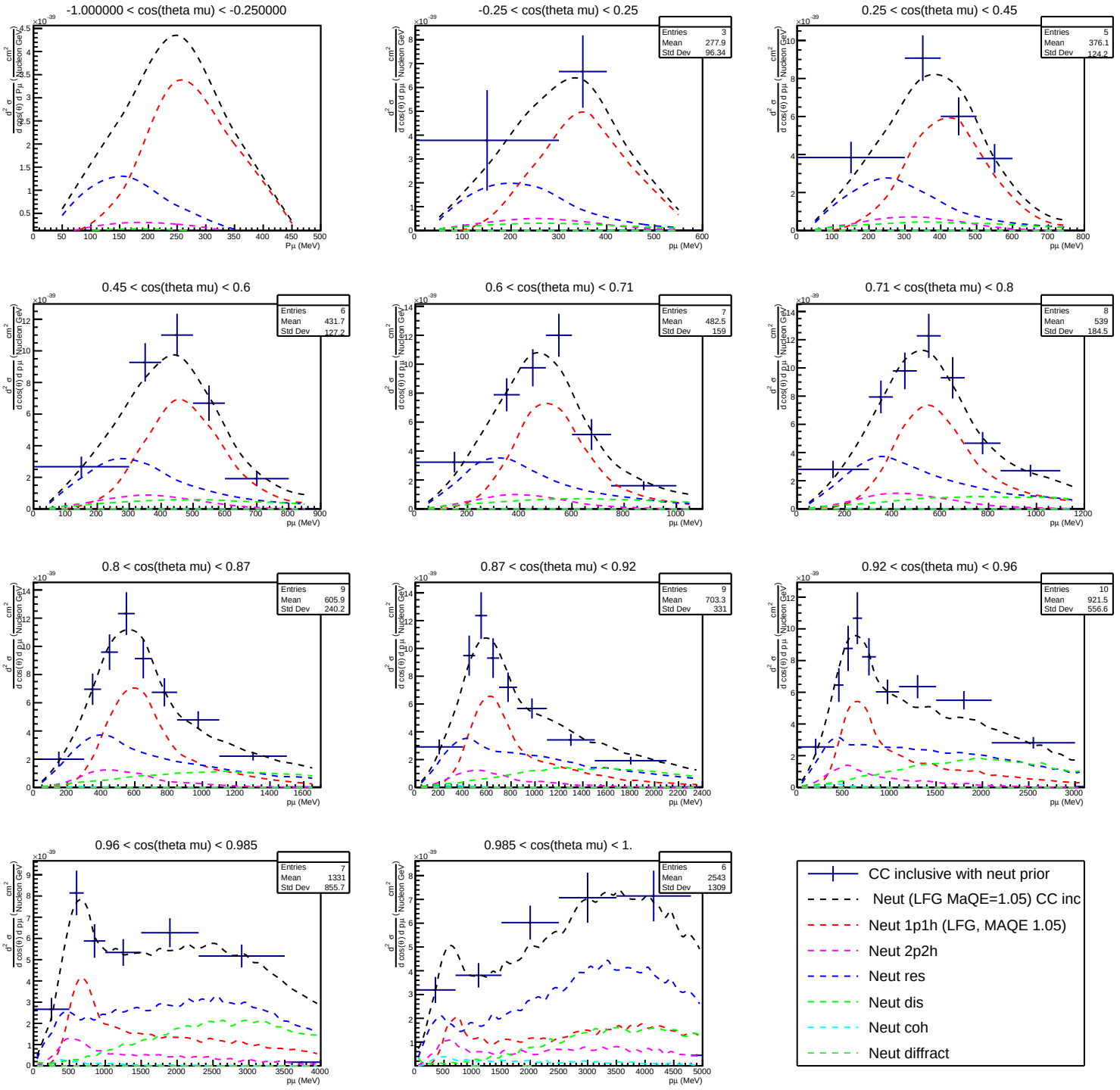

FIGURE 6.5: T2K CC inclusive cross section MC prediction with Neut LFG compared to the data

model inaccuracies. Following this discussion, the axial mass is an effective parameter that can vary with the nucleus and the neutrino energy.
The comparison between the previous NEUT version and our implementation is shown in figure 6.6 with the full line being NEUT using RFG model and the dashed line NEUT using LFG model. This comparison is done using the default axial mass value of the respective model. We can see that both models give nearly the same double differential cross section with respect to the muon momentum and angle. The main difference is that muons are predicted to have a slightly lower momentum for the LFG.

In NEUT, we modify the axial mass value of the RFG model to have the same as the one used in the LFG model and the resulting 1p1h double differential cross section with respect to muon kinematics is shown figure 6.7. Here, we can see that, for the RFG, by comparing both blue lines, for the muon kinematics, using a lower axial mass reduces the double differential cross section.We expected such a behavior as in the cross section calculation, as defined in chapter 3, a lower axial mass means a lower axial form factor. Thus the nucleon tensor is smaller and the cross section is reduced. This reduction does not reproduce exactly the LFG double differential cross section (red line), as seen for forward and low angle muons.

We show in figures 6.8 and 6.9 the differential cross section with respect to the neutrino energy using T2K flux for the default axial mass (6.8) and using the same axial mass (6.9). As expected, this differential cross section is lower for figure 6.8 and the same for figure 6.9. But for both figures, the cross section curve is sightly shifted towards lower neutrino energy for the LFG compared to RFG. Thus the LFG model favors, albeit only a little, lower neutrino energies compared to the RFG.

From figures 6.7 and 6.9, we can see that the change of model is not affecting much the leptonic part of the cross section. We will see mores differences in the momentum of the hadrons as shown later. We show the cross section differential with respect to the target nucleon momentum in figure 6.10 and product nucleon momentum in figure 6.11. The target nucleus momentum, shown in figure 6.10, is the core of the difference between the two models. The way this momentum is chosen differs, whereas the LFG model defines it depending on the nuclear medium density, the RFG model uses a fixed maximum, here around 220 MeV as a maximum. This give a target nucleon that can have higher momentum for the LFG model but most of the events will have a lower momentum. We should notice that the LFG model needs the kinematics to be correct, therefore having higher momentum means that lower neutrino energy is needed for the interaction, as we have seen in figure 6.9. The product nucleon momentum comparison, shown in figure 6.11, has a few interesting points. First the LFG model has less high momentum product

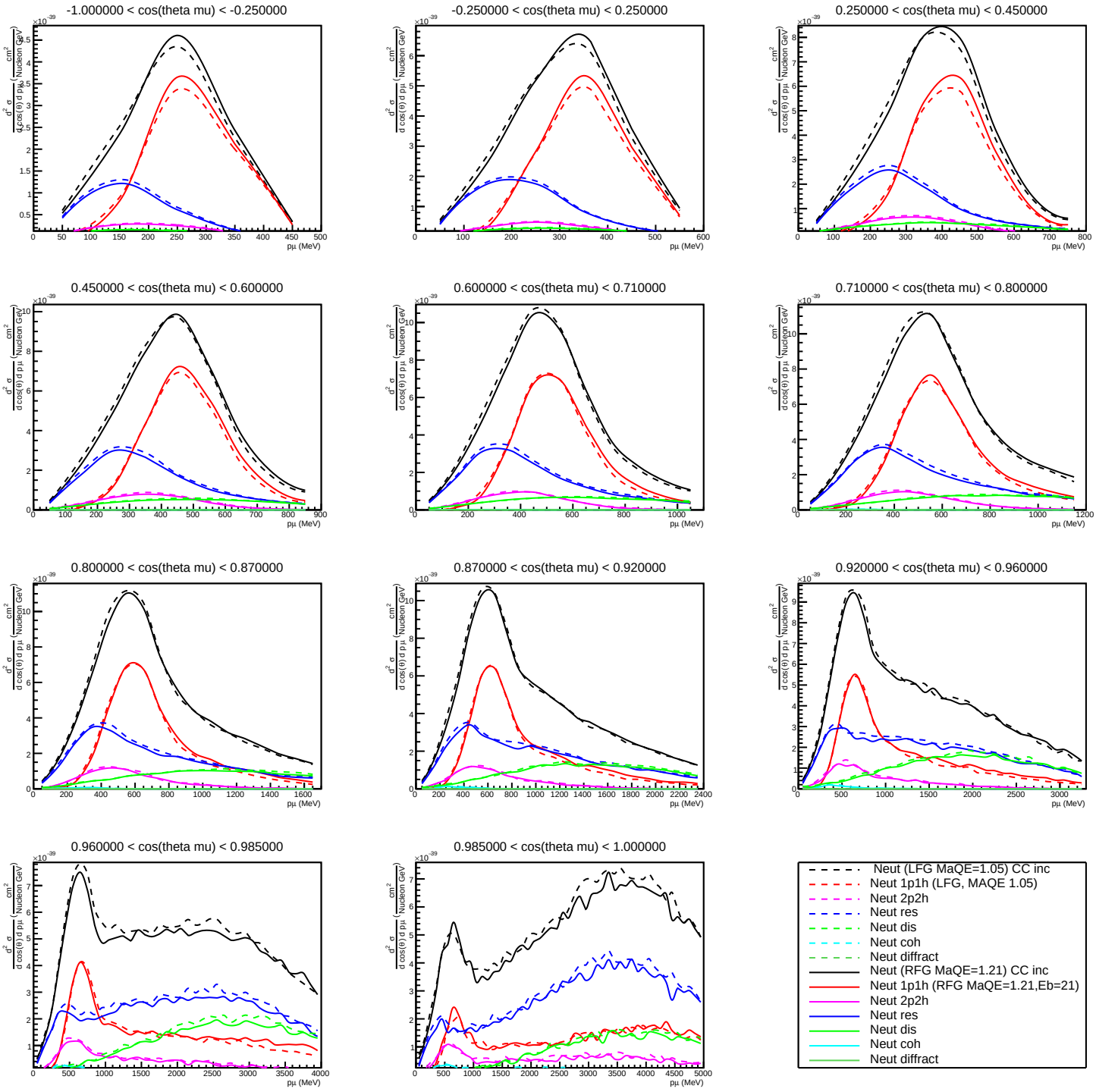

FIGURE 6.6: Comparison between the cross section of previous version of NEUT MC with RFG and the current version of NEUT with LFG with CC inclusive selection

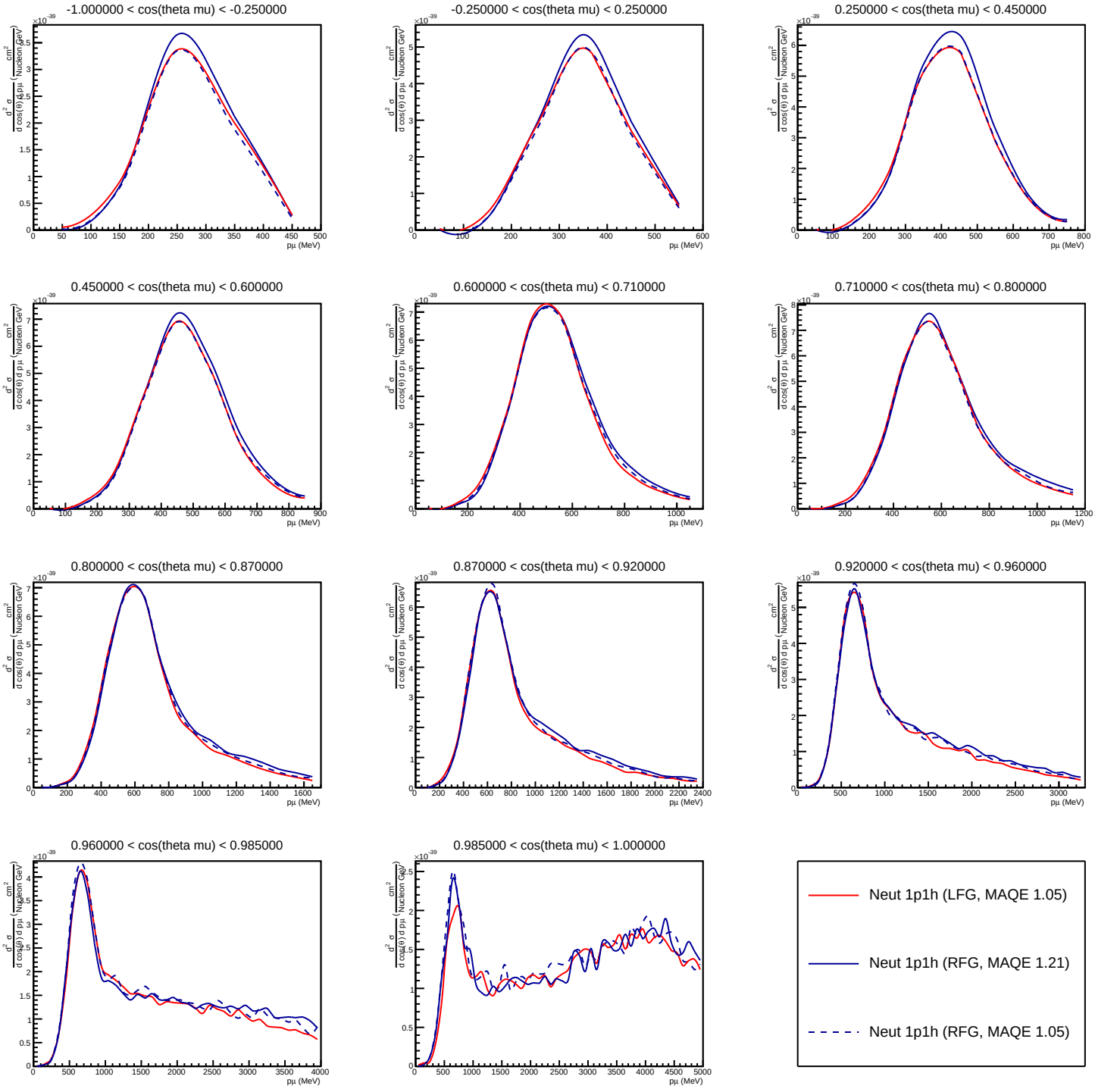

FIGURE 6.7: Comparison between the 1p1h interaction's cross section with CC inclusive selection for LFG (red), RFG with the same axial mass(doted blue) and RFG with neut default axial mass

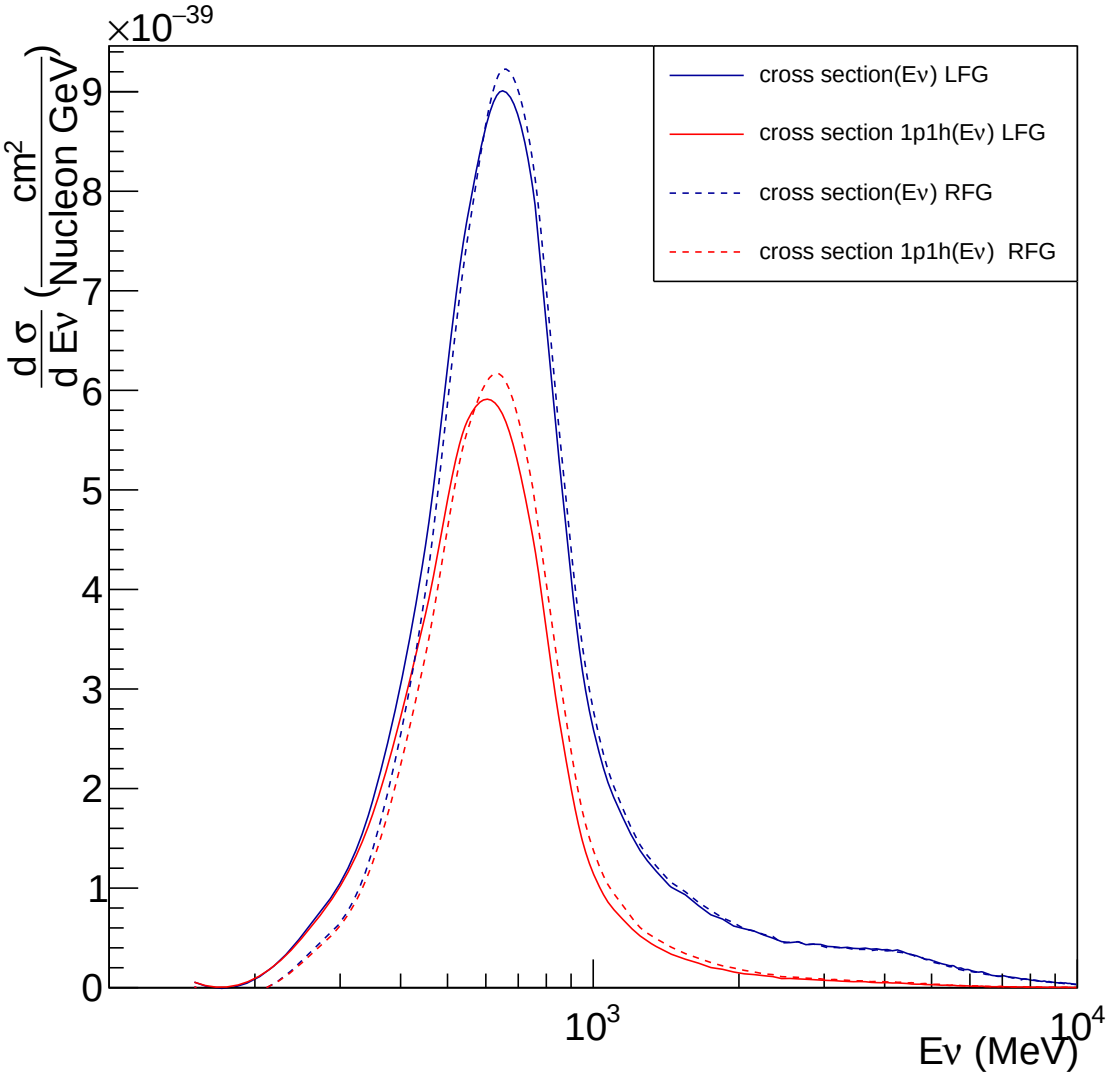

FIGURE 6.8: Comparison for the T2K flux convoluted differential cross section in neutrino energy using logarithmic scale (total in red and 1p1h in blue) between RFG (dashed line) and LFG (full line). The axial mass value used is 1.21 GeV for RFG and 1.05 GeV for LFG

nucleons than the RFG, second only the LFG model has the possibility to have lower than 200 MeV product nucleons bypassing the Pauli blocking as discussed in chapter 4. So even if the lepton component is similar, when we look at the proton we expect differences.

6.3.2 T2K CC0pion

In the study, the data are presented using muon momentum and angle between neutrino direction and muon. Those are the observables that can be directly detected in the

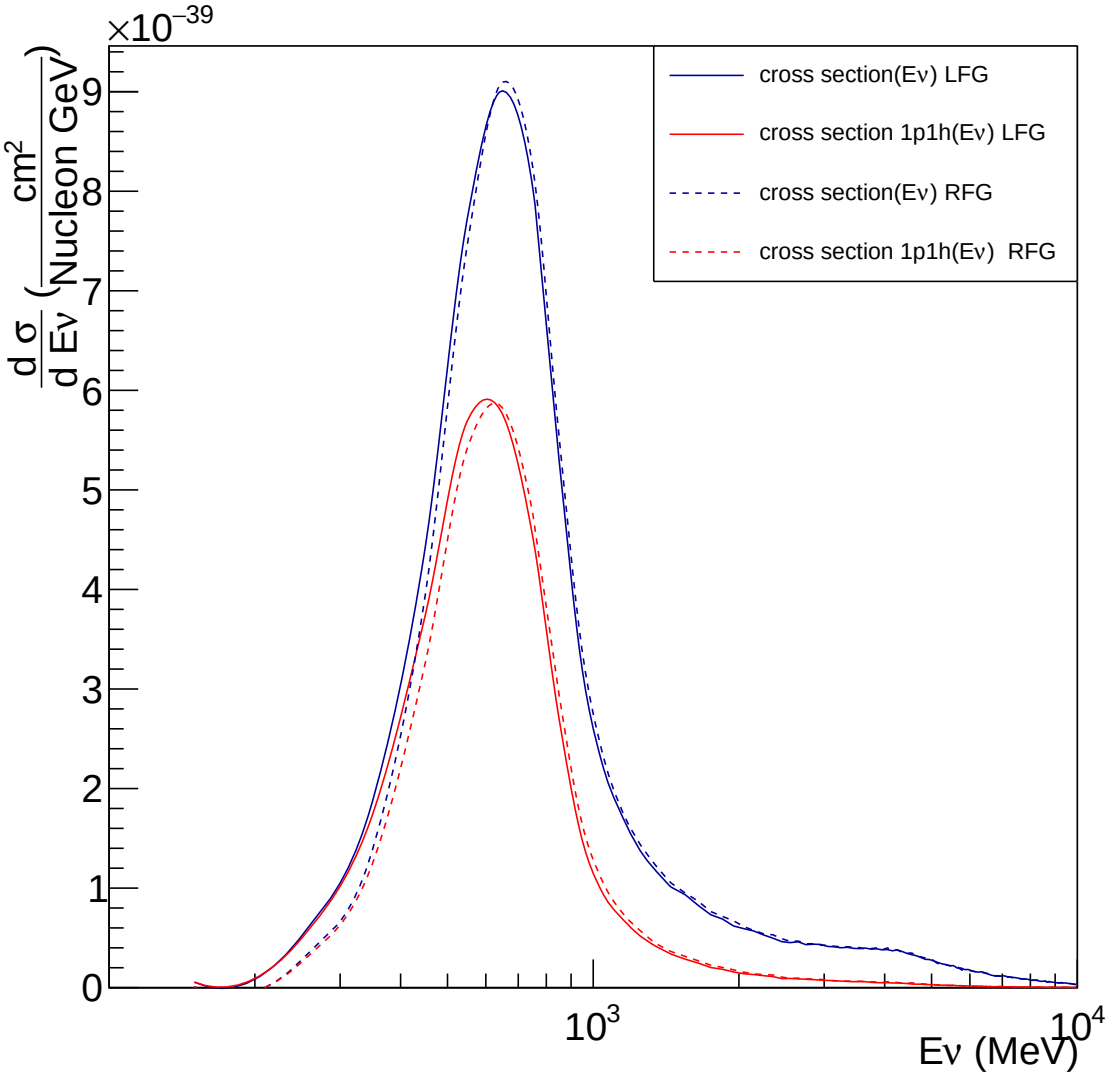

FIGURE 6.9: Comparison for the T2K flux convoluted differential cross section in neutrino energy using logarithmic scale (total in red and 1p1h in blue) between RFG (dashed line) and LFG (full line). The axial mass value used is 1.05 GeV for RFG and LFG

ND280 detector and should be less model dependent. The composition of the NEUT simulation output is presented in table 6.2. In this table, the "selected" events have a muon and no pion in the final state, and the "not selected" have either no muon, neutral current events, or a pion in the final state without taking into account the events interaction. So 44.1 % of the total events are detected as CC0pion events whereas 55.9 % are recognised as non CC0pion events whether there is no muon or a pion outside the nucleus. Again we have a majority of 1p1h (34.2 %) events compared to 2p2h (5.9 %) and CC1π without π detected (4.0 %) as secondary selected events. Considering the true signal as 1p1h and 2p2h interactions, we will have 40.1 % of events and 4.0 % of

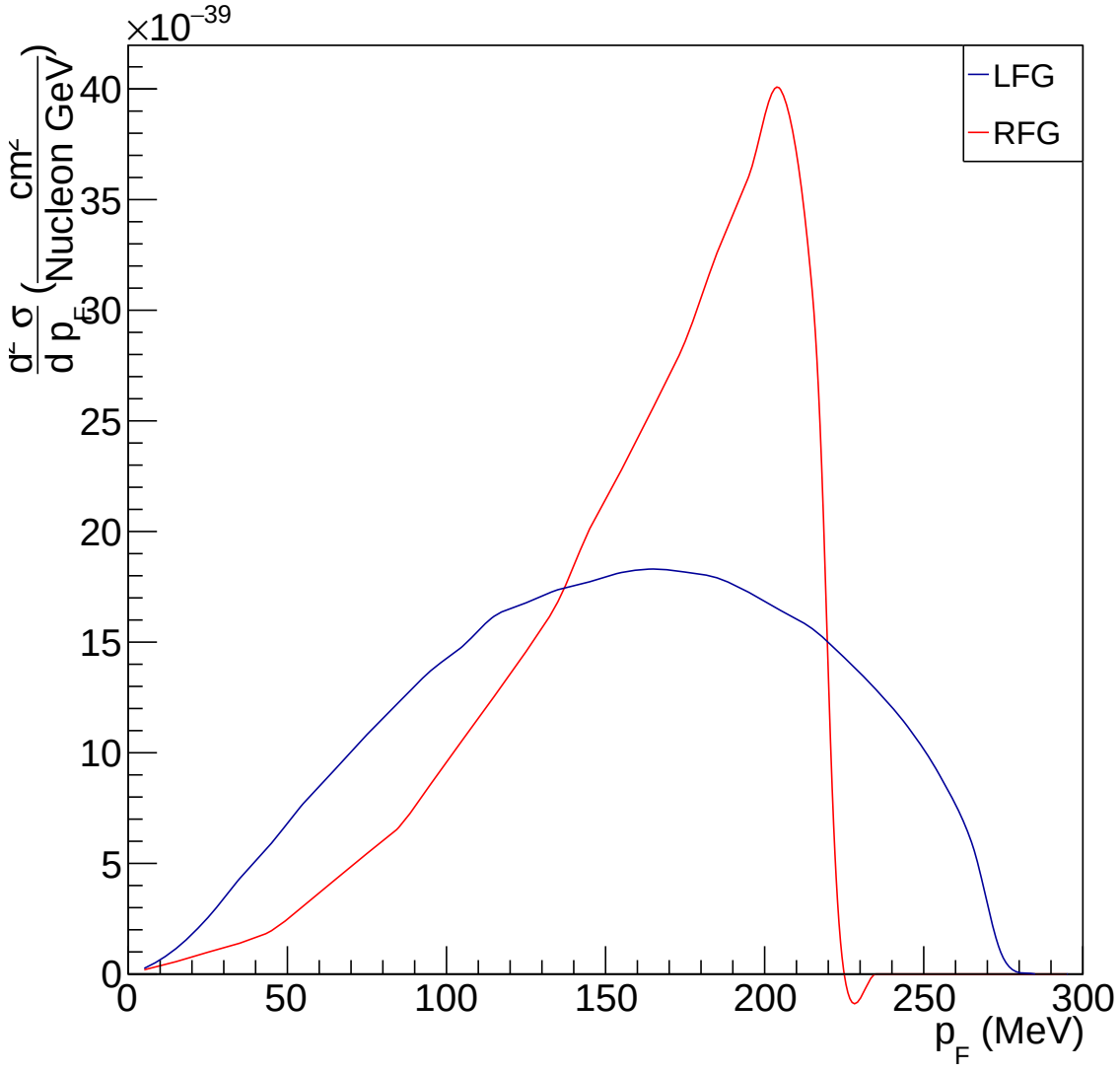

FIGURE 6.10: Differential cross section as function of the target nucleon momentum for RFG (red) and LFG (blue)

	selected (no π detected)			not selected	
interaction	1p1h	2p2h	CC (1π)	CC 1π	NC
event (%)	34.2	5.9	4.0	29.25	26.65

TABLE 6.2: Composition of selected and non selected events for a NEUT file output using the T2K flux and T2K CC0pion selection method

backgrounds in the selected sample. All the other events are rejected by the selection. The comparison between data and NEUT simulation cross section is shown in figure 6.12. In this figure, to represent the double differential, each graph correspond to a neutrino-muon angle. And the X-axis binning of each graph is chosen as the muon momentum. The top-left graph is the backward muon with $-1 < cos(\theta) < 0$, while the

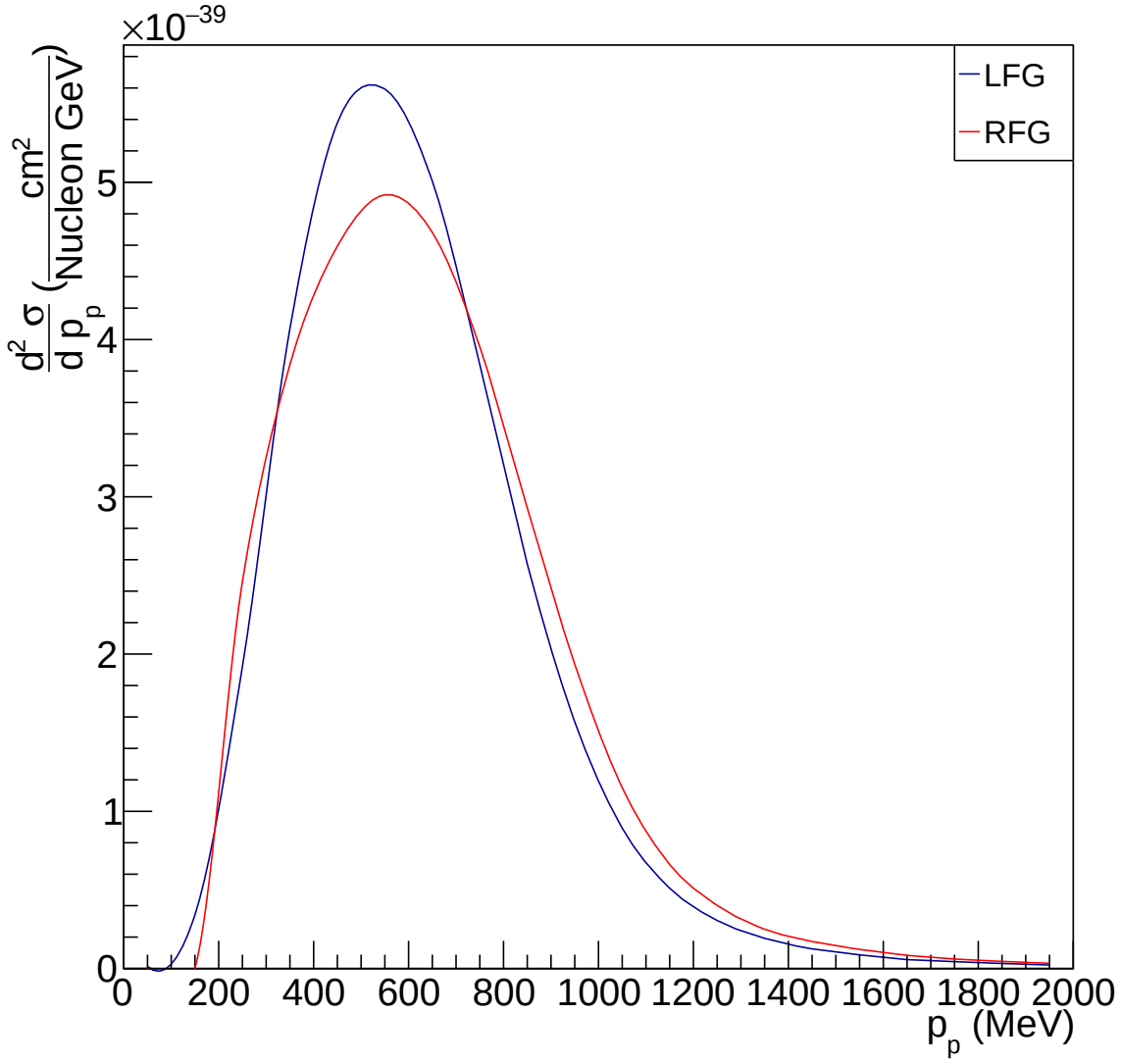

FIGURE 6.11: Differential cross section as function of the product nucleon momentum for RFG (red) and LFG (blue)

bottom right plot shows the forward muon with $0.98 < cos(\theta) < 1$.
If we compare the general tendency, the simulation and the data are in a good agreement except for a few significant deviations. We can see that the data cross section show a peculiar behavior for the three most forward angle, after reaching the maximum cross section the cross section drops sharply and then goes up again before slowly decreasing or stabilizing for the most forward angle. This sharp drop is not predicted by NEUT and it is very significant for the angle $0.9 < cos(\theta) < 0.94$ and $0.98 < cos(\theta) < 1.0$. we have the second figures of the two most forward angle 6.13 and 6.14 for a more detailed NEUT prediction. This sharp drop is not seen in the CC inclusive data making difficult to draw any decisive conclusion. Actually this fact might be an indication of an experimental

effect on the extraction of the cross section.

We can see that the differences between the data and the MC are difficult to extract from the statistical fluctuations. Furthermore comparing data to cross section model in order to seek the limitation of the model and improve it further is complicated as the T2K CC0pion data is using $p_\mu \cos(\Theta)$ as variable whereas our model prefers $(q^0, q3)$, the transfer energy and momentum as variables.
Figure 6.15 shows a comparison between data and MC using transfer momentum and energy. To create this histogram we used the following procedure. For each event in the NEUT file:

- obtain $p_\mu, \cos(\Theta)$ and calculate $\frac{d^2\sigma^{MC}}{dp_\mu d\cos(\Theta)}$ for the MC events.
- calculate q^0 and $q3$, it is possible since we know the full kinematics of the MC event.
- find for the events the data bin with the corresponding $(p_\mu, \cos(\Theta))$ and obtain the $\frac{d^2\sigma^{data}}{dp_\mu d\cos(\Theta)}$ value for the data.
- calculate the ratio $R = \frac{d^2\sigma^{data}}{dp_\mu d\cos(\Theta)} / \frac{d^2\sigma^{MC}}{dp_\mu d\cos(\Theta)}$.
- Fill the 2D histogram R(q^0,$q3$).
- Average it by the number of events at each bin of (q^0,$q3$).

So we have realized the following equation:

$$< R(q^0, q3) >= \frac{1}{N} \sum \frac{d^2\sigma^{data}}{dp_\mu d\cos(\Theta)} / \frac{d^2\sigma^{MC}}{dp_\mu d\cos(\Theta)} \tag{6.1}$$

The idea is to concentrate the deviation in the region of momentum transfer ($q3$) and energy transfer (q^0) predicted by the model. This is a model dependent calculation that should allow to have an idea where the model deviates from data.

The resulting figure (6.15) shows a ratio from below 1 for high momentum transfer to above 1 for low momentum transfer. A tendency is visible, but it is not a smooth dependency. For comparison we show the same ratio for energy transfer versus momentum transfer using the cross section predicted by the previous NEUT version, using the RFG model for 1p1h, in figure 6.16. For the comparison the axial mass used for the previous NEUT version is 1.05 GeV. Between the two models we can see that the ratio is higher for the old NEUT version but the functional dependency is similar to each other. Since only the 1p1h model has changed between the two versions and we saw before that the main difference between the cross section model are not too strong with lepton kinematics, we can understand that there is not a strong difference between the models using

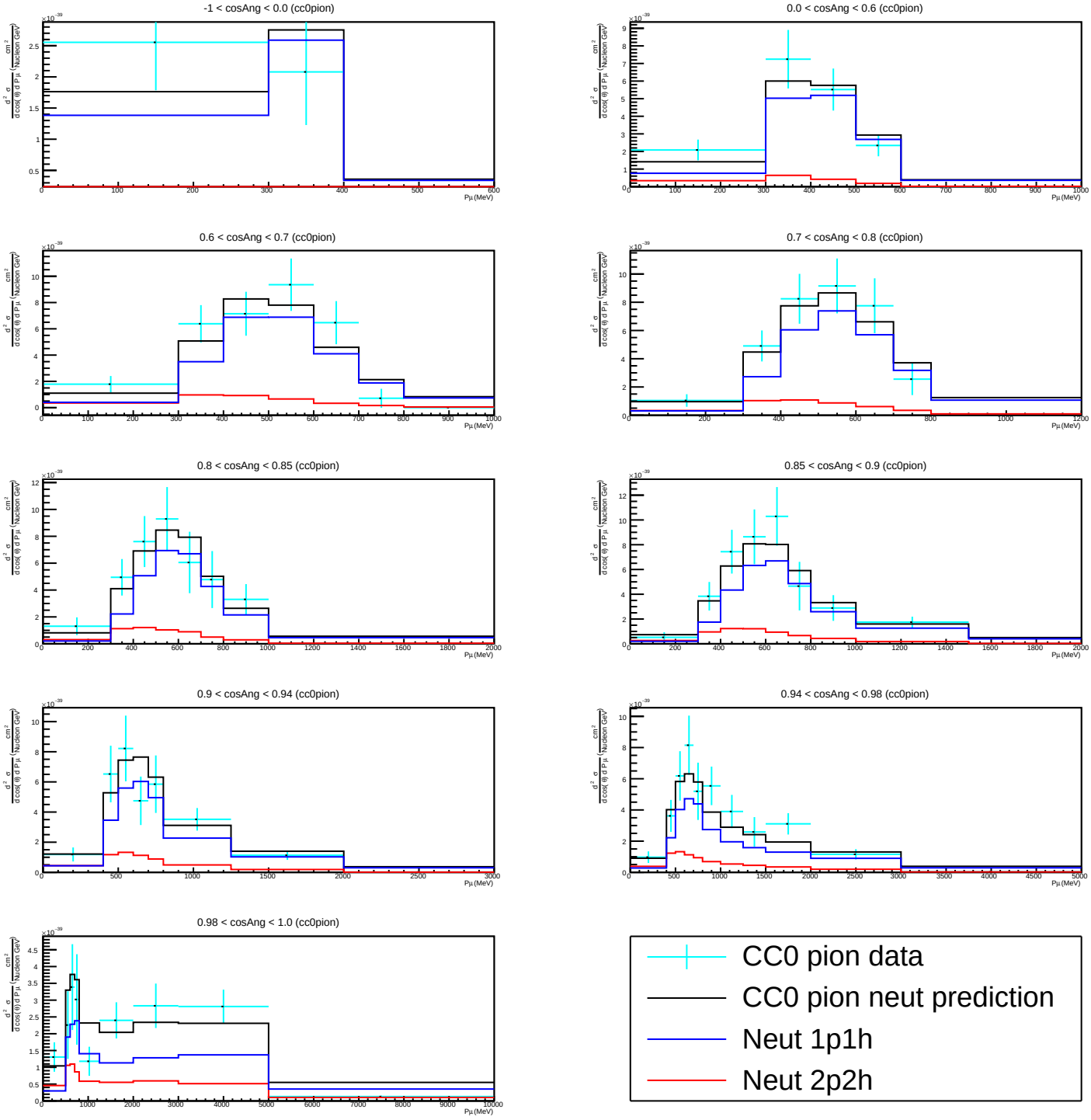

FIGURE 6.12: T2K CC0pion data and NEUT prediction using Nieves model for 1p1h and 2p2h

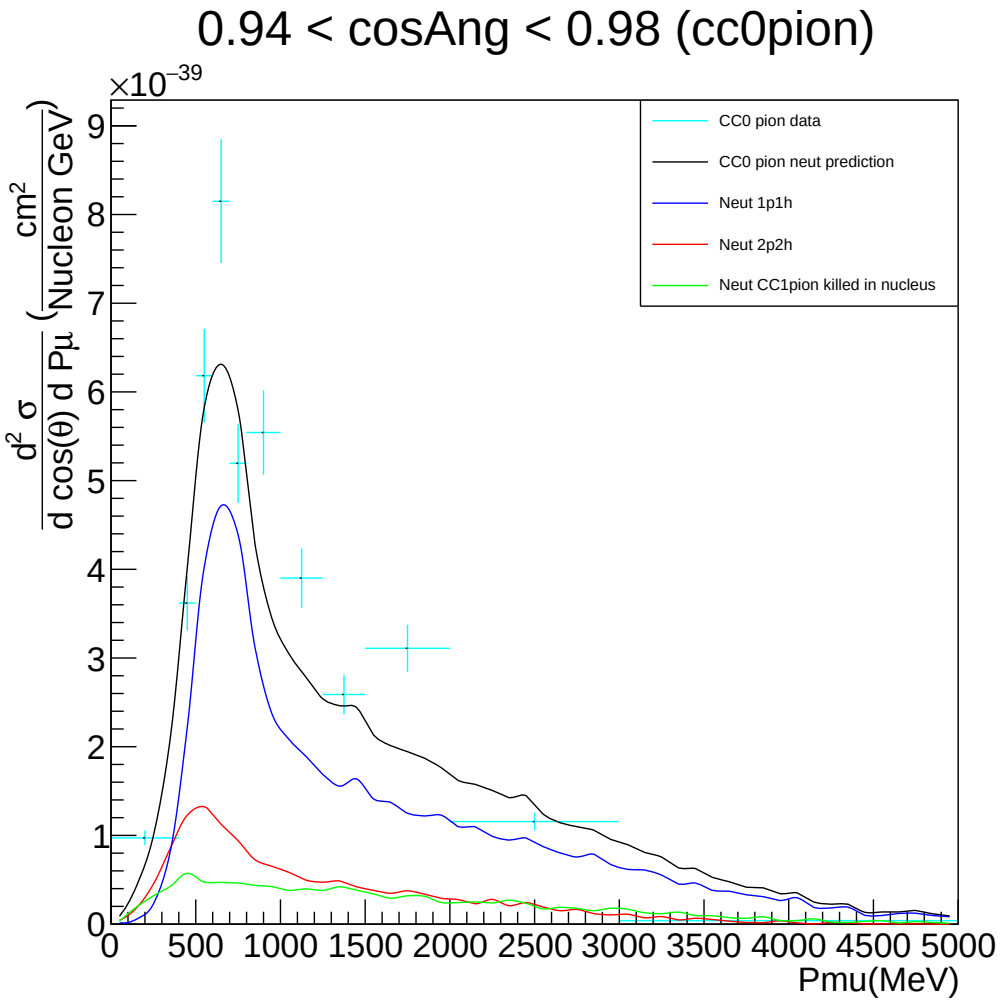

FIGURE 6.13: T2K CC0pion data versus NEUT prediction for the second most forward angle bin, $0.94 < cos(\theta) < 0.98$

the momentum transfer and energy transfer variables.

An idea to have a better understanding of this dependency is to use the scaling variable $\Psi'(q^0, q3)$ that has been presented for the SuSA model in the theory chapter. In order to build this plot, we use the figure 6.15.

Figure 6.17 shows the result of using the scaling variable on the average ratio data versus MC of figure 6.15. By using information from the MC we can distinguish between the interaction type of each event allowing to have the interaction type probability for each Ψ' value. This is shown in figure 6.18. We can see that each interaction takes a specific value range of the scaling variable, with the 1p1h interaction being confined between $\Psi' = -1.2$ and $\Psi' = 1.2$. CCQE is by far the main contribution to the ratio between those two values. 2p2h events take a wider range of Ψ' values between -1 and 6 and background events have Ψ' values between 0 and 6. With this method, we have projected using physically based arguments the (q^0,$q3$) two dimensional plot into a one dimension plot. We have been also able to separate the different interaction contribution regions,

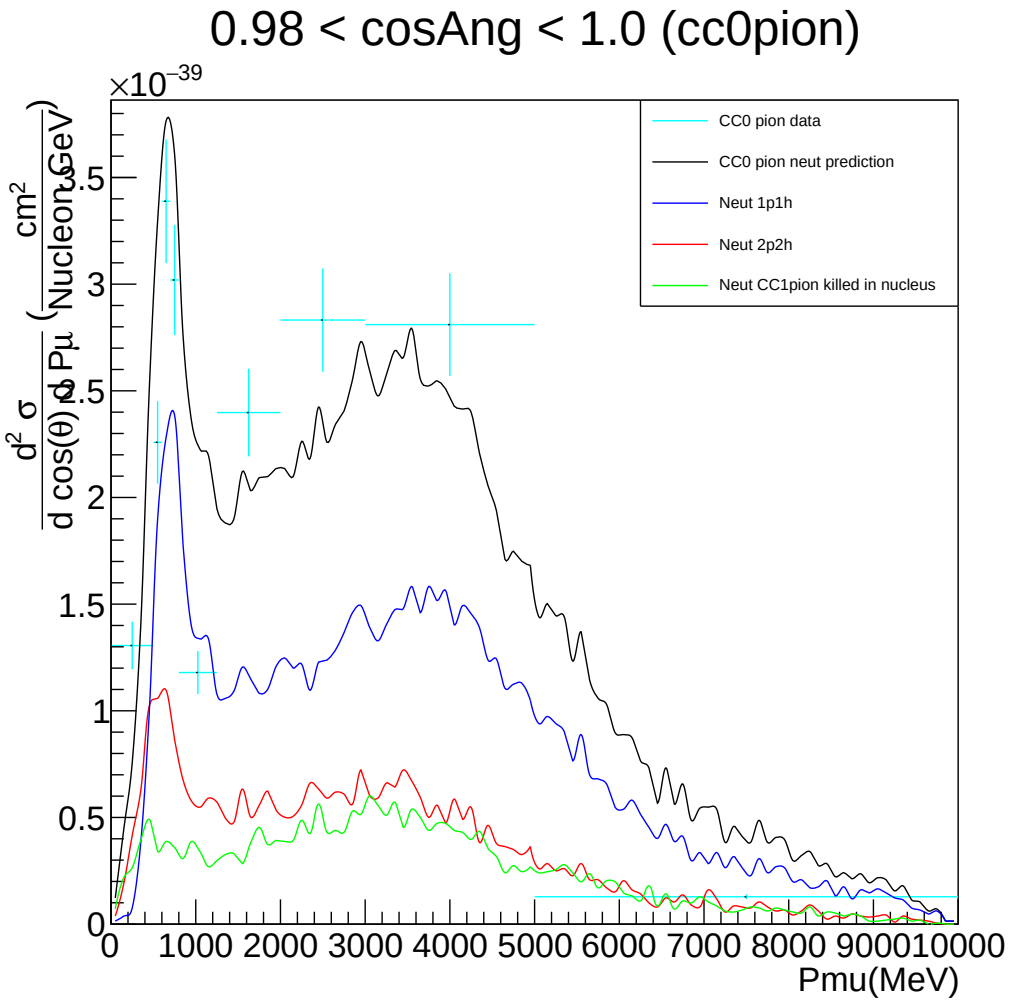

FIGURE 6.14: T2K CC0pion data versus NEUT prediction for the most forward angle bin, $0.98 < cos(\theta) < 1$

with 1p1h being the main interaction for Ψ' between -1 and 1 with some 2p2h events from -0.5 to 1. In this -1 to 1 region we can see that the events are spread into some sort of a gaussian with the 1p1h events contributing to it, see figure 6.18. This gaussian has two aspects: the peak position and the width. According to what we know from the implementation of the scaling variable the peak position is related to the nucleus Binding Energy and the width is related to the Fermi momentum spread. As we can see there is no background events below $\Psi' = 0$. And from Ψ' values between 0 and 1 the background (CC resonance, DIS, etc...) events are very low compare to the 1p1h and 2p2h events. The background events has thus little effect on the ratio and can be ignored in this region. For $\Psi' > 1$, we do not have any 1p1h events and the number of 2p2h and background events is the same so it has to be taken into account.

Returning to figure 6.17, we can focus on the region of Ψ' between -1 and 1, there the ratio data MC is rising from R = 0.9 to R = 1.2 and it passes to R = 1 at $\Psi' = -0.4$

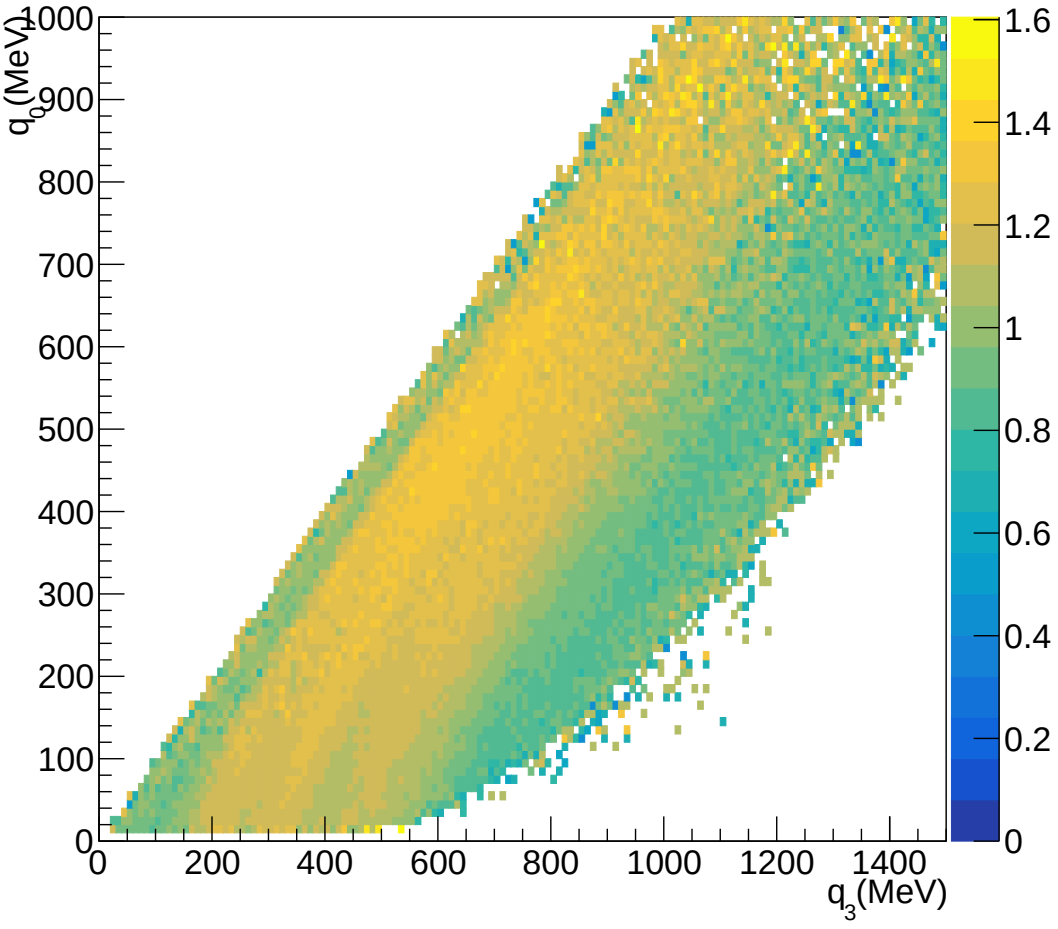

FIGURE 6.15: Average ratio data divided by MC for LFG (energy transfer versus momentum transfer)

approximatively, when 2p2h events began to be more relevant. This means that at low Ψ' values, inferior to $\Psi' = 0$, the MC is overestimating the 1p1h cross section. For higher Ψ', the MC events combining 1p1h and 2p2h interactions are underestimating the data cross section. Beyond $\Psi' = 1$, where the background is of the same order as the 2p2h interaction, the data cross section is underestimated by the MC.

Figure 6.19 shows the ratio of cross section between data and MC in function of Ψ' with the previous NEUT version using the RFG model for 1p1h events.
We compare the results from the two NEUT version in function of the Ψ' variable in figure 6.20. For Ψ' lower than 0, where the 1p1h interaction is the only interaction, we see that ratio for the old NEUT version is slightly lower than for the new version.So for the momentum transfer and energy transfer variables corresponding to the Ψ', the RFG model has a higher cross section than the LFG model. We had shown that in the ratio plot in function of (q^0, q_3) seemed to have the same behavior for the two NEUT version

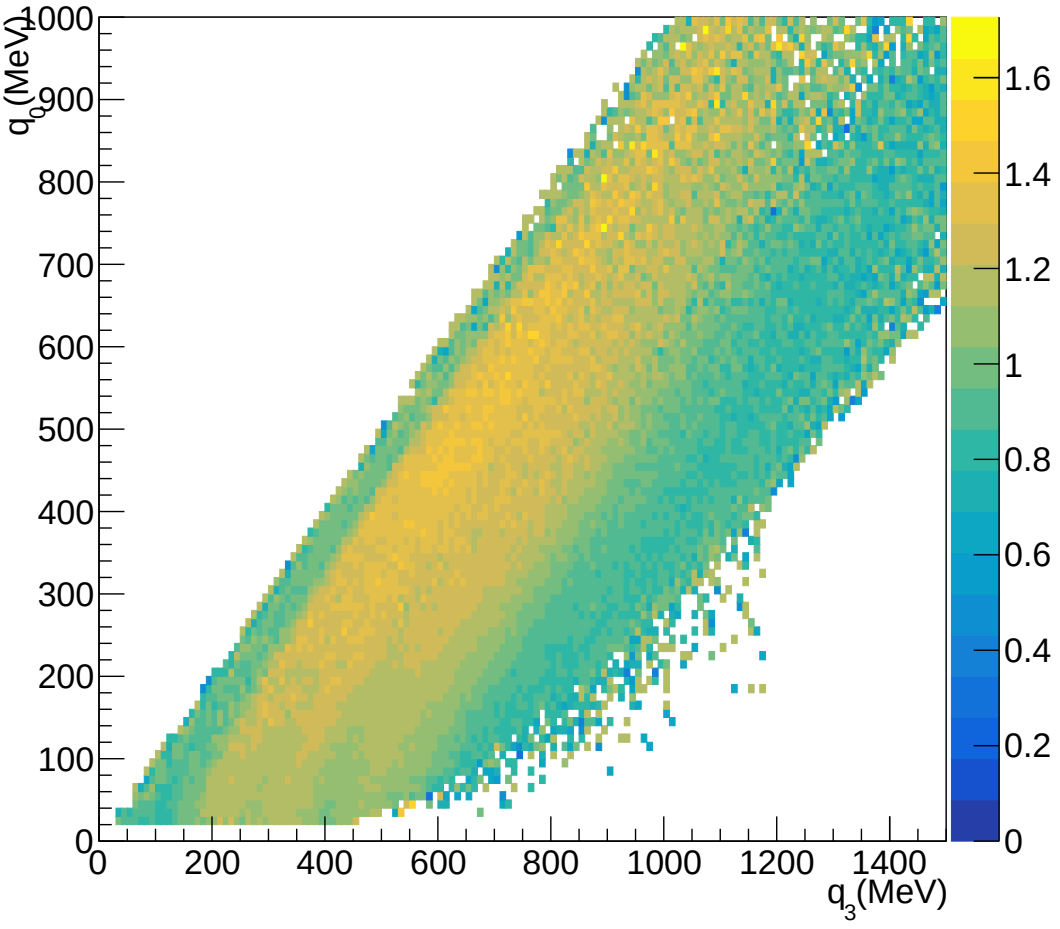

FIGURE 6.16: Average ratio data divided by MC for RFG (energy transfer versus momentum transfer)

but the ratio seemed higher for the previous version. This similarity in behavior between the two models should come from the fact that the transfer variable are computed from the lepton part of the interaction, leading to less significant difference. We also see that in the case of 1p1h the ratio is lower for the previous NEUT version, and it is more logical since we saw in the CC inclusive comparison of model that the predicted cross section for the RFG model was a bit higher than for the LFG model.

Then for Ψ' higher than 0, we see that the ratio for both old and new version of NEUT slowly become the same. In this region the 1p1h interaction has an important background of 2p2h interaction events so the behavior could be due to that interaction. But the 2p2h model used in the two model is the same it should be unlikely to have too much of an effect. Using the scaling variable, we can see that the difference between the models is represented by a small difference in the curve slope. With the definition of the scaling variable, the only differences between the models that are taken into account here should be the elements that affect the energy transfer and momentum transfer.

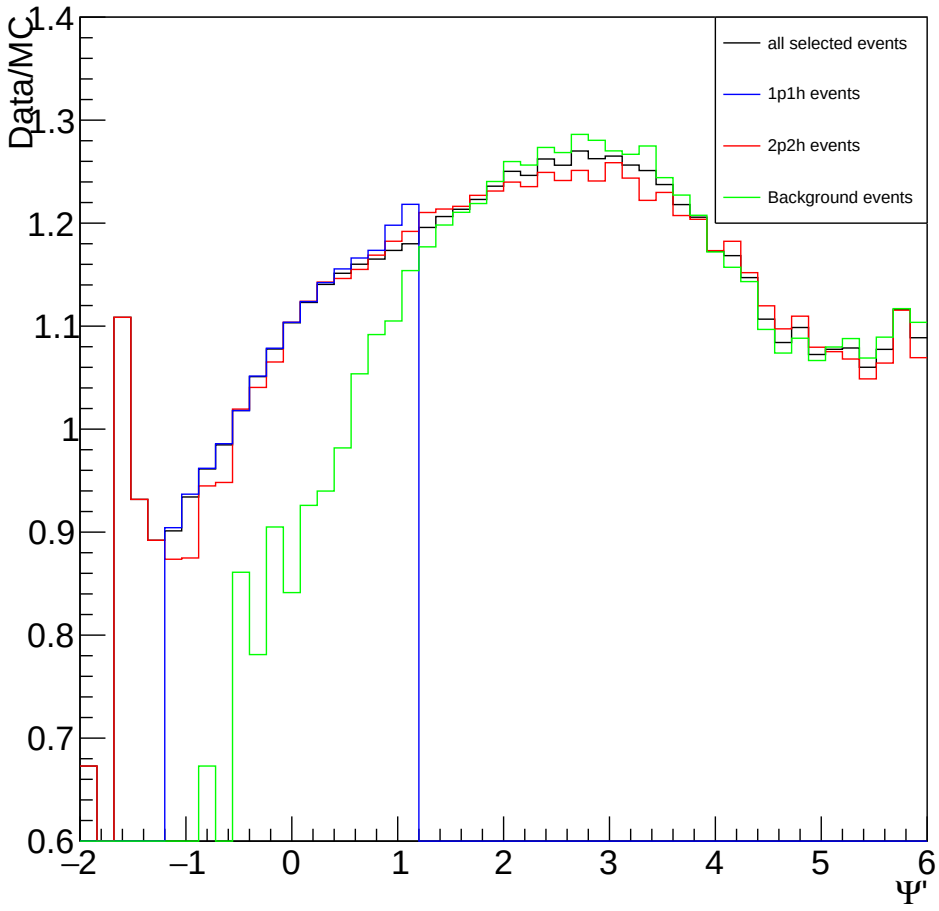

FIGURE 6.17: Comparison data MC for LFG model (Ψ'), black line is all selected events, blue line is 1p1h events, red line is 2p2h events, green line is background events

This study indicates the regions in which the model needs to be improved. With the small difference seen between the two 1p1h models and the way the scaling variable is computed we can make some guess on the improvement needed. The scaling variable should be dependent of the parameters affecting the energy transfer and momentum transfer. The Binding Energy is a good candidate.

In both model, an energy required to excite the nucleus from the initial state to the final state is removed from the energy transfer. It is called the Binding Energy, and they are not exactly computed in the same way for the RFG and the LFG models. This energy value depend on the nature of the nucleus and of the incident lepton. And there is one common assumption in the computation, the initial nucleus is taken at its Fermi level and the final nucleus is produced at its Fermi level too, so not in an excited state. Also the removed nucleon need the smallest energy to exit the nucleus. This lead to the Binding Energy to be of fixed value for a nucleus. As an example, for the neutrino on Carbon target the Binding Energy is of 25 MeV for the RFG model and 17 MeV for the

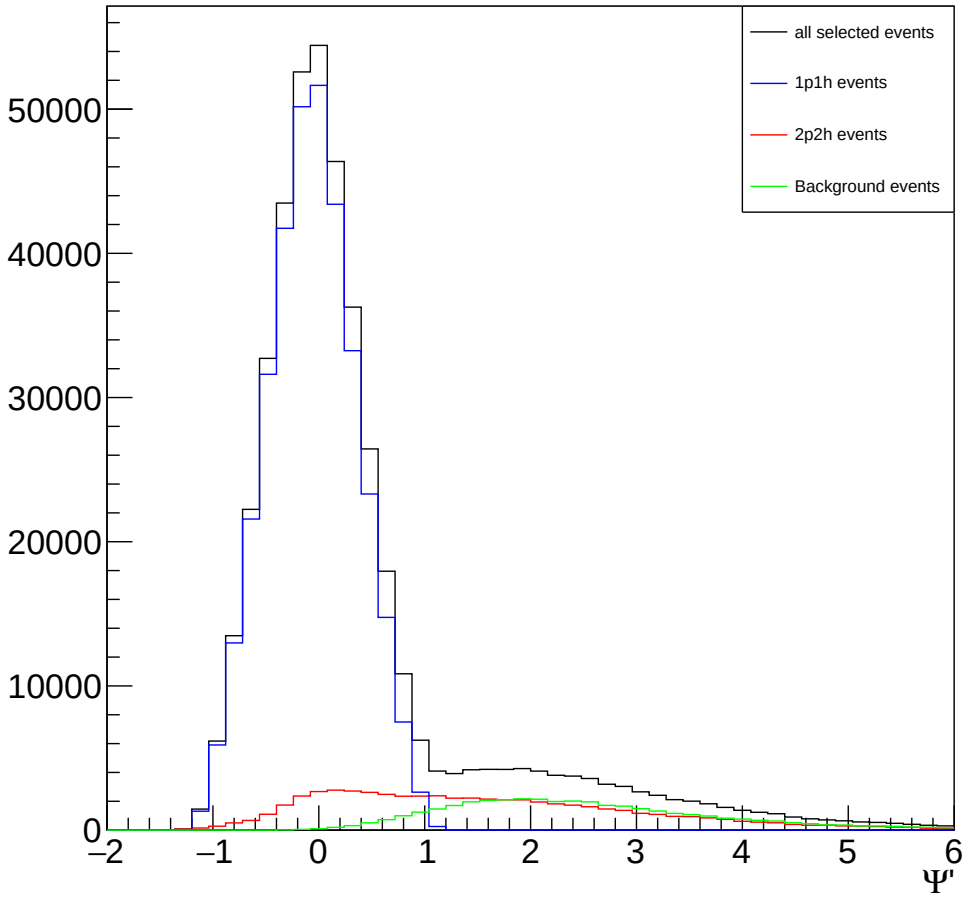

FIGURE 6.18: Number of events for each Ψ' value for each interaction, black line is all selected events, blue line is 1p1h (LFG model) events, red line is 2p2h events, green line is background events

LFG model. In a CCQE interaction the nucleus can be produced in an excited state. In this case the energy consumed by the reaction is the excited state energy with the lowest energy necessary to remove a nucleon from the nucleus. In the models it could be represented by a randomized value between reasonable value of 0 to tens of MeV for the binding energy of each events.

Moreover, we will test this method with other data sets to see if the results are comparable.

6.3.3 MiniBooNE

The composition of the NEUT simulation output for this CCQE-like selection with the MiniBooNE flux is shown in figure 6.3. As this experiment is on-axis, the neutrino

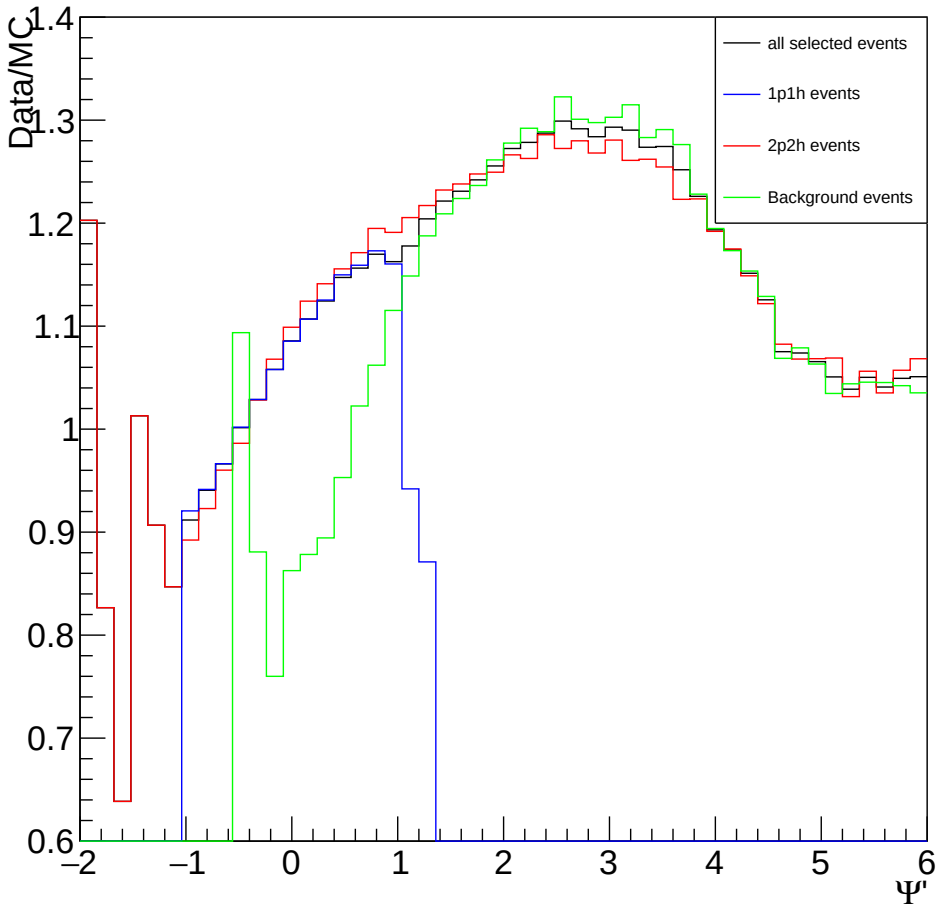

FIGURE 6.19: Comparison data MC for RFG model (Ψ'), black line is all selected events, blue line is 1p1h events, red line is 2p2h events, green line is background events

	selected			not selected	
interaction	1p1h	2p2h	CC 1π	CC 1π	NC
events (%)	34.0	6.6	7.1	25.7	26.6

TABLE 6.3: Composition of selected and non selected events for a NEUT file output using the MiniBooNE flux and MiniBooNE CCQE-like selection method

energy flux is more broad and we have more 2p2h events than for the T2K flux. Also with the additional background we discussed during the event selection, we have a higher background selected than with the T2K CC0π study. The MiniBooNE results are presented using double differential cross sections with respect to the outgoing muon momentum and neutrino-muon angle. The figures in 6.21 show that we have the proper order of magnitude but the shape is not well described. Particularly for high angle and low momentum muons the simulation seems to underpredict the data and for the forward angle the peak of the MC cross section prediction is lower than the data. The underprediction behavior can be seen for every forward angle plot and we can assume

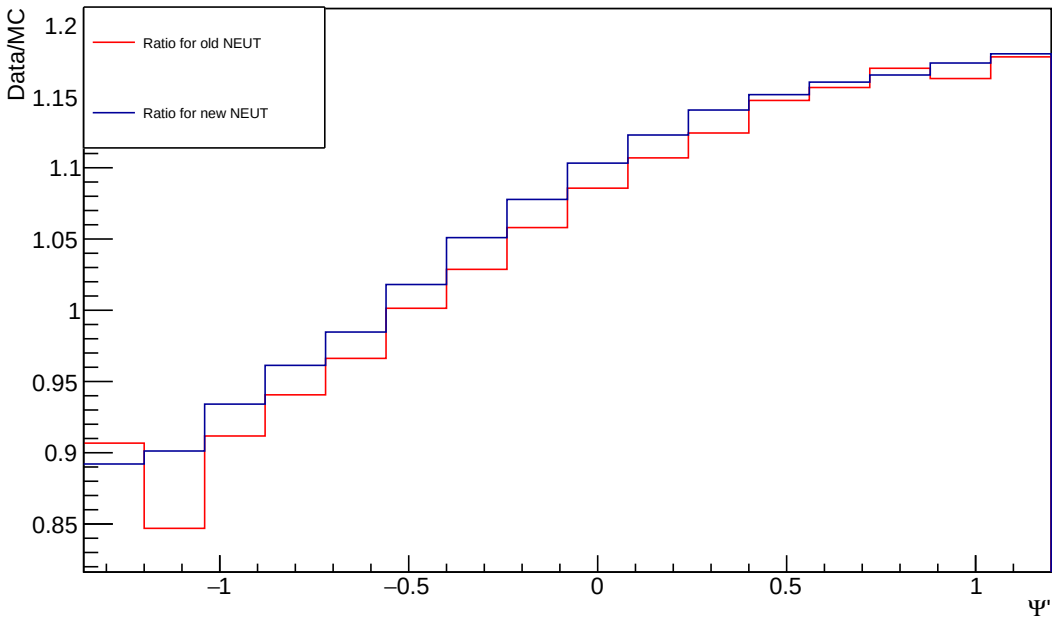

FIGURE 6.20: Comparison data MC in function of Ψ' for the old (in red) and new (in blue) version of NEUT with CC0pion selection. Ψ' lower than 0 with nearly only 1p1h interaction and Ψ' higher than 0 with 1p1h and 2p2h interactions

that it should be the same behavior for the backward angle plot but the binning of the data is not enough to confirm this expectation. The fact that every plot shows the same behavior should indicate that there exists a fundamental underlying issue. We assume that this does not come directly from the 1p1h model since this behavior would have also shown up in the T2K CC0pion analysis. The other possibility would be the background selection, either the background is not reproduced properly or we do not understand properly how the background was selected. First, we verified that the background selection was properly understood. Then, we tested that removing the π^0 background only made the cross section prediction worse. So background correction in the data could be one of the issue but there are others possibilities. The issue could come from neutrino flux uncertainty or the Binding Energy has a larger effect at lower neutrino energy.

We also use the CC0pion set of data from MiniBooNE to verify if we can confirm the result of the previous study for CC0pion with T2K data. The idea is that the events selected should be the same in both studies, the CC0pion of T2K and the CCQE-like of MiniBooNE, the only change between the two is the neutrino flux and the fact that the background is not exactly the same. We compute the ratio data divided by MC and applying the method presented in the CC0pion study we create figure 6.22 of the ratio with respect to energy transfer versus momentum transfer. We already see a significant difference in respect to the T2K CC0pion data, the ratio is higher for high transfer

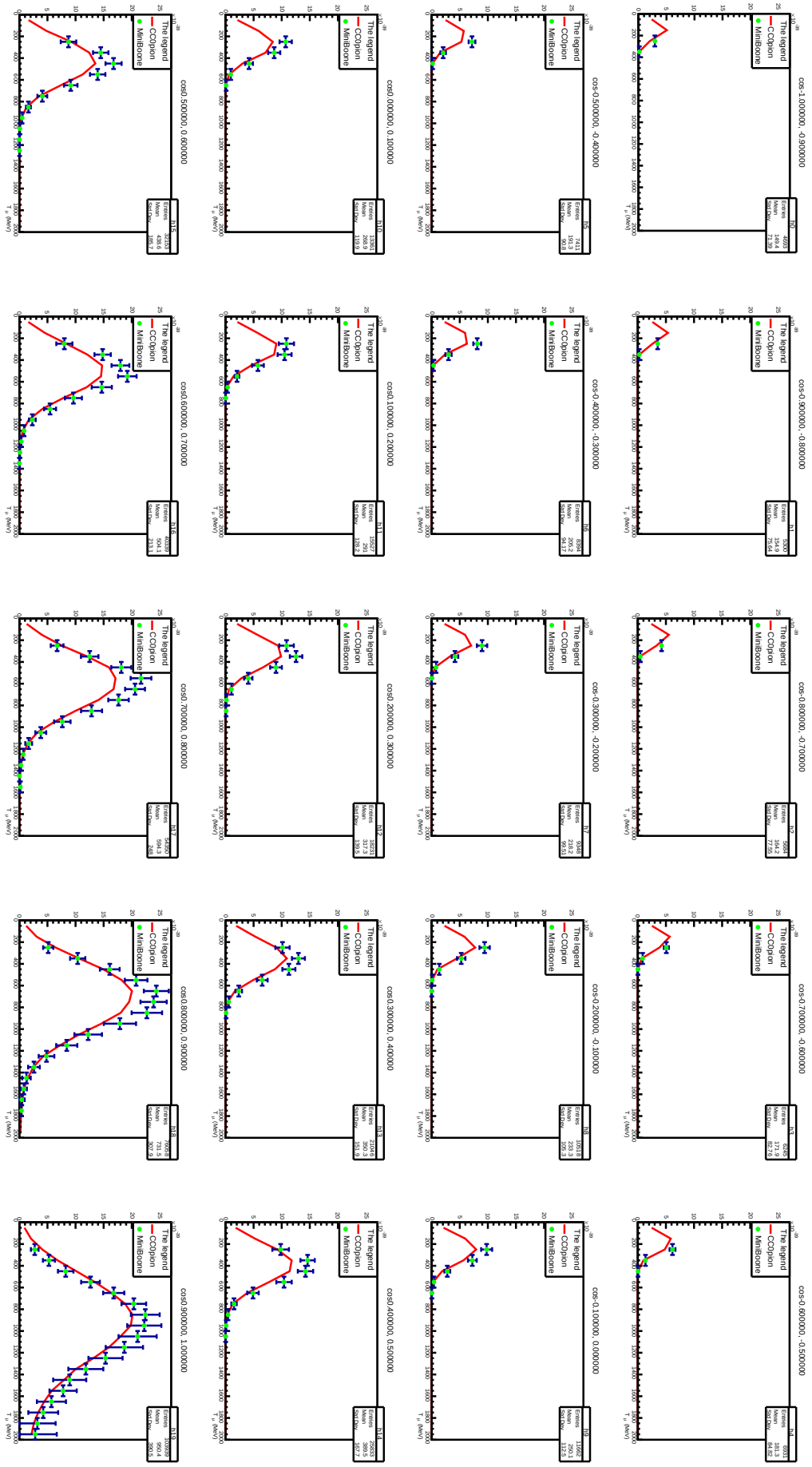

FIGURE 6.21: MiniBooNE comparison data MC using muon angle $cos(\theta)$ and transverse momentum T_μ. Data is shown with green dot with error bar in blue. The red line is CCQE-like selection prediction

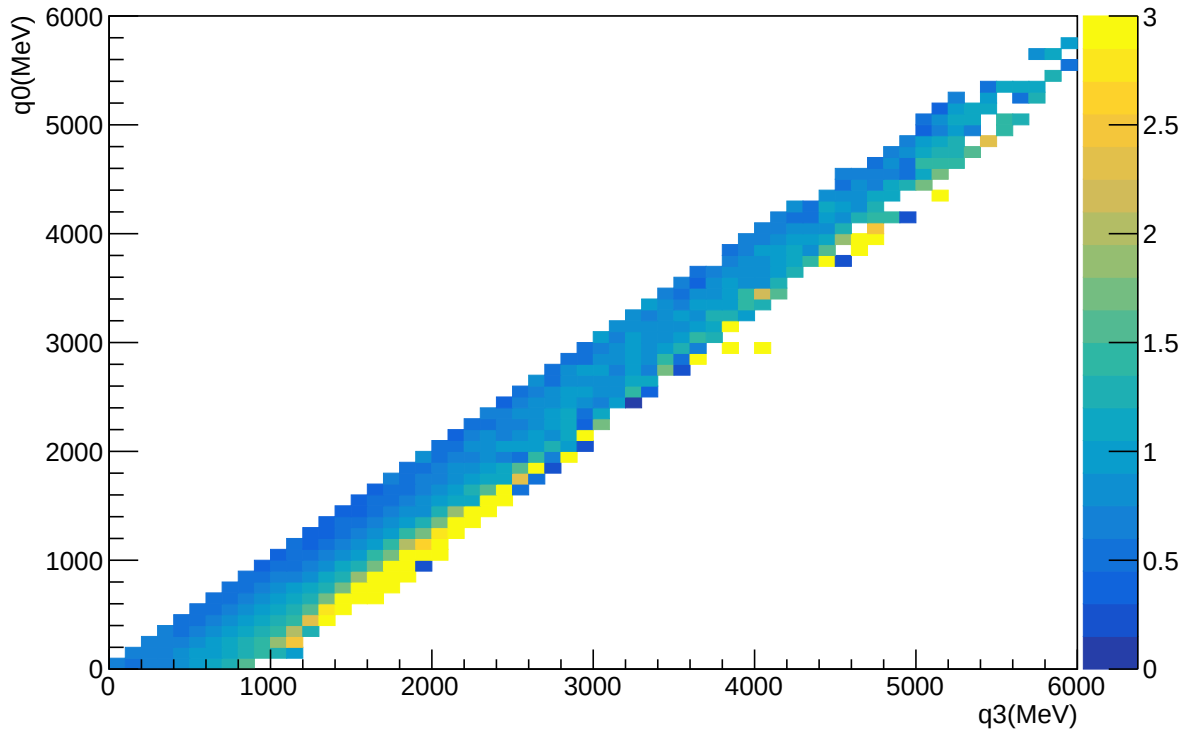

FIGURE 6.22: Ratio data divided by MC for energy transfer (q0) versus momentum transfer (q3) with MiniBooNE CCQE-like data

momentum and goes down for low transfer momentum. It seems the ratio behaves in the opposite way for MiniBooNE data than for T2K data. This is a very interesting tendency as it might bring some light to the origin of the discrepancies.
In figure 6.23, we show the number of events in function of Ψ' for 1p1h, 2p2h and CCQE-like interaction. And figure 6.24 shows the ratio between the data and MC cross section in function of Ψ' for 1p1h, 2p2h and CCQE-like interaction. The first comment to do is that we find the expected Ψ' values for both 1p1h and 2p2h, meaning that 1p1h takes Ψ' values between -1.2 and 1.2 and 2p2h has values going from -1 to 6. Then the ratio is higher than 1 for Ψ' lower than -0.4 and goes down as the scaling variable increases, going to around 0.75 for $\Psi' = 1.2$ and towards 0.55 for higher Ψ' value. This means that the MC prediction underestimates the cross section for low Ψ' and overestimates it for high Ψ'. This behavior is the exact opposite than the result we have with the CC0pion data study from T2K. We can think of a few possibilities about why does this happen:

- One option is the difference of background in both selections. But it cannot be the only reason as the background should be small for $\Psi' < 0.5$.
- The flux is different between the two experiments, meaning that the neutrino energy range is not the same but by definition the scaling variable is independent

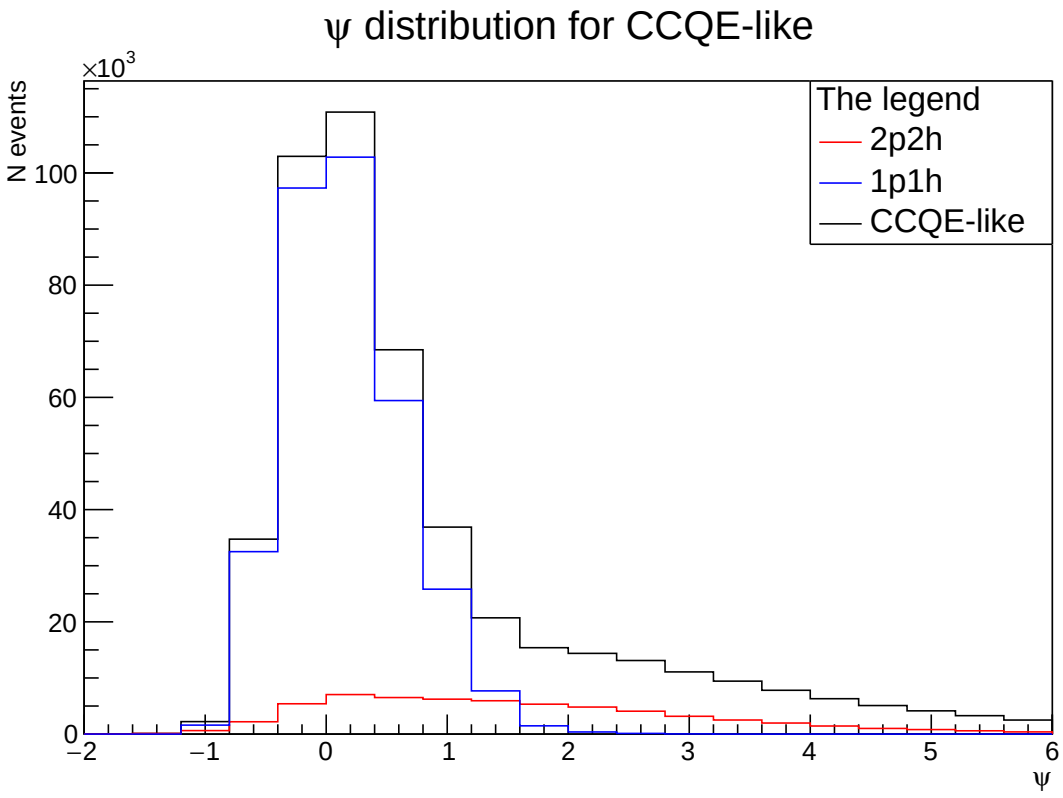

FIGURE 6.23: number of events versus Ψ' for 1p1h, 2p2h and CCQE-like for MiniBooNE data

of the neutrino energy as it is shown in figure 6.25.

- Some of the possible changes in the model, such as Binding Energy, will have an impact that depend on the neutrino energy. It could be reasonable that the difference of behaviour between the two sets of data came from a difference of effect of such parameters.

Even if we have no concrete indication from where the problem is, the Ψ' seems to be very sensitive to the way of detecting deviation and it should be used to evaluate data-MC comparison in the future.

6.3.4 MINERvA

6.3.4.1 Anti-neutrino

The composition of the NEUT simulation output interaction for the MINERvA anti-neutrino flux is presented in table 6.4. The MINERvA flux is of higher energy, therefore it is expected that there are more CC1π events than there is of 1p1h but with the selection used most of them are rejected. In this study, the double differential cross

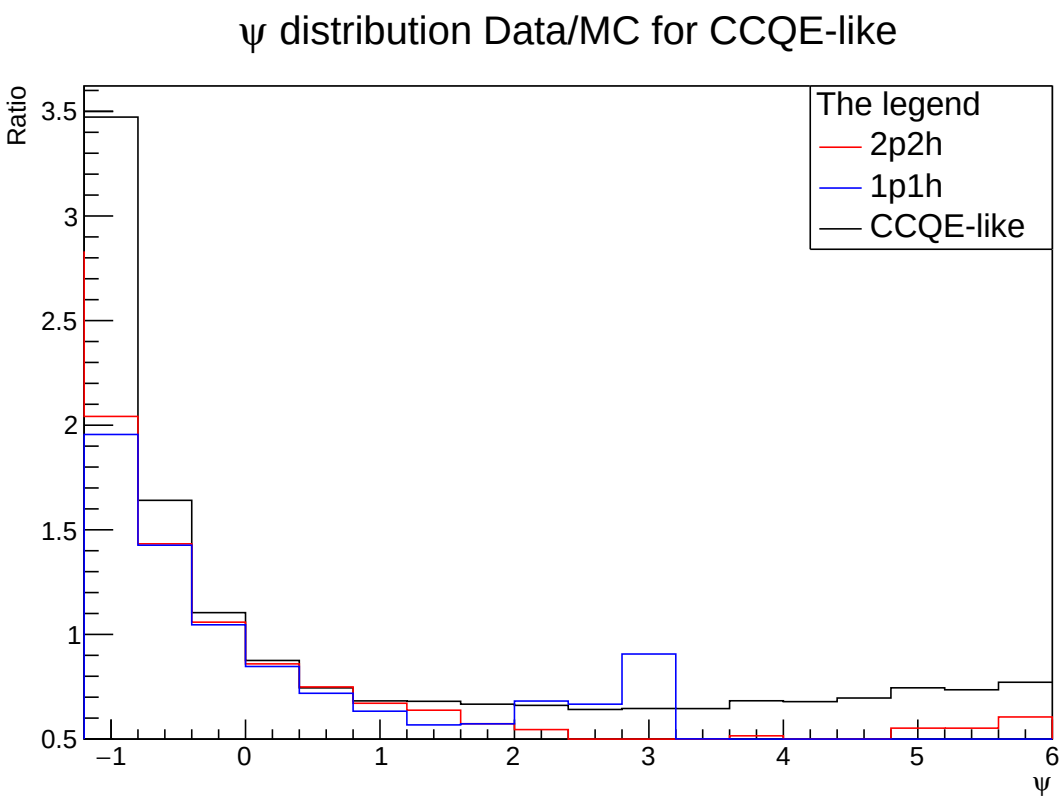

FIGURE 6.24: Ratio data divided by MC versus Ψ' for 1p1h and 2p2h and CCQE-like for MiniBooNE data

	selected			not selected	
interaction	1p1h	2p2h	CC 1π	CC 1π	NC
events (%)	17.8	4.8	4.4	45.8	27.2

TABLE 6.4: Composition of selected and non selected events for a NEUT file output using the MINERvA flux and MINERvA anti-neutrino CCQE-like selection method

section is presented with respect to transverse (p_T) and longitudinal (p_L) anti-muon momentum with $p_T = p_\mu * \sin(\Theta)$ and $p_L = p_\mu * \cos(\Theta)$. The comparison between the data and the neut prediction is shown in figure 6.26. From the study, most of the CCQE-like interactions happen in the kinematic region limited by $1.5\ GeV < p_L < 4\ GeV$ and $0.15\ GeV < p_T < 0.7\ GeV$ and it is confirmed by the simulation results. In addition, the simulation shows that with the detector region of acceptance we lose few events with low μ^+ momentum, with $p_L < 1.5\ GeV$. The data maximum cross section is for the kinematic region confined between $1.5GeV < p_L < 4GeV$ and $0.15 < p_T < 0.7GeV$, and the MC shown that the regions that are not covered by this MINERvA study are not too relevant in terms of cross section.

The data and the MC prediction show a good agreements with only a few relevant differences. The main relevant difference is shown for a kinematic region delimited by $2.5GeV < p_L < 3.5GeV$ and $0.25 < p_T < 0.7GeV$ as the MC show an underprediction

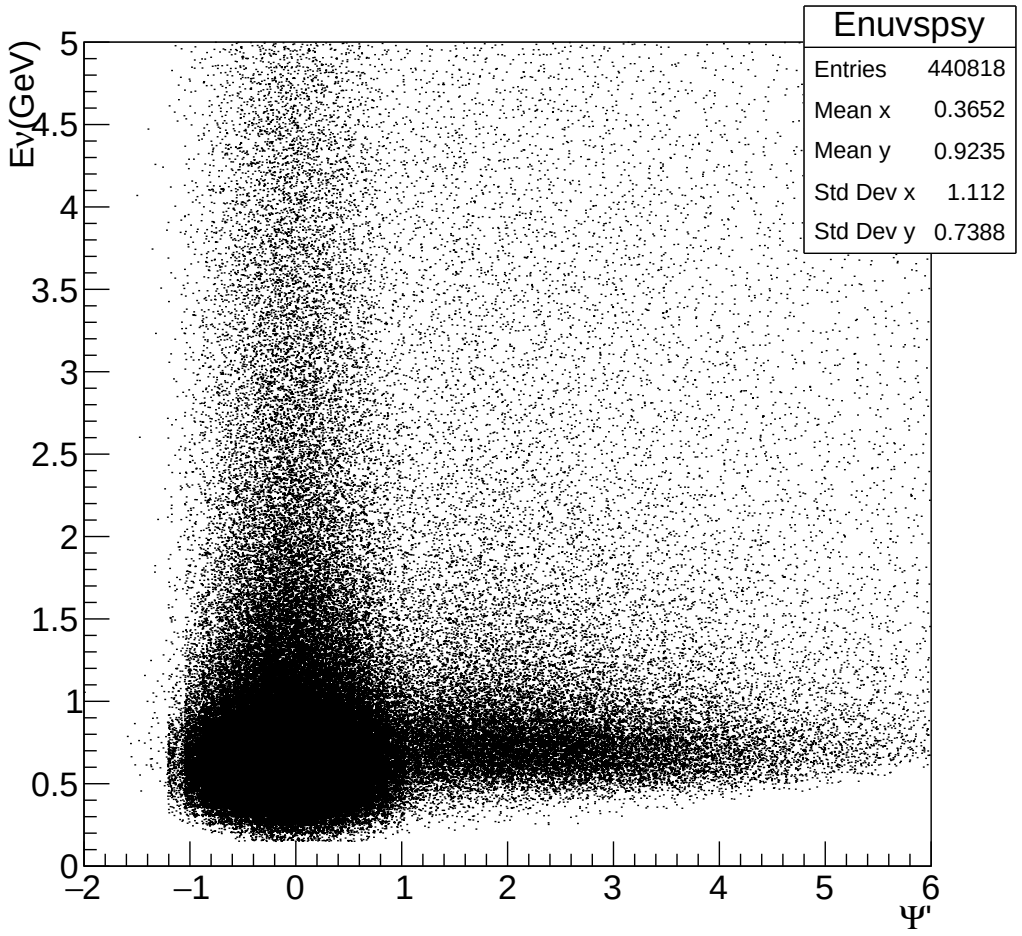

FIGURE 6.25: Distribution of the neutrino energy (GeV) events for each Ψ' value

of the data cross section.

We reproduce the method we used for the CC0pion studies of T2K and CCQE-like of MiniBooNE, and directly calculate and present the results with the scaling variable. This should be a valid comparison as again the selection of events is similar to the other study. The kinematics limits used in this study should not affect the result as most of the cross section is inside those limits.

The numbers of events versus Ψ' is presented in figure 6.27, and it is the same kind of number obtained in the previous analysis but there is a peak of 1p1h interaction close to $\Psi' = 0$. That peak come from anti-neutrino interactions with hydrogen for which the scaling principles do not apply. The anti-neutrino interaction on hydrogen are considered to be interaction on free nucleon in the NEUT MC. As such, there is no binding energy nor other nuclear effect correction added to the interaction, giving the shape of the Ψ' distribution.

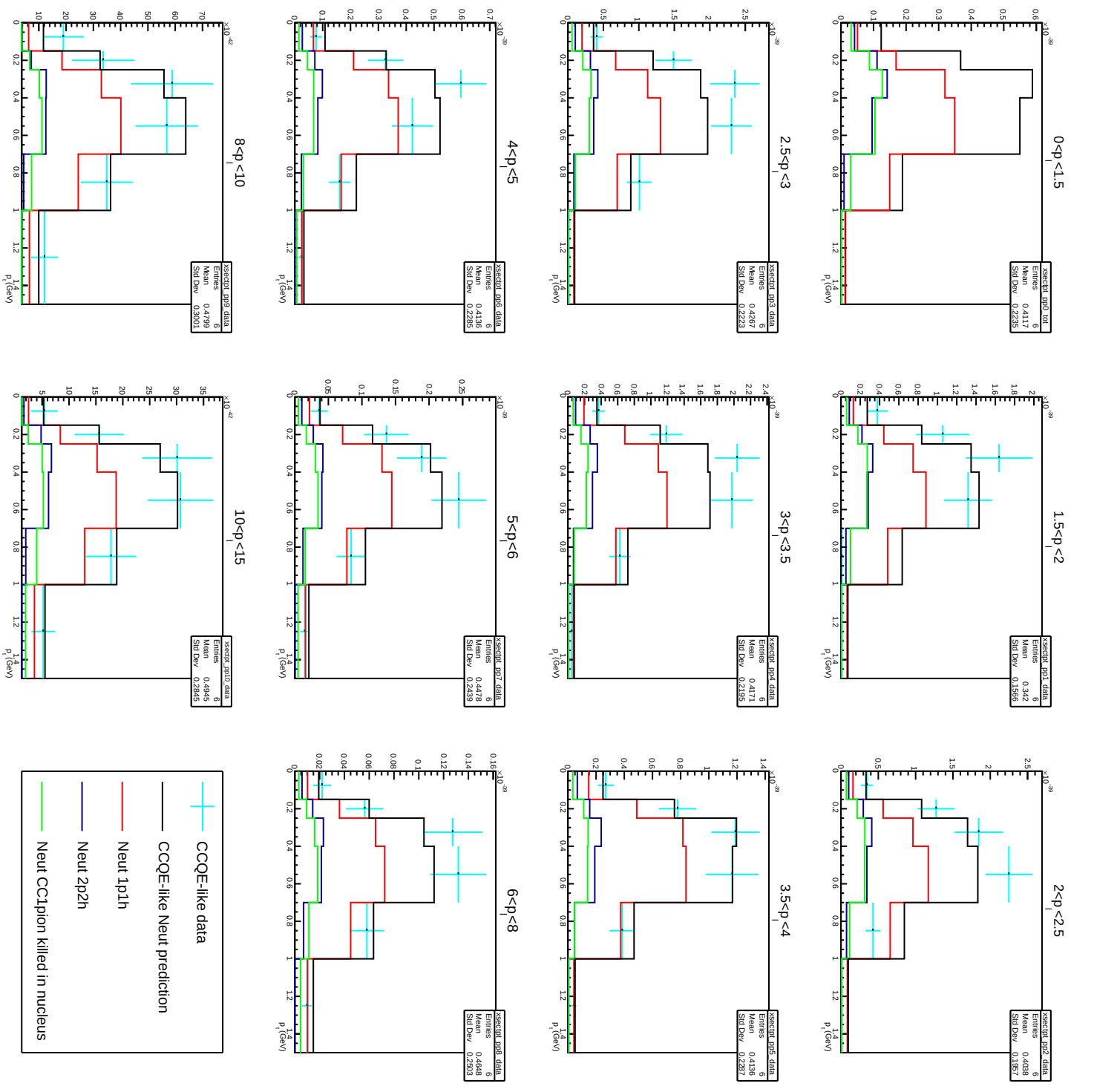

FIGURE 6.26: Comparison between data and NEUT MC prediction for MINERvA anti-neutrino double differential cross section with respect the transverse anti-muon momentum for each bin of longitudinal anti-muon momentum.

	selected			not selected	
interaction	1p1h	2p2h	CC 1π(not detected)	CC 1π	NC
events (%)	9.2	2.5	3.0	61.5	23.8

TABLE 6.5: Composition of selected and non selected events for a NEUT file output using the MINERvA flux and MINERvA neutrino CC0pion-like selection method

The resulting ratio versus Ψ' distribution is shown in figure 6.28, and for 1p1h interaction, that it still confined between -1.2 and 1.2, the ratio goes from 0.85 to 1.06 increasing with the scaling variable and passing to 1 around $\Psi' = 0.2$. That means our MC is overpredicting the cross section for low Ψ' values and underpredicting the cross section for high Ψ' values. It is the same behavior as the T2K CC0pion study, we can now confirm that the method used is correct and the problem of prediction encountered for the MiniBooNE study may come from the data of this study of from effects that are enhanced at low neutrino energies such as the Binding Energy. In figure 6.28, we can see the effect of the anti-neutrino interaction on hydrogen with the gap around $\Psi' = 0$ for 1p1h interaction where the peak of anti-neutrino hydrogen interaction is. The effect of this interaction that should be limited to a single Ψ' value are spread out due to the way we compute it, with the shifting energy, E_{shift}, that change the energy transfer in function of the momentum transfer. It seems to compensate over a few bins with the specific shape to be further analysed in another study.

6.3.4.2 Neutrino

The interactions composition of the NEUT simulation output for the MINERvA neutrino study is presented in table 6.5. We can see that most of the events are CC 1π as expected from the MINERvA flux and most of them are rejected by the selection. The aim of the study is to constraint nuclear effects in neutrino interaction by measuring particular transverse variables. Those variables have been proposed in [94] to obtain information on the nuclear initial and final states effect.The variable, $\delta\phi_T$ and $\delta\alpha_T$, are schematized in figure 6.29. Before defining the transverse variables in neutrino nucleus interactions, we determine an imbalance, $\delta\overrightarrow{p}$ between the initial neutrino momentum and the sum of the final state lepton and hadron momentum. This imbalance is defined as the sum of the target nucleon motion and all the intranuclear momentum exchange, meaning all nucleon correlations and the final state interaction. So the imbalance is, in the limit where there is no intranuclear momentum exchange, the transverse target nucleon momentum.

The schematic representation of figure 6.29 shows the decomposition of the interaction kinematic into longitudinal and transverse component with respect to the neutrino

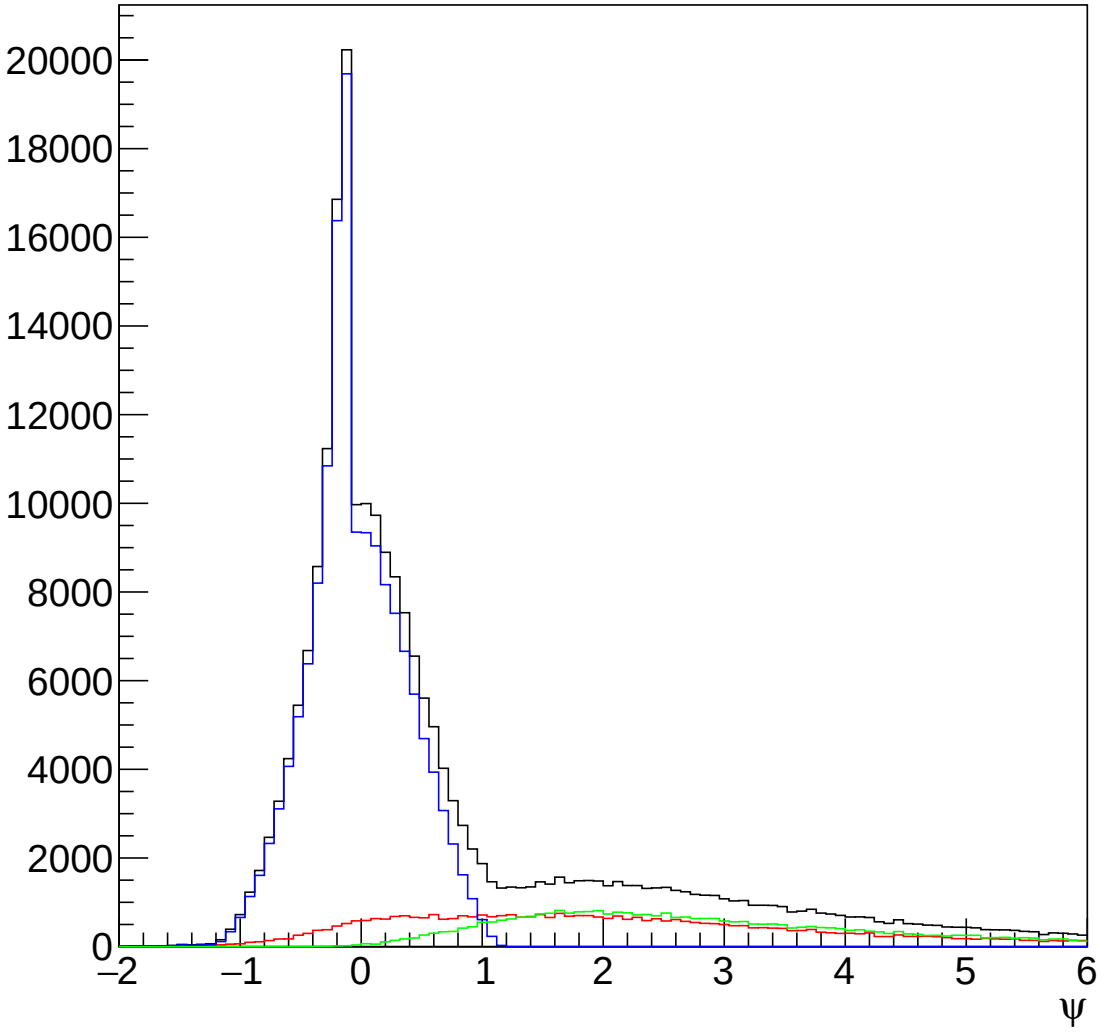

FIGURE 6.27: number of events for each interaction using NEUT MC in function of the scaling variable for MINERvA anti-neutrino CC0pion-like study. Black line is all selected events, blue line is 1p1h events, red line is 2p2h events, green line is selected CC-others events

direction. So the energy-momentum conservation can be written:

$$p_\nu = p_L^l + p_L^{N'} - \delta p_L \tag{6.2}$$

$$\overrightarrow{0} = \overrightarrow{p}_T^{\,l} + \overrightarrow{p}_T^{\,N'} - \delta \overrightarrow{p}_T \tag{6.3}$$

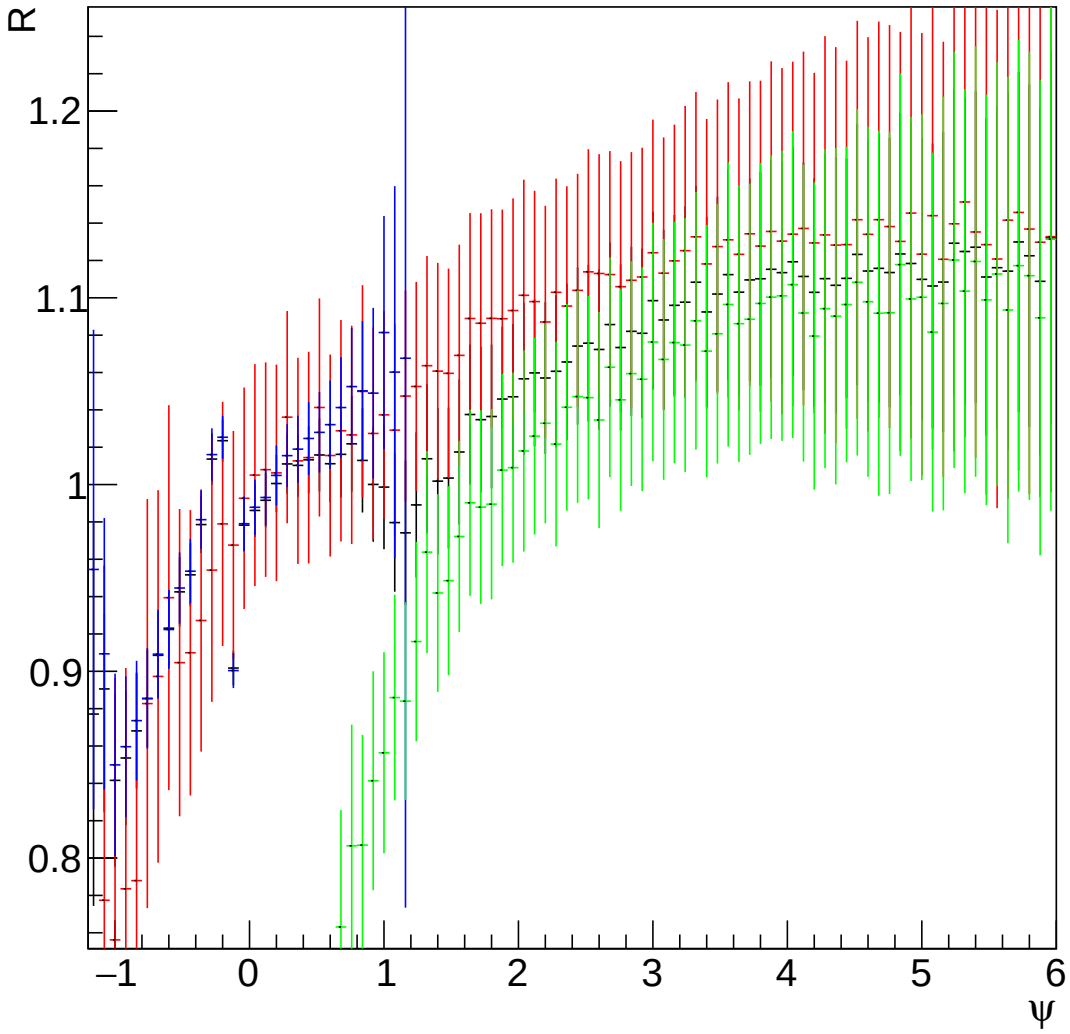

FIGURE 6.28: Ratio data divided by NEUT MC using the scaling variable Ψ' for MINERvA anti-neutrino CC0pion-like study. Black line is all selected events, blue line is 1p1h events, red line is 2p2h events, green line is selected CC-others events

where $\overrightarrow{p_\nu} = \overrightarrow{E_\nu}$ is the neutrino momentum, $\overrightarrow{p^l}$ the lepton momentum and $\overrightarrow{p^{N'}}$ the proton momentum. Then the transverse variables are defined as

$$\delta\phi_T = arccos\frac{-\overrightarrow{p}^l_T.\overrightarrow{p}^{N'}_T}{p^l_T p^{N'}_T} \tag{6.4}$$

$$\delta\alpha_T = arccos\frac{-\overrightarrow{p}^l_T.\delta\overrightarrow{p}_T}{p^l_T \delta p_T} \tag{6.5}$$

With the transverse variables properly defined, we can use them for the comparison between data and simulation.

Figure 6.30 shows the differential cross section in respect to $\delta\phi_T$ and figure 6.31 shows

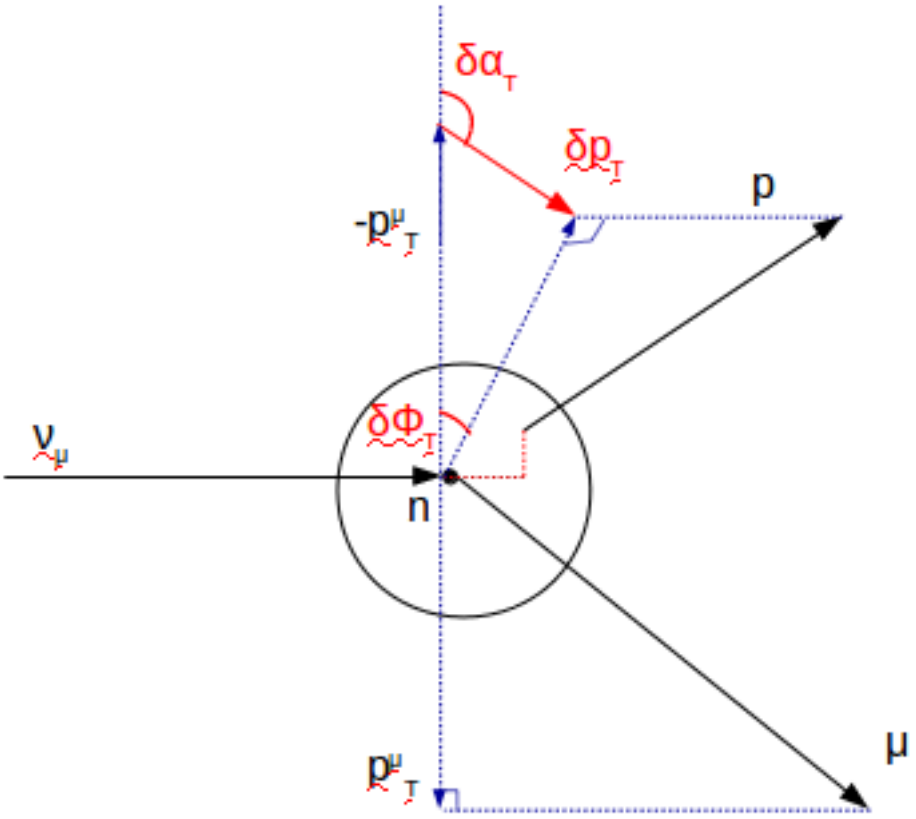

FIGURE 6.29: Schematic definition of the transverse kinematics from [94]

the differential cross section in respect to $\delta\alpha_T$. The comparison between prediction and data using the $\delta\phi_T$ variable shows that there is a good agreement in general with only small deviations. It seems for this variable every backward event is either 2p2h or RES, DIS and others background, with nearly no 1p1h events. For very forward events, $\delta\phi_T < 20°$, we have the majority of the 1p1h events, with very few 2p2h or Res events. As for the high angle events, neither interactions are dominant.

The differential cross section in respect to $\delta\alpha_T$ is more interesting. For the most forward angles, $\delta\alpha_T < 20°$ the simulation is underpredicting the cross section. Then, for most of the angles, $60° < \delta\alpha_T < 150°$, the simulation is overpredicting the cross section. At backward angles, $150° < \delta\alpha_T < 180°$, we see that as the data cross section diminishes the simulation prediction stabilizes. The behavior of the 1p1h differential cross section prediction is the same as for the total differential cross section prediction except it continues to increase for backward events. These results show that the different models used here still have limitation on the predictions.

We show the different non-transverse variables in figures 6.32, 6.33, 6.34. For the muon kinematic, both momentum (6.32) and angle (6.33), we see that data and NEUT

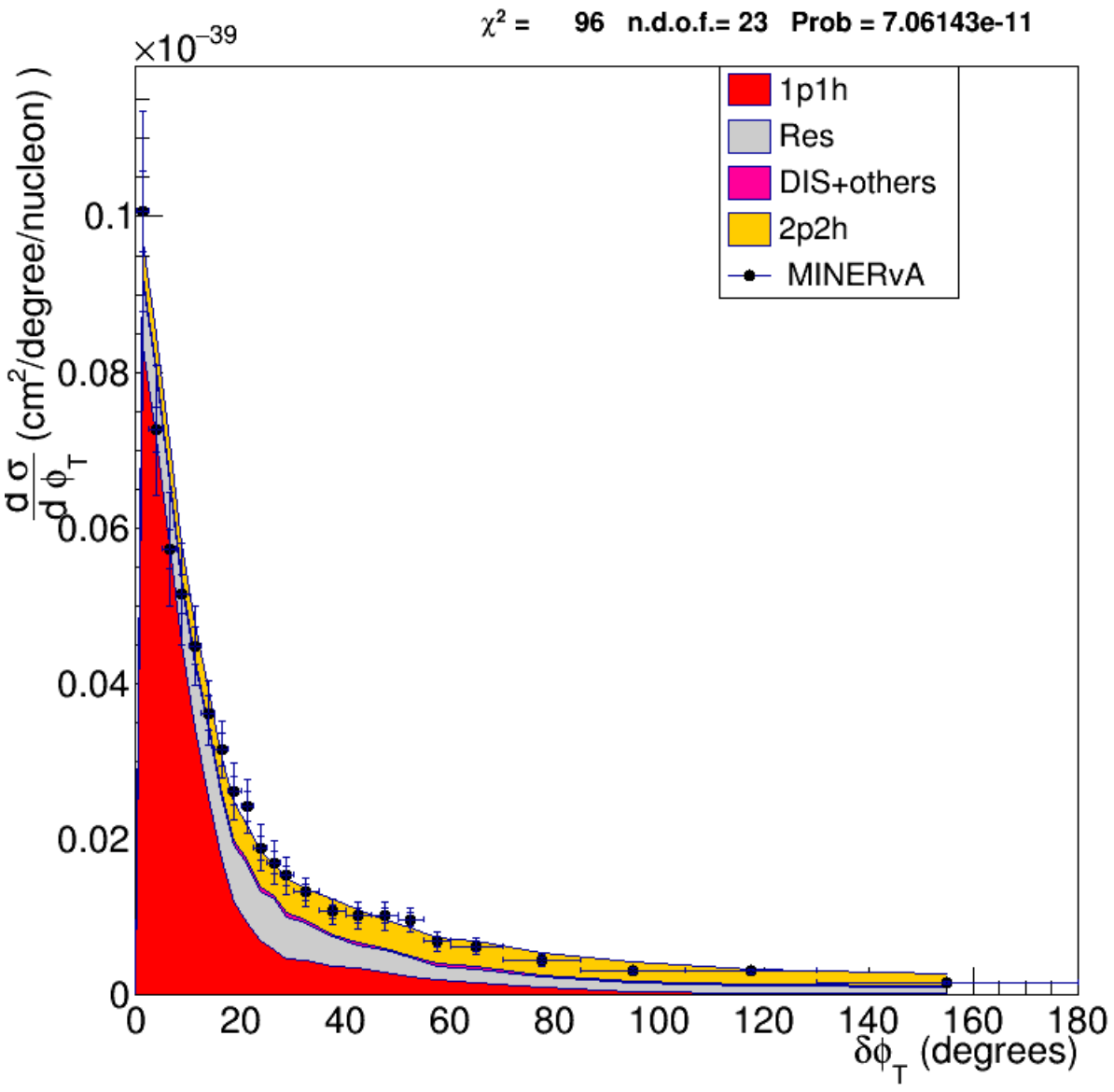

FIGURE 6.30: comparison between NEUT MC and data for the differential cross section in $\delta\phi_T$ of neutrino with MINERvA data.

prediction have an overall good agreement. We can see an interesting behavior in muon momentum where there is a slight overprediction by NEUT between 3 and 4 GeV and an underprediction around 7 GeV. Whereas for the muon angle, we only see punctual deviation prediction. For the proton momentum (6.34) we see an overall good agreement, with some slight overprediction by the MC between 0.7 and 0.8 GeV and some underprediction around 1.1 GeV. For these variables, we cannot separate the different interactions as we could in the $\delta\phi_T$ variable prediction. We also see that, apart from the muon momentum variable, the other non-transverse variables only show punctual deviation from the data cross section and not some dependency like the $\delta\alpha_T$ variable

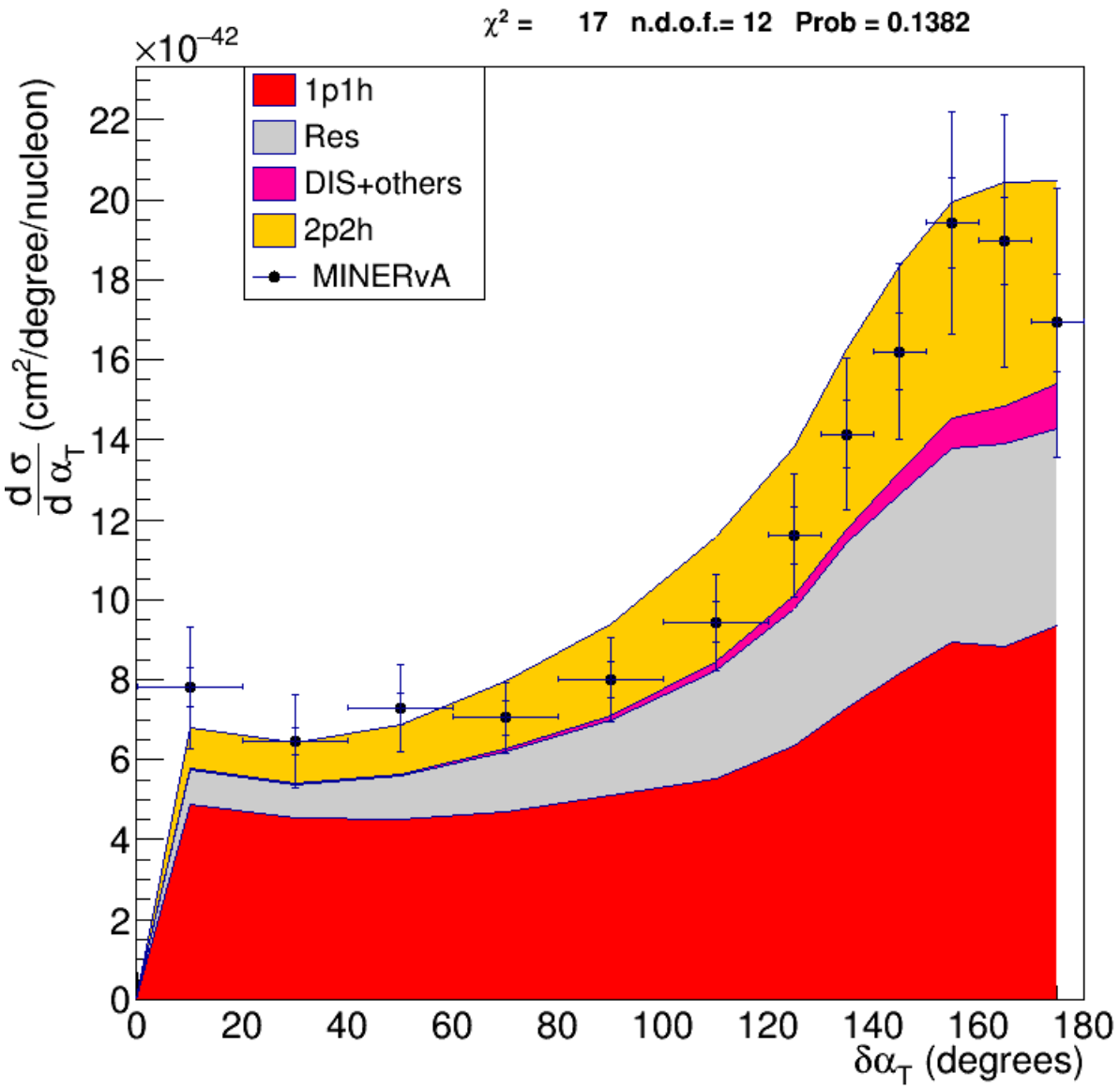

FIGURE 6.31: comparison between NEUT MC and data for the differential cross section in $\delta\alpha_T$ of neutrino with MINERvA data.

prediction.

Since the transverse variable are used to obtain nuclear information, the difference of prediction between the previous model used in NEUT, the RFG model, and the one we implemented should be significant. We expect that the difference in nucleus modelization to have an important impact on these variables. We shown in figure 6.35 and 6.36 the cross section comparison between the MINERvA data and the prediction by the simulation when using the RFG model for 1p1h interaction for the two transverse variables $\delta\phi_T$ and $\delta\alpha_T$. For the $\delta\phi_T$ variable, the cross section shows a clear overprediction by the simulation for forward angle. We also see a slight underprediction for high angle.

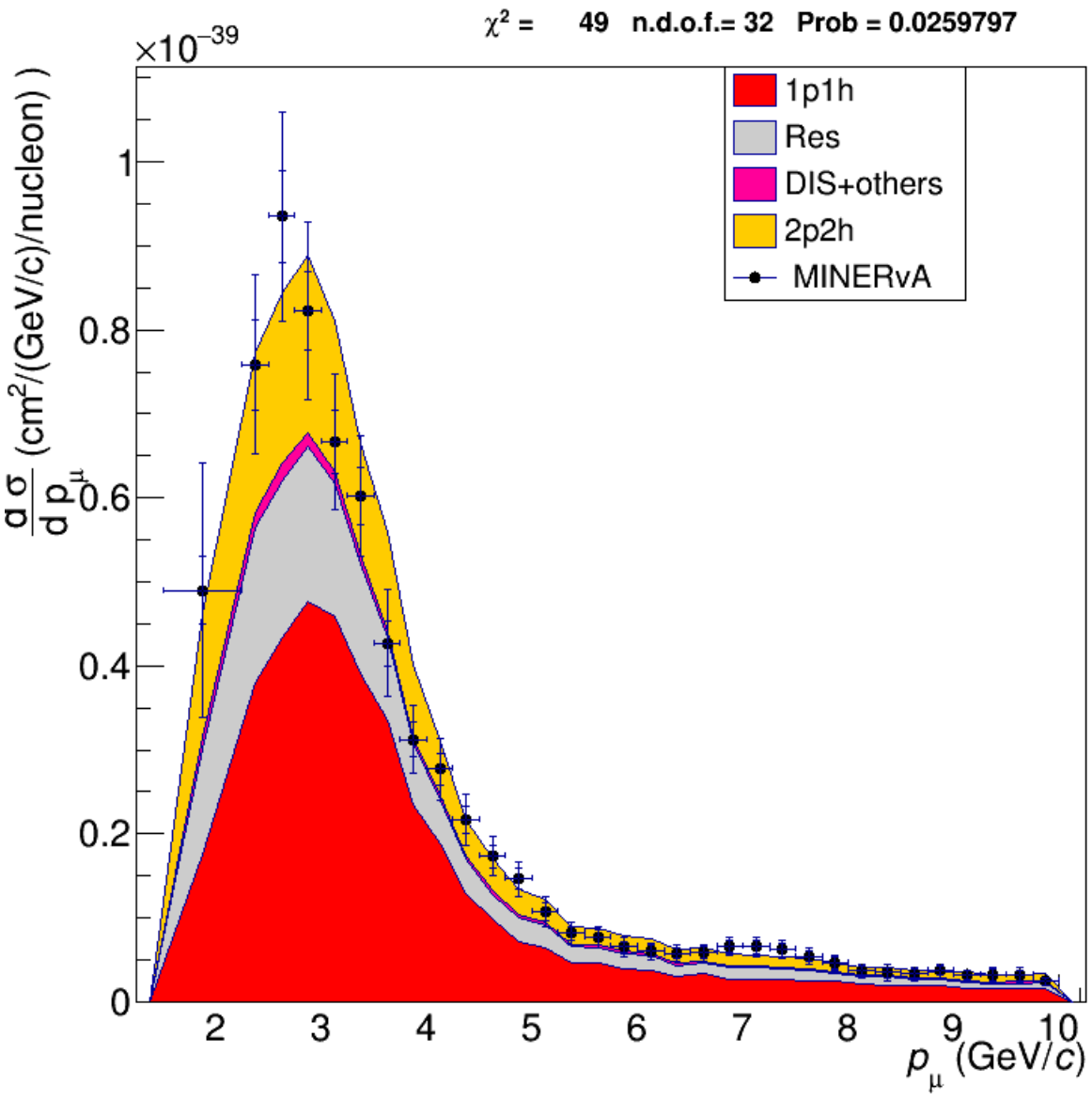

FIGURE 6.32: comparison between NEUT MC and data for the differential cross section in p_μ of neutrino with MINERvA data.

As for the $\delta\alpha_T$ variable, the shape of the data is not reproduced by the simulation. We can see that the simulation overpredicts the cross section for $\delta\alpha_T < 150°$.
For both transverse variables, using the RFG model for the 1p1h interaction leads to a different shape of the cross section compared to the LFG model. This result proves that the LFG model with its more realistic nuclear modelization than the RFG, has a better cross section prediction for hadron related variables.

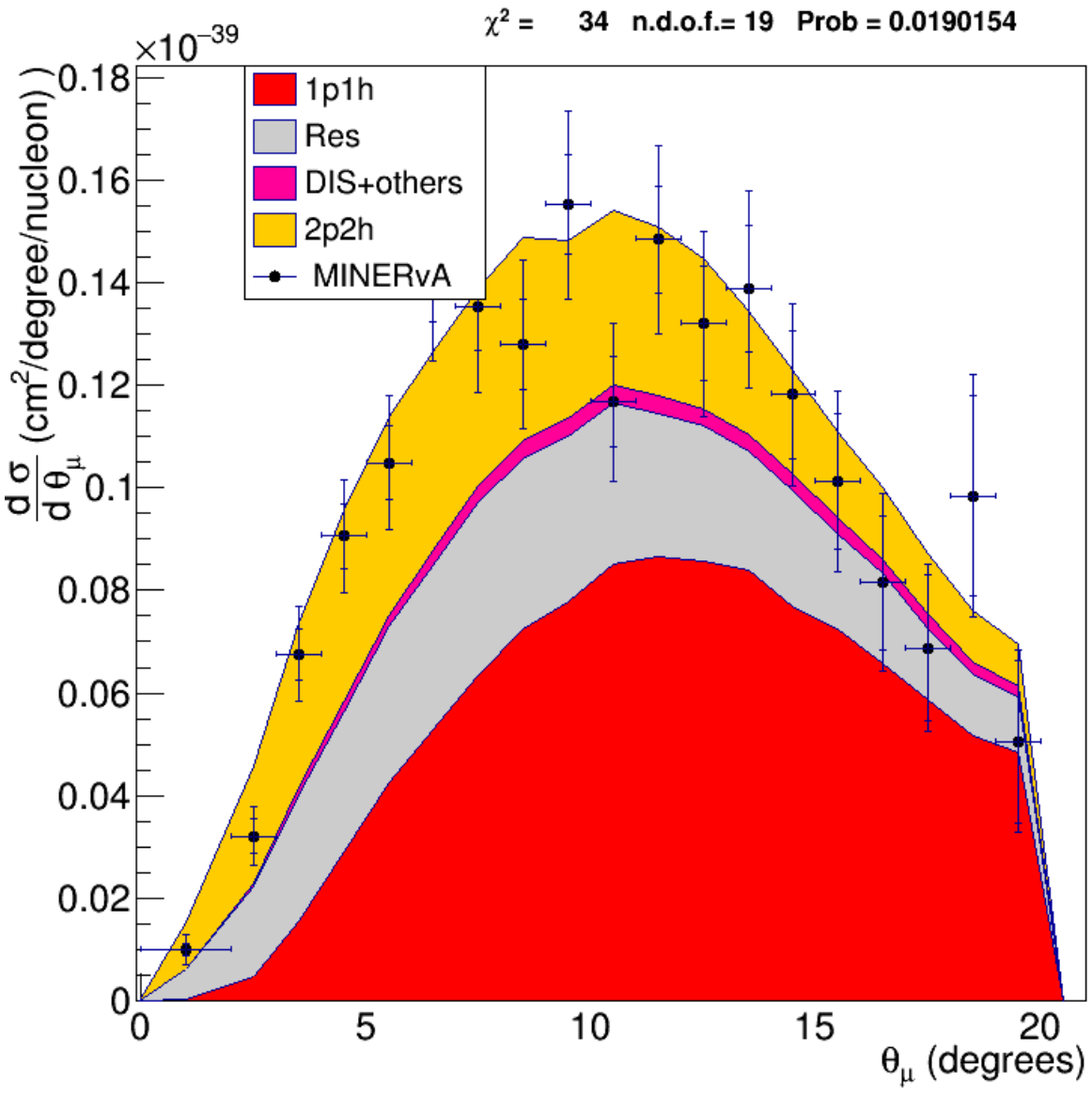

FIGURE 6.33: comparison between NEUT MC and data for the differential cross section in θ_μ of neutrino with MINERvA data.

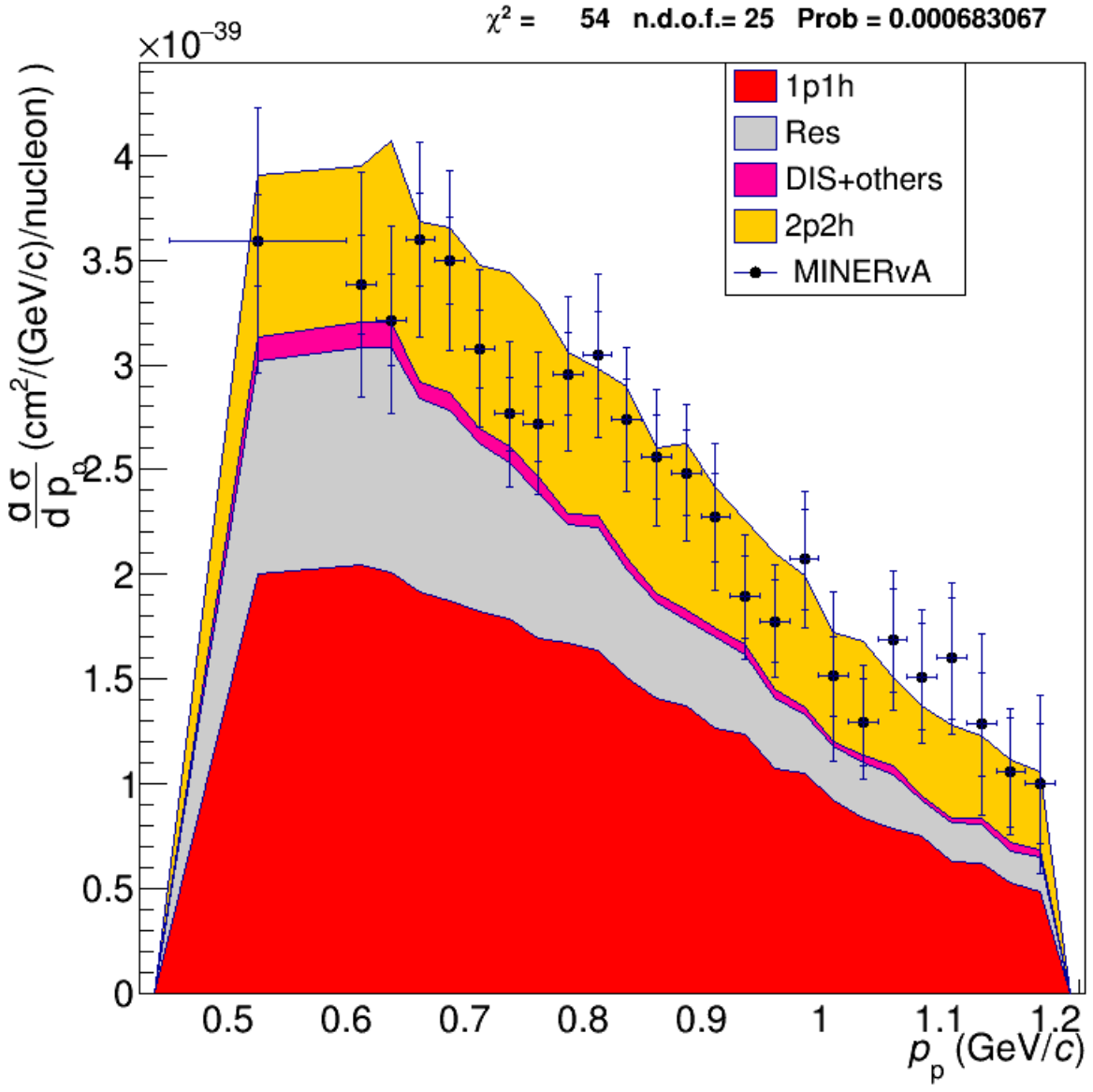

FIGURE 6.34: comparison between NEUT MC and data for the differential cross section in p_p of neutrino with MINERvA data.

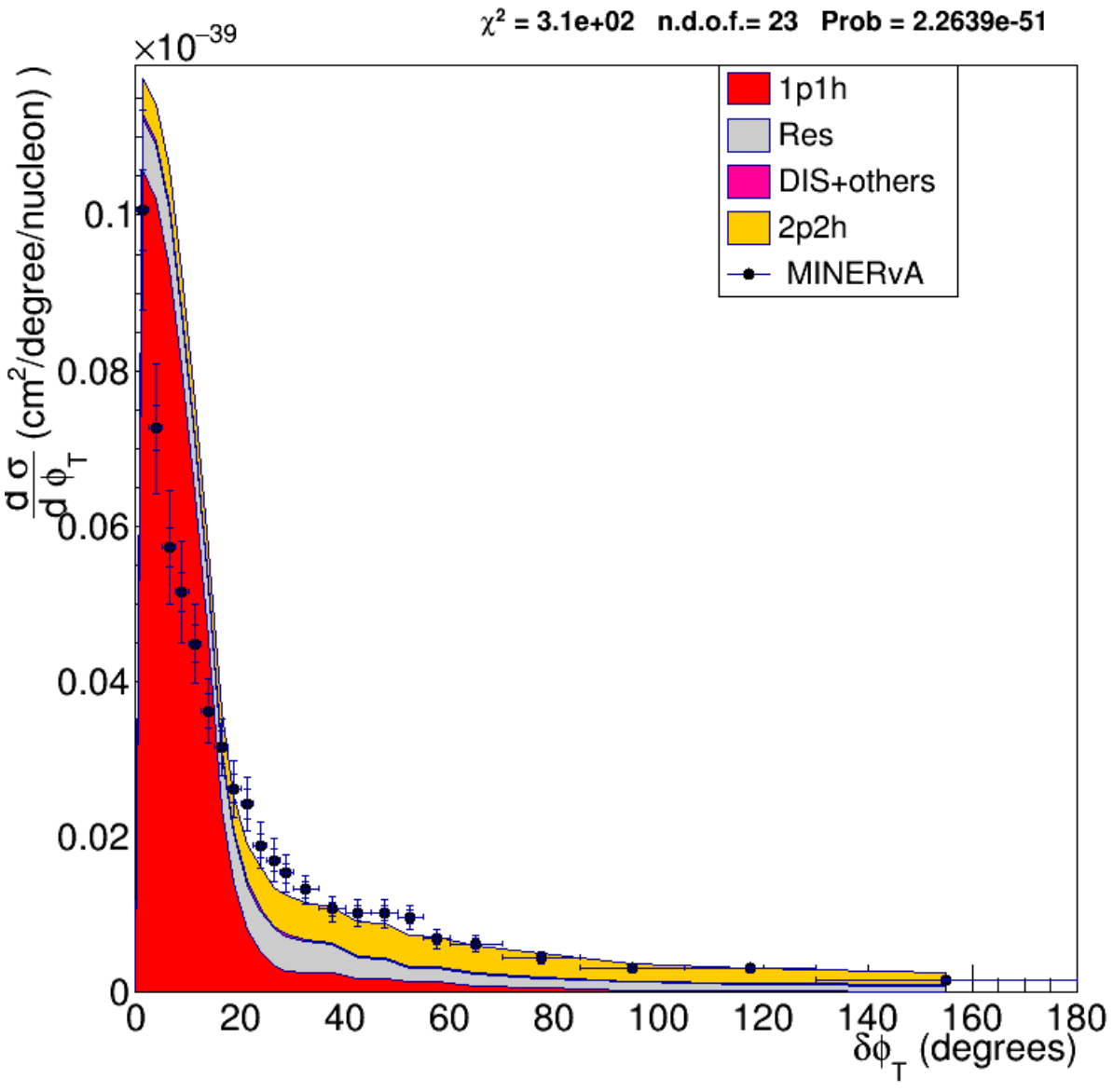

FIGURE 6.35: comparison between simulation and data for the differential cross section in $\delta\phi_T$ of neutrino with MINERvA data. 1p1h model used is the previous NEUT model.

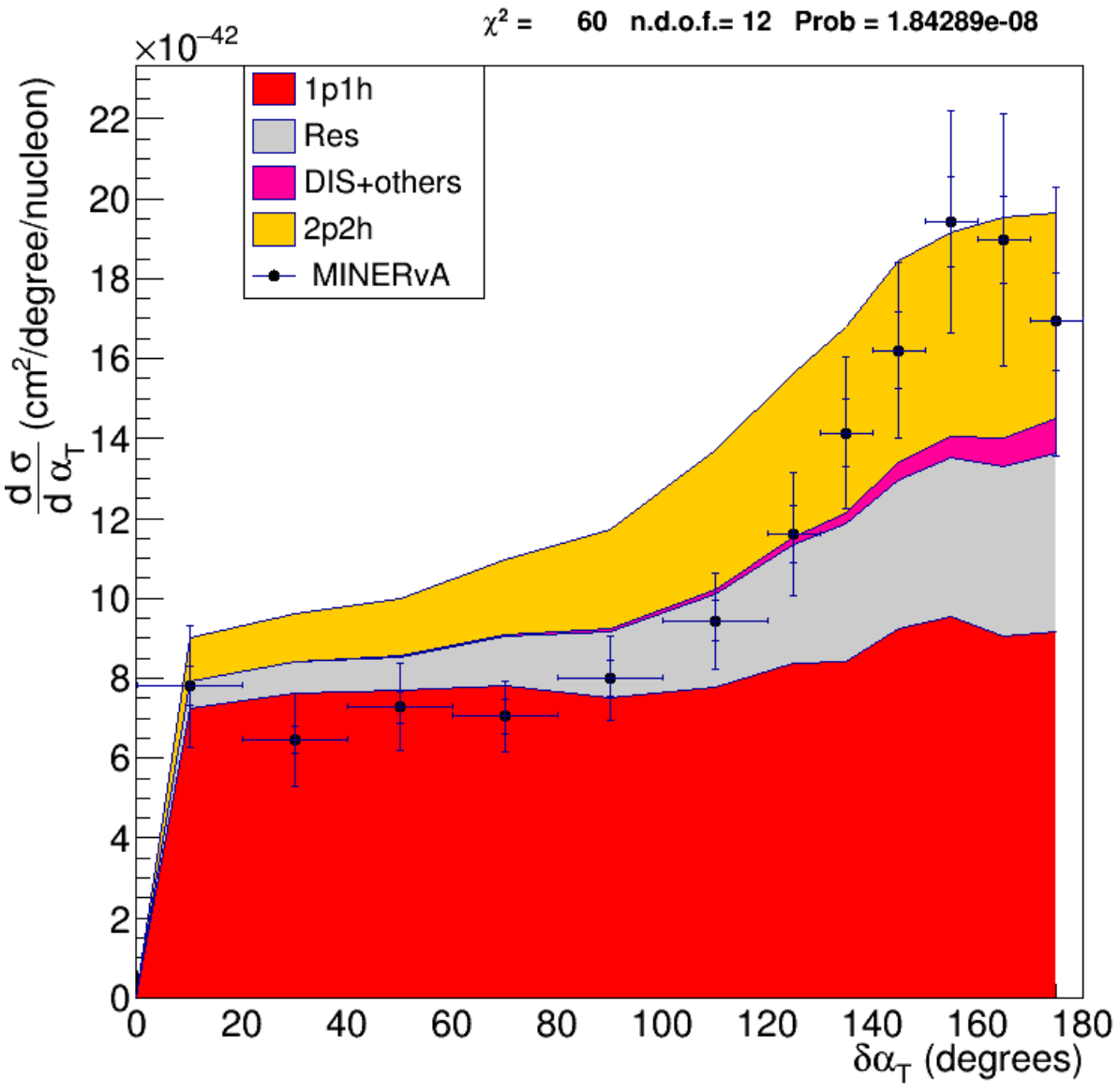

FIGURE 6.36: comparison between MC and data for the differential cross section in $\delta\alpha_T$ of neutrino with MINERvA data. 1p1h model used is the previous NEUT model.

Chapter 7

Conclusion

In this thesis, we have presented the model which we have implemented in NEUT. We have been using a neutrino nucleus scattering interaction model developed by Nieves et al [72]. The main characteristic of this model is the use of a local Fermi gas for the nucleus. This allows the cross section computation to provide the complete interaction kinematics. Using this cross section calculation model we have developed a Monte Carlo simulation predicting the interaction kinematics.

We have implemented the MC in the neutrino event generator and verified that the implementation was done without any error by comparing the output of the MC before and after the implementation. With the completion of the implementation, the LFG model has been made to be the default model used in the newest version of NEUT.
We tested the new version of NEUT using cross section studies from three different experiments, T2K, MiniBooNE and MINERvA. For the comparison with T2K data we used two studies, one in which the selected events had no pion, the so-called CC0π, and one in which the only selection criteria was to have a muon in the final state, called CC inclusive. For the MiniBooNE data we used a study with a selection of events without pion and the MINERvA studies used had a similar condition but with added kinematics constraints due to the detector geometry. Out of the two MINERvA studies we used, one was realized using anti-neutrinos and the other used neutrinos and was realized using the transverse variables. The NEUT predictions were in good agreement with the T2K and MINERvA data but showed discrepancy with the MiniBooNE data. We discussed that this discrepancy could be the results of either the background events or some energy dependent parameters in the mode.

One of the important verification we had to do was to compare the prediction of NEUT using the LFG based model we implemented with NEUT using the RFG model that was

used before to show that the use of this model is an improvement. The comparison shows that cross section prediction are not too different if you observe the lepton kinematics. Even more, some of these differences are due to a nucleus modelisation parameter, the axial mass. The axial mass is not chosen to be of the same value for each model as a result of it being determine by the best accuracy value to reproduce the scattering data. The old and new version of NEUT show significant difference when one uses the hadron variables. This difference were expected as the modelisation of the nucleus is the main difference between the two models. The result shows that with the prediction of the kinematics of the new model we will not affect significantly the study using only lepton kinematics but once a study include selection based on hadron kinematics, such as a CC inclusive study with one proton in the final state, the new model will have a significantly different prediction than the old one. This is verified in the transverse variable study of the MINERvA experiment where the new model gives prediction closer to the data cross section than the previous one for all the hadron related variables.
The comparison we performed between the NEUT cross section prediction and the data cross section using the transfer energy and momentum on one side and the scaling variable on the other side had the goal to see the limits of the model. We see that using the transfer energy and momentum showed a complex dependency on both variable but it was unclear how to obtain any information from this so we tried to use the scaling variable. There we had a clear dependency on the scaling variable and we could distinguish to a certain extend between the different interactions. With this we could find one of the limitations of the model, the removal energy that is defined as a fixed value in the model. This parameter depends on the nature of the nucleus and whether the interaction is with neutrino or anti-neutrino and is used to represent the minimal energy required to extract the nucleon from the nucleus. But in reality the energy used during the interaction can be higher or lower if the nucleus is not at rest. Thus using a fixed value is a simplification that could be improved using a randomized value. The first test on using a randomized value for the removal energy showed some promising results with the average ratio becoming flatter in function of the scaling variable. But it will require a dedicated study.

To summarize, we have built a working MC simulation for the CCQE interaction using the LFG model developed by Nieves et al. [72] This MC is now the basic option for CCQE interaction in NEUT, one of the official neutrino event generator of the T2K collaboration. And we have explored some of the limitation of the model.

Appendix A

Implementation of the model inside NEUT generator

The Monte Carlo simulation of the LFG has been implemented in NEUT. The implementation necessitated to build an interface between the two programs. The first role of this interface is to have the variable defined in NEUT be assigned to the equivalent variable in the MC. In this appendix, we will discuss how this interface is build. The interface has two principal functions that are directly called by NEUT, one to obtain the cross section and one for the kinematics. These two functions also use another function to initialize the MC.

A.1 Initialization

In NEUT, the generator parameters are specified in a card as we explained in chapter 5.2. Whereas in the LFG MC simulation, the nucleus information are stored in table and has to be selected before calculation of the cross section and kinematics. The interface contains an initialization function that is called each time the principal functions of the interface are used. This initialization function reads the parameters in NEUT and rewrites the configuration card of the MC. Then the MC is initialized according to the process described in chapter 4.2. Once the initialization is done once and the look-up table are written, this process will not be repeated.

A.2 Cross section

NEUT selects the cross section channel by selecting one interaction type (CCQE,CCRes, etc..) for a given neutrino energy, neutrino type and nuclei. The LFG code has pre-computed the cross section as function of the energy and stored into look-up tables. Look-up table are stored in files so the initialization process is faster and calculation are done only once. The interface use this function to return the cross section. The function takes as parameter inputs an energy value of the neutrino, a neutrino type and whether this is an antineutrino or not. The type of nuclei is obtained from the parameters value written in the NEUT card with its atomic numbers. The cross section is then obtained by asking the MC to calculate the value of the cross section using the look-up table and the following function:

```
1   int ibin = (int) ((Enu+Enubin*0.001)/Enubin);
2
3   Precompindx pindx(id,nuclei);
4
5   double a0 = IntCrossSection[pindx][ibin];
6   double a1 = IntCrossSection[pindx][ibin+1];
7
8   int binmax = Emax/Enubin;
9
10  double cross_section;
11
12  if( ibin+1  < binmax )
13     cross_section = (a1-a0)/Enubin*(Enu-Enubin*(double)ibin)+a0;
14  else if ( ibin >= binmax  )
15     cross_section = IntCrossSection[pindx][binmax-1];
16  else if ( ibin < binmax )
17    cross_section = a0;
18  else
19    cross_section = 0.0;
20
21  return cross_section;
```

Listing A.1: Function used to read the look-up table

This function take energy value with a minimum depending on the type of neutrino and a maximum up to 9.5 GeV, energy value beyond is taken to be 9.5 GeV. For energy values below 3 MeV for electron neutrino, 150 MeV for muon neutrino and 3.5 GeV for tau neutrino the cross section is taken to be 0. The cross section is linearly interpolated and returned.

$$\mathrm{P}= \begin{vmatrix} \mathrm{E}_1 & \mathrm{E}_2 & \mathrm{E}_3 & \mathrm{E}_4 \\ \mathrm{P}_x^1 & \mathrm{P}_x^2 & \mathrm{P}_x^3 & \mathrm{P}_x^4 \\ \mathrm{P}_y^1 & \mathrm{P}_y^2 & \mathrm{P}_y^3 & \mathrm{P}_y^4 \\ \mathrm{P}_z^1 & \mathrm{P}_z^2 & \mathrm{P}_z^3 & \mathrm{P}_z^4 \end{vmatrix} \quad \mathrm{idpart}= \begin{vmatrix} \mathrm{id}_1 \\ \mathrm{id}_2 \\ \mathrm{id}_3 \\ \mathrm{id}_4 \end{vmatrix} \quad \mathrm{parent}= \begin{vmatrix} \mathrm{id}_{parent1} \\ \mathrm{id}_{parent2} \\ \mathrm{id}_{parent3} \\ \mathrm{id}_{parent4} \end{vmatrix}$$

TABLE A.1: Vectors built for the function to transfer the kinematics information

A.3 Kinematics

This function takes as parameter inputs the type of neutrino and whether this is an antineutrino or not, the energy value of the neutrino and the direction of the neutrino. Once again nucleus information is taken from the parameters value written in the NEUT card with its atomic numbers. Three vectors are build here, they will be used to store the kinematics, the particles identity and its parent in the function as shown in table A.1. The function run the MC using the entry parameters. During the MC run, the kinematics parameters used are the neutrino energy, E_ν, depending on the lepton kinetic energy, t_{lep}, neutrino lepton angle, $\theta_{\nu lep}$, radial position of interaction in the nucleus and target nucleon momentum, R, the transfer energy and momentum, $q0$ and dq, the target nucleon momentum, p_t, and angle, θ_{tp}. The kinematics is then computed from those parameters, adding two angle taken randomly between 0 and π, ϕ_1 and ϕ_2. These two angles are the azimuth angles of the outgoing lepton and the target nucleon that are not constrained by the interaction due to symmetry. The energy is computed through the formula $E = \sqrt{m^2 + p^2}$ and the vectors are built using the following function:

```
1         SUBROUTINE comptmomentum(dnu)
2        IMPLICIT REAL*8 (A-H,O-T,V-Z)
3        IMPLICIT COMPLEX*16 (U)
4
5  C      DATA DPI/3.141592653589793D0/
6
7        COMMON/datos/dpi,hbarc,GF0,DMNU,DMA
8        COMMON/datos2/dmneutrino,dmlepton,dmi,dmf,
9       f     coscabibbo,dmuon,dmelectron,dmtau,xuma
10       DIMENSION dt1(3),dt2(3),dt3(3),dnu(3)
11       DIMENSION y(3),clone(3)
12       DIMENSION vPnu(4),vPmu(4),vPn(4),vPp(4),vq(4)
13       COMMON/fourvectors/vPnu,vPmu,vq,vPn,vPp
14
15       COMMON/ENERGY/Enu,Emu,Eq,En,Ep
16       COMMON/ANGLE/theta,thetap
17       COMMON/momentum/pm,dqt,dPt,P
18       COMMON/coulomb/coul
19
20 #ifndef __GFORTRAN__
21       INTEGER*4 IDUM
22       REAL*4    RLU
23       EXTERNAL  RLU
24 #endif
```

```
25
26          DPI = 3.141592653589793D0
27    #ifdef __GFORTRAN__
28          CALL RANDOM_NUMBER(A)
29    #else
30          A = RLU(IDUM)
31    #endif
32          PHI=2.D0*DPI*A
33
34          ct=dcos(theta)
35          st=dsin(theta)
36
37          cp=dcos(phi)
38          sp=dsin(phi)
39    C
40    C  Reference system
41    C
42          dnunorm = dsqrt(dnu(1)*dnu(1)+dnu(2)*dnu(2)+dnu(3)*dnu(3))
43
44          dt3(1)  = dnu(1)/dnunorm
45          dt3(2)  = dnu(2)/dnunorm
46          dt3(3)  = dnu(3)/dnunorm
47    c
48    c If dt3 is parallel to y then use x as perpendicular.
49    c
50          if( dt3(2).eq.1 ) then
51             y(1) = 1.
52             y(2) = 0.
53             y(3) = 0.
54          else
55             y(1) = 0.
56             y(2) = 1.
57             y(3) = 0.
58          endif
59
60          dt1(1) =  y(2)*dt3(3)-y(3)*dt3(2)
61          dt1(2) =  y(3)*dt3(1)-y(1)*dt3(3)
62          dt1(3) =  y(1)*dt3(2)-y(2)*dt3(1)
63
64          dt1norm = dsqrt(dt1(1)*dt1(1)+dt1(2)*dt1(2)+dt1(3)*dt1(3))
65
66          dt1(1)  = dt1(1) / dt1norm
67          dt1(2)  = dt1(2) / dt1norm
68          dt1(3)  = dt1(3) / dt1norm
69
70          dt2(1) =  dt3(2)*dt1(3)-dt3(3)*dt1(2)
71          dt2(2) =  dt3(3)*dt1(1)-dt3(1)*dt1(3)
72          dt2(3) =  dt3(1)*dt1(2)-dt3(2)*dt1(1)
73    C
74    C   Energy
75    C
76          vPnu(1) = Enu
77          vPmu(1) = Emu
78          vq(1)   = Eq
79          vPn(1)  = En
```

```
80          vPp(1)   = Ep
81    c
82    C     coulomb potential modification
83    c
84          Emuloc=Emu-coul
85
86          if( Emuloc.lt.(DMF*hbarc) ) then
87             Emuloc = DMF*hbarc
88          endif
89
90          pmuloc=DSQRT(Emuloc**2-(DMF*hbarc)**2)
91    C
92    C     3-momentum for the lepton.
93    C
94          do i = 2 , 4
95             vPnu(i)= dt3(i-1)*Enu
96             vPmu(i)=(dt3(i-1)*ct + dt1(i-1)*st*cp + dt2(i-1)*st*sp)*pm
97             clone(i-1)=vPmu(i)*pmuloc/pm
98    c         vq(i)=vPnu(i)-vPmu(i)
99             vq(i)=vPnu(i)-clone(i-1)
100         enddo
101   C
102   C  Build the new reference system along q3
103   C
104         vqnorm = dsqrt(vq(2)*vq(2)+vq(3)*vq(3)+vq(4)*vq(4))
105
106         dt3(1)   = vq(2) / vqnorm
107         dt3(2)   = vq(3) / vqnorm
108         dt3(3)   = vq(4) / vqnorm
109
110         if( dt3(2).eq.1 ) then
111            y(1) = 1
112            y(2) = 0
113            y(3) = 0
114         else
115            y(1) = 0
116            y(2) = 1
117            y(3) = 0
118         endif
119
120         dt1(1) =  y(2)*dt3(3)-y(3)*dt3(2)
121         dt1(2) =  y(3)*dt3(1)-y(1)*dt3(3)
122         dt1(3) =  y(1)*dt3(2)-y(2)*dt3(1)
123
124         dt1norm = dsqrt(dt1(1)*dt1(1)+dt1(2)*dt1(2)+dt1(3)*dt1(3))
125
126         dt1(1)   = dt1(1) / dt1norm
127         dt1(2)   = dt1(2) / dt1norm
128         dt1(3)   = dt1(3) / dt1norm
129
130         dt2(1) =  dt3(2)*dt1(3)-dt3(3)*dt1(2)
131         dt2(2) =  dt3(3)*dt1(1)-dt3(1)*dt1(3)
132         dt2(3) =  dt3(1)*dt1(2)-dt3(2)*dt1(1)
133
134   #ifdef __GFORTRAN__
```

```
135         CALL RANDOM_NUMBER(B)
136  #else
137         B = RLU(IDUM)
138  #endif
139         PHIP=2.D0*DPI*B
140
141         ctp=dcos(thetap)
142         stp=dsin(thetap)
143
144         cpp=dcos(phip)
145         spp=dsin(phip)
146  C
147  C      3-momentum for the hadrons.
148  C
149         do i = 2 , 4
150            vPn(i)=dPt*(dt3(i-1)*ctp + dt1(i-1)*stp*cpp + dt2(i-1)*stp*spp)
151            vPp(i)= vq(i)+vPn(i)
152
153         enddo
154
155  c       print*,En,dsqrt(En*En-vPn(2)*vPn(2)-vPn(3)*vPn(3)-vPn(4)*vPn(4))
156  c       print*,P-dsqrt(vPp(2)*vPp(2)+vPp(3)*vPp(3)+vPp(4)*vPp(4)),ctp
157
158         RETURN
159         END
```

LISTING A.2: construction of the kinematics vectors.

The energy and these vectors are then written in the 4*4 vector. The MC returns to the interface the complete kinematics of the four particles, the identity of each of these particles, their origin and the radial position of interaction. In the interface, two angles are randomly generated, one between 0 and 2π, called ϕ, and the other with its cosinus between $-$ and 1, called θ. With those two angle, the position of interaction inside the nucleus is computed the following way:

$$x = R * \sin\theta * \cos\phi \tag{A.1}$$

$$y = R * \sin\theta * \sin\phi \tag{A.2}$$

$$z = R * \cos\theta \tag{A.3}$$

Once the MC has filled the vectors the function translate them into the equivalent NEUT data structure.

Bibliography

[1] J. Chadwick. Intensitatsverteilung im magnetischen spektrum der b -strahlen von radium b+c. *Vehr der Deutschen Physikalishen Ges.*, 16, 1914.

[2] J. Chadwick. Possible existence of a neutron. *Nature*, 129, 1932.

[3] W. Heisenberg. Uber den bau der atomkerne. *Zeitschrift fur Physik*, 77:1, 1932.

[4] E. Fermi. Versuch einer theorie der -strahlen. *Zeitschrift fur Physik*, 88:161, 1934.

[5] F. Reines and C. L. Cowan. The neutrino. *Nature*, 178:446, Setptember 1956.

[6] F. Reines and C. L. Cowan. Free antineutrino absorption cross section. i. measurement of the free antineutrino absorption cross section by protons. *Phys. Rev.*, 113, January 1959.

[7] T. D. Lee and C. N. Yang. Question of parity conservation in weak interactions. *Phys. Rev.*, 104(254), 1956.

[8] C. S. Wu et al. Experimental test of parity conservation in beta decay. *Phys. Rev.*, 105(769), 1957.

[9] R. Feynman abd M. Gell-Mann. Theory of the fermi interaction. *Physical Review*, 109(193), 1958.

[10] E. Sudarshan and R. Marshak. Chirality invariance and the universal fermi interaction physical. *Physical Review*, 109(1860), 1958.

[11] J. C. Street and E. C. Stevenson. New evidence for the existence of a particle of mass intermediate between the proton and electron. *Phys. Rev.*, 52, November 1937.

[12] G. P. S. Occhialini C. M. G. Lattes, H. Muirhead and C. F. Powell. Processes involving charged mesons. *Nature*, 159, May 1947.

[13] B. Pontecorvo. Electron and muon neutrino. *Sov. Phys. JETP.*, 37(1236), 1960.

[14] G.Danby et al. Observation of high-energy neutrino reactions and the existence of two kinds of neutrinos. *Psysical Review Letters*, 9(36), 1962.

[15] S. L. Glashow. Partial-symmetries of weak interactions. *Nucl. Phys.*, 22, 1961.

[16] S. Weinberg. A model of leptons. *Physical Review Letters*, 19(1264), 1967.

[17] A. Salam. Weak and electromagnetic interactions. *Proceedings of the Eighth Nobel Symposium*, page 367, 1968.

[18] UA1 Collaboration. Experimental observation of isolated large transverse energy electrons with associated missing energy at sqrt(s)=504 gev. *Physics Letters B*, 122, February 1983.

[19] UA2 Collaboration. Observation of single isolated electrons of high transverse momentum in events with missing transverse energy at the cern pp collider. *Physics Letters B*, 122, March 1983.

[20] Gargamelle Neutrino Collaboration. Observation of neutrino-like interactions without muon or electron in the gargamelle neutrino experiment. *Nuclear Physics B*, 73:1, 1974.

[21] NuTeV Collaboration. Precise determination of electroweak parameters in neutrino-nucleon scattering. *Physical Review Letters*, 88(091802), 2002.

[22] P. W. Higgs. Broken symmetries, massless particles and gauge fields. *Physics Letter*, 12, 1964.

[23] Raymond Davis. A review of the homestake solar neutrino experiment. *Progree in Particle and Nuclear Physics*, 32:13–32, 1994.

[24] B. Pontecorvo. Neutrino experiments and the problem of conservation of leptonic charge. *Journal of Experimental and Theoretical Physics*, 26, 1968.

[25] Z. Maki et al. Remarks on the unified model of elementary particles. *Progress of Theoretical Physics*, 28, 1962.

[26] M. Tanabashi, K. Hagiwara, K. Hikasa, K. Nakamura, Y. Sumino, F. Takahashi, J. Tanaka, K. Agashe, G. Aielli, C. Amsler, M. Antonelli, D. M. Asner, H. Baer, Sw. Banerjee, R. M. Barnett, T. Basaglia, C. W. Bauer, J. J. Beatty, V. I. Belousov, J. Beringer, S. Bethke, A. Bettini, H. Bichsel, O. Biebel, K. M. Black, E. Blucher, O. Buchmuller, V. Burkert, M. A. Bychkov, R. N. Cahn, M. Carena, A. Ceccucci, A. Cerri, D. Chakraborty, M.-C. Chen, R. S. Chivukula, G. Cowan, O. Dahl, G. D'Ambrosio, T. Damour, D. de Florian, A. de Gouvêa, T. DeGrand, P. de Jong, G. Dissertori, B. A. Dobrescu, M. D'Onofrio, M. Doser, M. Drees, H. K. Dreiner,

D. A. Dwyer, P. Eerola, S. Eidelman, J. Ellis, J. Erler, V. V. Ezhela, W. Fetscher, B. D. Fields, R. Firestone, B. Foster, A. Freitas, H. Gallagher, L. Garren, H.-J. Gerber, G. Gerbier, T. Gershon, Y. Gershtein, T. Gherghetta, A. A. Godizov, M. Goodman, C. Grab, A. V. Gritsan, C. Grojean, D. E. Groom, M. Grünewald, A. Gurtu, T. Gutsche, H. E. Haber, C. Hanhart, S. Hashimoto, Y. Hayato, K. G. Hayes, A. Hebecker, S. Heinemeyer, B. Heltsley, J. J. Hernández-Rey, J. Hisano, A. Höcker, J. Holder, A. Holtkamp, T. Hyodo, K. D. Irwin, K. F. Johnson, M. Kado, M. Karliner, U. F. Katz, S. R. Klein, E. Klempt, R. V. Kowalewski, F. Krauss, M. Kreps, B. Krusche, Yu. V. Kuyanov, Y. Kwon, O. Lahav, J. Laiho, J. Lesgourgues, A. Liddle, Z. Ligeti, C.-J. Lin, C. Lippmann, T. M. Liss, L. Littenberg, K. S. Lugovsky, S. B. Lugovsky, A. Lusiani, Y. Makida, F. Maltoni, T. Mannel, A. V. Manohar, W. J. Marciano, A. D. Martin, A. Masoni, J. Matthews, U.-G. Meißner, D. Milstead, R. E. Mitchell, K. Mönig, P. Molaro, F. Moortgat, M. Moskovic, H. Murayama, M. Narain, P. Nason, S. Navas, M. Neubert, P. Nevski, Y. Nir, K. A. Olive, S. Pagan Griso, J. Parsons, C. Patrignani, J. A. Peacock, M. Pennington, S. T. Petcov, V. A. Petrov, E. Pianori, A. Piepke, A. Pomarol, A. Quadt, J. Rademacker, G. Raffelt, B. N. Ratcliff, P. Richardson, A. Ringwald, S. Roesler, S. Rolli, A. Romaniouk, L. J. Rosenberg, J. L. Rosner, G. Rybka, R. A. Ryutin, C. T. Sachrajda, Y. Sakai, G. P. Salam, S. Sarkar, F. Sauli, O. Schneider, K. Scholberg, A. J. Schwartz, D. Scott, V. Sharma, S. R. Sharpe, T. Shutt, M. Silari, T. Sjöstrand, P. Skands, T. Skwarnicki, J. G. Smith, G. F. Smoot, S. Spanier, H. Spieler, C. Spiering, A. Stahl, S. L. Stone, T. Sumiyoshi, M. J. Syphers, K. Terashi, J. Terning, U. Thoma, R. S. Thorne, L. Tiator, M. Titov, N. P. Tkachenko, N. A. Törnqvist, D. R. Tovey, G. Valencia, R. Van de Water, N. Varelas, G. Venanzoni, L. Verde, M. G. Vincter, P. Vogel, A. Vogt, S. P. Wakely, W. Walkowiak, C. W. Walter, D. Wands, D. R. Ward, M. O. Wascko, G. Weiglein, D. H. Weinberg, E. J. Weinberg, M. White, L. R. Wiencke, S. Willocq, C. G. Wohl, J. Womersley, C. L. Woody, R. L. Workman, W.-M. Yao, G. P. Zeller, O. V. Zenin, R.-Y. Zhu, S.-L. Zhu, F. Zimmermann, P. A. Zyla, J. Anderson, L. Fuller, V. S. Lugovsky, and P. Schaffner. Review of particle physics. *Phys. Rev. D*, 98:030001, Aug 2018. URL https://link.aps.org/doi/10.1103/PhysRevD.98.030001.

[27] P. Vogel C. Bemporad, G. Gratta. Reactor-based neutrino oscillation experiments. *Rev. Mod. Phys*, 74, March 2002.

[28] B.T. Cleveland et al. Measurement of the solar electron neutrino flux with the homestake chlorine detector. *Astrophysical Journal*, 496, 1998.

[29] D. R. Williams. Sun fact sheet. *NASA Goddard Space Flight Center*, July 2013.

[30] H. A. Bethe and C. L. Critchfield. The formation of deuterons by proton combination. *Phys. Rev.*, 54, august 1938.

[31] H. A. Bethe. Energy production in stars. *Phys. Rev.*, 55, March 1939.

[32] B.T.Cleveland et al. Measurement of the solar electron neutrino flux with the homestake chlorine detector. *Astrophys. J.*, 496, 1998.

[33] P.A. Cerenkov. Visible emission of clean liquids by action of radiation. *Doklady Akademii Nauk SSSR*, 2, 1934.

[34] The SNO collaboration. The sudbury neutrino observatory. *Nucl.Instrum.Meth. A*, 449, 2000.

[35] V. Agrawal et al. Atmospheric neutrino flux above 1 gev. *Phys Rev. D*, 53(3), February 1996.

[36] M. Honda T.K. Gaisser. Flux of atmospheric neutrinos. *Ann.Rev.Nucl.Part.Sci.*, 52, 2002.

[37] J. Wentz et al. Simulation of atmospheric muon and neutrino fluxes with corsika. *Phys. Rev. D*, 67(073020), April 2003.

[38] K. Abe et al. (T2K Collaboration). Indication of electron neutrino appearance from an accelerator-produced off-axis muon neutrino beam. *Phys. Rev. Lett.*, 107 (041801), July 2011.

[39] Y. Fukuda et al. (Super-Kamiokande Collaboration). The super-kamiokande detector. *Nucl.Instrum.Meth. A*, 501, January 2002.

[40] T2K collaboration. Measurements of the t2k neutrino beam properties using the ingrid on-axis near detector. *Nuclear Instruments and Methods in Physics Research Section A: Accelerators, Spectrometers, Detectors and Associated Equipment*, 694, 2012.

[41] T2K Collaboration. T2k neutrino flux prediction. *Physical Review D*, 87(012001), 2013.

[42] P. Amaudruz et al. The t2k fine-grained detectors. *Nuclear Instruments and Methods in Physics Research Section A: Accelerators, Spectrometers, Detectors and Associated Equipment*, 696:1, 2012.

[43] N. Abgrall et al. Time projection chambers for the t2k near detectors. *Nuclear Instruments and Methods in Physics Research Section A: Accelerators, Spectrometers, Detectors and Associated Equipment*, 637:25, 2011.

[44] D. Allan et al. The electromagnetic calorimeter for the t2k near detector nd280. *Journal of Instrumentation*, 8, 2013.

[45] S. Aoki et al. The t2k side muon range detector (smrd). *Nuclear Instruments and Methods in Physics Research Section A: Accelerators, Spectrometers, Detectors and Associated Equipment*, 698:135, 2013.

[46] S. Assylbekov et al. The t2k nd280 off-axis pizero detector. *Nuclear Instruments and Methods in Physics Research Section A: Accelerators, Spectrometers, Detectors and Associated Equipment*, 686:48, 2012.

[47] MiniBooNE Collaboration. A search for electron antineutrino appearance at the m2 1 ev2 scale. *Phys.Rev.Lett.*, 103(111801), 2009.

[48] MicroBooNE Collaboration. Design and construction of the microboone detector. *JINST*, 12(P02017), 2017.

[49] G. P. Zeller J. A. Formaggio. From ev to eev: Neutrino cross sections across energy scales. *REVIEWS OF MODERN PHYSICS*, 84, July-September 2012. URL http://dx.doi.org/10.1103/RevModPhys.84.1307.

[50] Geoffrey F. Chew and Gian Carlo Wick. The impulse approximation. *Phys. Rev.*, 85, February 1952.

[51] J. Nieves A. Gil and E. Oset. Many body approach to the inclusive (e,e) reaction from the quasielastic to the excitation region. *Nucl. Phys. A.*, 627, 1997.

[52] R. G. Newton. Optical theorem and beyond. *Am. J. Phys.*, 44, 1976.

[53] R. E. Cutkosky. Singularities and discontinuities of feynman amplitudes. *Journal of Mathematical Physics*, 1, 1960.

[54] E. Oset R. C. Carrasco. Interaction of real photons with nuclei from 100 to 500 mev. *Nucl. Phys. A*, 536, January 1992.

[55] R.G. Sachs Ernst F. J. and K.C. Wali. Electromagnetic form factors of the nucleon. *Phys. Rev.*, 119, 1960.

[56] S. Galster et al. Elastic electron-deuteron scattering and the electric neutron form factor at four-momentum transfers 5fm2¡2¡14fm2. *Nucl. Phys. B*, 32, Feb 1971.

[57] P. Fernndez De Crdoba H. C. Chiang, E. Oset. Muon capture revisited. *Nucl. Phys. A*, 510, April 1990.

[58] A.B. Migdal. Theory of finite fermi systems and applications to atomic nuclei. *Interscience Publishers, a division of John Wiley and Sons, New York*, 1967.

[59] J. Wambach G.W. Brown J. Speth, V. Klemt. The influence of the pi and rho exchange potential on magnetic properties of nuclei. *Nucl. Phys. A*, 343, 1980.

[60] E. Oset S. K. Singh. Quasielastic neutrino (antineutrino) reactions in nuclei and the axial-vector form factor of the nucleon. *Phys. Rev. A*, 542, June 1992.

[61] M. J. Vicente Vacas J. Nieves, I. Ruiz Simo. Inclusive charged-current neutrino-nucleus reactions. *Phys rev C*, 83(045501), February 2011.

[62] M. Valverde E. Hernandez, J. Nieves and M. J. Vicente Vacas. N(1232) axial form factors from weak pion production. *Phys. Rev. D*, 81:085046, 2010.

[63] J.D. Bjorken. Asymptotic sum rules at infinite momentum. *Phys Rev.*, 179(1547), March 1969.

[64] R. P. Feynman. Very high-energy collisions of hadrons. *Phys. Rev. Lett*, 23(1415), December 1969.

[65] R. Yoshida M. Klein. Collider physics at hera. *Prog.Part.Nucl.Phys.*, 61, 2008.

[66] G. B. West. Electron scattering from atoms, nuclei and nucleons. *Phys. Rep.*, 18, June 1975.

[67] J. A. Caballero T. W. Donnelly A. Molinari J. E. Amaro, M. B. Barbaro and I. Sick. Using electron scattering superscaling to predict charge-changing neutrino cross sections in nuclei. *Phys. Rev. C*, 71(015501), January 2005.

[68] J. A. Caballero. General study of superscaling in quasielastic (e,e) and (,) reactions using the relativistic impulse approximation. *Phys. Rev. C*, 74(015502), July 2006.

[69] T. W. Donnelly and Ingo Sick. Superscaling in inclusive electron-nucleus scattering. *Phys. Rev. Lett.*, 82(3212), April 1999.

[70] Guillermo Daniel Megias Vazquez. Charged-current neutrino interactions with nucleons and nuclei at intermediate energies. may 2017.

[71] J. Jourdan. Quasi-elastic response functions. the coulomb sum revisited. *Nucl. Phys. A*, 603(117), 1996.

[72] J. E. Amaro J. Nieves and M. Valverde. Inclusive quasielastic charged-current neutrino-nucleus reactions. *Phys. Rev. C*, 70(055503), 2004.

[73] Y.Hayato. Neut. *Nucl. Phys. B*, 112, 2002.

[74] P.A. Rodrigues et al. (MINERvA Collaboration). Identification of nuclear effects in neutrino-carbon interactions at low three-momentum transfer. *Phys. Rev. Lett.*, 116(071802), February 2016.

[75] R. A. Smith and E. J. Moniz. Neutrino reactions on nuclear targets. *Nucl. Phys. B*, 43, 1972.

[76] S. Fantoni I. Sick O.Benhar, A. Fabrocini. Spectral function of finite nuclei and scattering of gev electrons. *Nucl. Phys. A.*, 579, 1994.

[77] Dieter Rein and Lalit M. Sehgal. Neutrino excitation of baryon resonances and single pion production. *Annals Phys.*, 133, 1981.

[78] Krzysztof M. Graczyk and Jan T. Sobczyk. Lepton mass effects in weak charged current single pion production. *Phys. Rev. D*, 77(053003), 2008.

[79] E. Reya M. Glck and A. Vogt. Dynamical parton distributions revisited. *Eur. Phys. J. C*, 5, 1998.

[80] A. Bodek and U. K. Yang. Modeling neutrino and electron scattering inelastic cross-sections in the few gev region with effective lo pdfs tv leading order. *2nd International Workshop on Neutrino-Nucleus Interactions in the Few GeV Region (NuInt 02)*, December 2002.

[81] M. Levine Jihn E. Kim, Paul Langacker and H. H. Williams. A theoretical and experimental review of the weak neutral current: A determination of its structure and limits on deviations from the minimal su(2)-l x u(1) electroweak theory. *Rev. Mod. Phys.*, 53(211), 1981.

[82] Dieter Rein and Lalit M. Sehgal. Coherent pi0 production in neutrino reactions. *Nucl. Phys. B*, 223, 1983.

[83] The T2K Collaboration. Measurement of coherent + production in low energy neutrino-carbon scattering. *Phys. Rev. Lett.*, 117(192501), 2016.

[84] D. Rein and L. M. Sehgal. Pcac and the deficit of forward muons in pi+ production by neutrinos. *Phys. Lett. B*, 657, 2007.

[85] Ch. Berger and Lalit M. Sehgal. Pcac and coherent pion production by low energy neutrinos. *Phys. Rev. D*, 79(053003), 2009.

[86] The T2K collaboration. The t2k neutrino flux prediction. *Phys. Rev. D*, 87(012001), January 2013.

[87] The MiniBooNE collaboration. The neutrino flux prediction at miniboone. *Phys. Rev. D*, 79(072002), April 2009.

[88] The MINERvA collaboration. Neutrino flux predictions for the numi beam. *Phys. Rev. D*, 94(092005), 2016.

[89] The T2K collaboration. Measurement of inclusive double-differential charged-current cross section with improved acceptance in the t2k off-axis near detector. *Phys. Rev. D*, 98(012004), 2018.

[90] The T2K collaboration. Measurement of double-differential muon neutrino charged-current interactions on c 8 h 8 without pions in the final state using the t2k off-axis beam. *Phys. Rev. D*, 93(112012), 2016.

[91] The MiniBooNE collaboration. First measurement of the muon neutrino charged current quasielastic double differential cross section. *Phys.Rev.D*, 81(092005), 2010.

[92] The MINERvA collaboration. Measurement of the muon anti-neutrino double-differential cross section for quasi-elastic scattering on hydrocarbon at e3.5 gev. *Phys. Rev. D*, 97(052002), 2018.

[93] The MINERvA collaboration. Measurement of final-state correlations in neutrino muon-proton mesonless production on hydrocarbon at e=3 gev. *Phys. Rev. Lett.*, 121(022504), 2018.

[94] S. Dolan G. Barr D. Coplowe Y. Uchida D. Wark M.O. Wascko A. Weber T. Yuan X.-G. Lu, L. Pickering. Measurement of nuclear effects in neutrino interactions with minimal dependence on neutrino energy. *Phys. Rev. C*, 94(015503), 2016.